Eur. Phys. J. C (2024) 84:757
https://doi.org/10.1140/epjc/s10052-024-12994-1

THE EUROPEAN PHYSICAL JOURNAL C

Regular Article - Experimental Physics

Search for flavour-changing neutral-current couplings between the top quark and the Higgs boson in multi-lepton final states in 13 TeV pp collisions with the ATLAS detector

ATLAS Collaboration[*]

CERN, 1211 Geneva 23, Switzerland

Received: 4 April 2024 / Accepted: 7 June 2024 / Published online: 29 July 2024

Abstract A search is presented for flavour-changing neutral-current interactions involving the top quark, the Higgs boson and an up-type quark ($q = u, c$) with the ATLAS detector at the Large Hadron Collider. The analysis considers leptonic decays of the top quark along with Higgs boson decays into two W bosons, two Z bosons or a $\tau^+\tau^-$ pair. It focuses on final states containing either two leptons (electrons or muons) of the same charge or three leptons. The considered processes are $t\bar{t}$ and Ht production. For the $t\bar{t}$ production, one top quark decays via $t \to Hq$. The proton–proton collision data set analysed amounts to (140 fb^{-1}) at ($\sqrt{s} = 13$ TeV). No significant excess beyond Standard Model expectations is observed and upper limits are set on the $t \to Hq$ branching ratios at 95 % confidence level, amounting to observed (expected) limits of $\mathcal{B}(t \to Hu) < 2.8\,(3.0) \times 10^{-4}$ and $\mathcal{B}(t \to Hc) < 3.3\,(3.8) \times 10^{-4}$. Combining this search with other searches for tHq flavour-changing neutral-current interactions previously conducted by ATLAS, considering $H \to b\bar{b}$ and $H \to \gamma\gamma$ decays, as well as $H \to \tau^+\tau^-$ decays with one or two hadronically decaying τ-leptons, yields observed (expected) upper limits on the branching ratios of $\mathcal{B}(t \to Hu) < 2.6\,(1.8) \times 10^{-4}$ and $\mathcal{B}(t \to Hc) < 3.4\,(2.3) \times 10^{-4}$.

Contents

1 Introduction

Following the discovery of the Higgs boson at the Large Hadron Collider (LHC) by the ATLAS and CMS experiments in 2012 [1,2], several measurements have probed properties of the particle. In addition to Higgs boson couplings to fermions and gauge bosons, which agree well with the Standard Model (SM) predictions [3,4], further interactions can be investigated to search for evidence of possible new physics in the Higgs sector. A possibility is that the Higgs boson has an interaction involving two up-type quarks of different generations, denoted by tHq where $q = (u, c)$, leading to $gq \to Ht$ production and $t \to Hq$ decay. These are flavour-changing neutral-current (FCNC) interactions, forbidden at tree-level in the SM and suppressed at higher orders due to the Glashow–Iliopoulos–Maiani (GIM) mech-

[*] e-mail: atlas.publications@cern.ch

anism [5]. The SM predictions for the $t \rightarrow Hq$ branching ratios $\mathcal{B}(t \rightarrow Hq)$ are very small, around 10^{-15} [6–10], and beyond the sensitivity of the LHC. However, in the framework of new physics models such as two-Higgs-doublet models (2HDMs) [11], the minimal supersymmetric SM (MSSM) [12–15], supersymmetric models with R-parity violation [16], quark-singlet models [17], and warped extra dimensions [18], the branching ratios of these processes are modified making them large enough to be measured at the LHC. For example, branching ratios of up to 10^{-3} are possible in 2HDMs without explicit flavour symmetry, since there are no symmetries explicitly forbidding tree-level FCNC interactions [19–26] in this model. The FCNC interaction can also mediate the production of a Higgs boson with a single top quark ($pp \rightarrow tH$) [27]. The SM prediction of the $pp \rightarrow tH$ cross-section is $74.3^{+0.4}_{-0.3}$ fb at $\sqrt{s} = 13$TeV [28].

The FCNC interactions are introduced using an effective field theory (EFT) framework, which is used for indirect searches for new physics [29]. Here the SM is regarded as a low-energy approximation of an ultraviolet complete theory containing new particles, whose masses are characterised by an energy scale $\Lambda = 1$ TeV. The new physics contributions are parameterised in terms of operators with mass dimension greater than four containing only the SM fields, scaled by dimensionless Wilson coefficients and inverse powers of Λ. In the case where only the tHu and tHc interactions are considered, the relevant operators are

$$\mathcal{O}^{qt}_{u\phi} = \left(\phi^\dagger\phi - \frac{v^2}{2}\right)(\bar{q}_L\, t_R)\tilde{\phi}$$
$$\mathcal{O}^{tq}_{u\phi} = \left(\phi^\dagger\phi - \frac{v^2}{2}\right)(\bar{t}_L\, q_R)\tilde{\phi}, \tag{1}$$

where q corresponds to an up or charm quark, depending on the FCNC coupling. The index u is the coupling to any up-type quark, t is the top-quark, ϕ denotes the Higgs boson field with v corresponding to the absolute value of its vacuum expectation value. The two left-handed quark doublet fields are $\bar{q}_L$ and $\bar{t}_L$, with q_R and t_R being the corresponding right-handed singlets. The operators are scaled with Wilson coefficients $C^{qt}_{u\phi}$ and $C^{tq}_{u\phi}$, and $1/\Lambda^2$ to give the relevant Lagrangian:

$$\mathcal{L}_{\text{EFT}} = \mathcal{L}_{\text{SM}} + \sum_{q=u,c}\left[\frac{C^{qt}_{u\phi}}{\Lambda^2}\mathcal{O}^{qt}_{u\phi} + \frac{C^{tq}_{u\phi}}{\Lambda^2}\mathcal{O}^{tq}_{u\phi}\right]. \tag{2}$$

In the case of $t\bar{t}$ production with a FCNC $t \rightarrow Hq$ decay, no kinematic differences between $\mathcal{O}^{qt}_{u\phi}$ and $\mathcal{O}^{tq}_{u\phi}$ are expected because the top quarks are produced unpolarised and the Higgs boson is a scalar particle. For $t \rightarrow Hq$ production, comparisons of simulations using either $\mathcal{O}^{qt}_{u\phi}$ or $\mathcal{O}^{tq}_{u\phi}$ have shown that differences between production rates and kinematic distributions are negligible in the phase space considered. Thus, the mean of both the couplings $C^{qt,tq}_{u\phi} = \frac{C^{qt}_{u\phi}+C^{tq}_{u\phi}}{2}$ is considered.

Both the ATLAS and CMS Collaborations have undertaken various searches for tHq FCNC processes, split by Higgs boson final state [30,30–38]. In this paper, a search is conducted using final states containing either two leptons (electrons or muons) of the same charge (2ℓSS, $\ell = e, \mu$) or three leptons, exactly two of which have the same charge (3ℓ, $\ell = e, \mu$). The ATLAS Collaboration searched for tHq FCNC couplings in 2ℓSS and 3ℓ final states using a partial Run 2 data sample of 36.1 fb^{-1} [32], resulting in observed (expected) 95% CL upper limits of $\mathcal{B}(t \rightarrow Hu) < 19(15) \times 10^{-4}$ and $\mathcal{B}(t \rightarrow Hc) < 16(15) \times 10^{-4}$. The strongest limits set by the ATLAS Collaboration come from a combination of searches in the $H \rightarrow b\bar{b}$, $H \rightarrow \gamma\gamma$ and $H \rightarrow \tau^+\tau^-$ channels using the full Run 2 data sample [35]. The obtained limits are $\mathcal{B}(t \rightarrow Hu) < 4.0(2.4) \times 10^{-4}$ and $\mathcal{B}(t \rightarrow Hc) < 5.8(3.0) \times 10^{-4}$. For the tHc coupling, these are the most stringent limits published to date. However, for the tHu coupling the strongest limits are set by a search conducted with the CMS detector in the $H \rightarrow \gamma\gamma$ channel [38], amounting to $\mathcal{B}(t \rightarrow Hu) < 1.9(3.1) \times 10^{-4}$.

The dominant Higgs-boson decay mode resulting in 2ℓSS and 3ℓ final states across production and decay processes is $H \rightarrow WW^*$, with $WW^* \rightarrow \ell\nu jj$ or $WW^* \rightarrow \ell\nu\ell\nu$ for the 2ℓSS and 3ℓ final state respectively. The corresponding Feynman diagrams are shown in Figs. 1, 2. Other Higgs-boson decay modes such as $H \rightarrow ZZ^*$ and $H \rightarrow \tau^+\tau^-$ can also meet the selection criteria. Based on the SM branching ratios of the Higgs boson and the top quark, approximately 73 % of all 2ℓSS signal events are expected from the $H \rightarrow WW^*$ decay mode, while the rest originate from leptonic $H \rightarrow \tau^+\tau^-$ decays. Less than 1 % of events are attributable to the $H \rightarrow ZZ^*$ decay mode. In the 3ℓ final state, the latter contributes more significantly, being responsible for 14 % of all events. The majority, accounting for 54 % of the 3ℓ signal events, originate from $H \rightarrow WW^*$ decays, while the remaining 32 % arise from $H \rightarrow \tau^+\tau^-$ events. These numbers do not take into account detector acceptance effects or selection requirements. Although the total number of events meeting the 2ℓSS and 3ℓ criteria is modest, the low statistical precision is balanced by minimal background contributions.

The strategy of the analysis is to first identify kinematic regions enriched in the signal process. In these regions, various reconstruction algorithms are implemented to create variables that can distinguish between the signal and several background processes. These reconstructed variables are combined into a single discriminant using a feed-forward neural network [39]. The same kinematic regions are used for the tHu and the tHc channel of the analysis, while individual

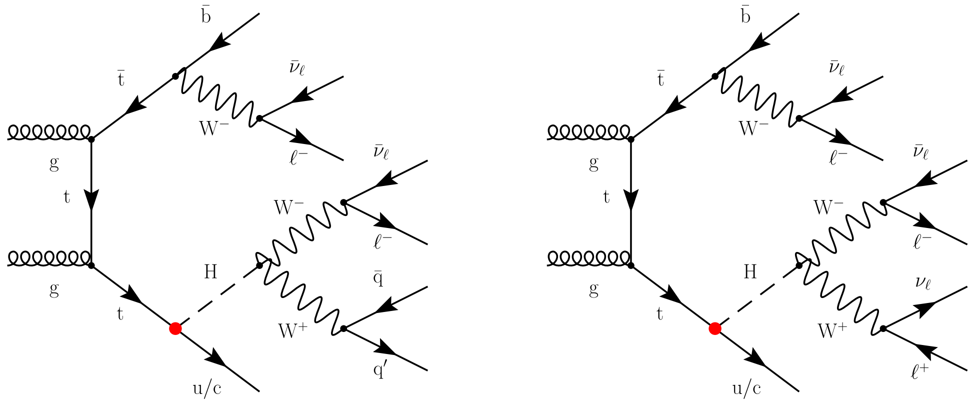

(a) (b)

Fig. 1 Example Feynman diagrams of the $t\bar{t}(t \to Hq)$ decay signal process resulting in **a** the 2ℓSS final state and **b** the 3ℓ final state. The FCNC vertex is highlighted in red

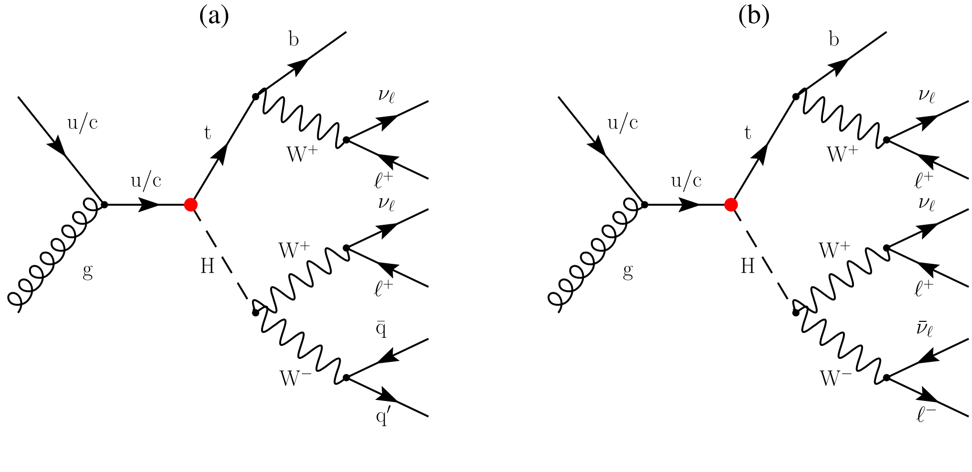

(a) (b)

Fig. 2 Example Feynman diagrams of the $gq \to Ht$ production signal process resulting in **a** the 2ℓSS final state and **b** the 3ℓ final state. The FCNC vertex is highlighted in red

neural networks are trained for each of the channels. Aside from this, the analysis strategy is identical for the tHu and the tHc channel. The distribution of the neural network output is then used as input to a maximum-likelihood fit, which considers statistical and systematic uncertainties. In addition to the signal-enriched regions, several regions enriched in specific background processes are included in the fit, to constrain the normalisation of these processes. If the fit shows evidence of a signal, the corresponding significance is determined. Otherwise, upper limits are set on the FCNC branching ratios and the Wilson coefficients of the EFT dimension-6 operators. Finally, the results of this analysis are statistically combined with those from other ATLAS searches for tHq FCNC interactions in different final states.

2 The ATLAS detector

The ATLAS detector [40] at the LHC covers nearly the entire solid angle around the collision point.[1] It consists of an inner tracking detector surrounded by a thin superconducting solenoid, electromagnetic and hadron calorimeters, and a muon spectrometer incorporating three large superconducting air-core toroidal magnets.

The inner-detector system (ID) is immersed in a 2 T axial magnetic field and provides charged-particle tracking in the range of $|\eta| < 2.5$. The high-granularity silicon pixel detector covers the vertex region and typically provides four measurements per track, the first hit normally being in the insertable B-layer (IBL) installed before Run 2 [41,42]. It is followed by the silicon microstrip tracker (SCT), which usually provides eight measurements per track. These silicon detectors are complemented by the transition radiation tracker (TRT), which enables radially extended track reconstruction up to $|\eta| = 2.0$. The TRT also provides electron identification information based on the fraction of hits (typically 30 in total) above a higher energy-deposit threshold corresponding to transition radiation.

[1] ATLAS uses a right-handed coordinate system with its origin at the nominal interaction point (IP) in the centre of the detector and the z-axis along the beam pipe. The x-axis points from the IP to the centre of

Footnote 1 continued
the LHC ring, and the y-axis points upwards. Cylindrical coordinates (r, ϕ) are used in the transverse plane, ϕ being the azimuthal angle around the z-axis. The pseudorapidity is defined in terms of the polar angle θ as $\eta = -\ln\tan(\theta/2)$. Angular distance is measured in units of $\Delta R \equiv \sqrt{(\Delta\eta)^2 + (\Delta\phi)^2}$.

The calorimeter system covers the pseudorapidity range $|\eta| < 4.9$. Within the region $|\eta| < 3.2$, electromagnetic calorimetry is provided by barrel and endcap high-granularity lead/liquid-argon (LAr) calorimeters, with an additional thin LAr presampler covering $|\eta| < 1.8$ to correct for energy loss in material upstream of the calorimeters. Hadron calorimetry is provided by the steel/scintillator-tile calorimeter, segmented into three barrel structures within $|\eta| = 1.7$, and two copper/LAr hadron endcap calorimeters. The solid angle coverage is completed with forward copper/LAr and tungsten/LAr calorimeter modules optimised for electromagnetic and hadronic energy measurements respectively.

The muon spectrometer (MS) comprises separate trigger and high-precision tracking chambers measuring the deflection of muons in a magnetic field generated by the superconducting air-core toroidal magnets. The field integral of the toroids ranges between 2.0 and 6.0 T m across most of the detector. Three layers of precision chambers, each consisting of layers of monitored drift tubes, cover the region $|\eta| < 2.7$ and are complemented by cathode-strip chambers in the forward region, where the detector occupancy is highest. The muon trigger system covers the range of $|\eta| < 2.4$ with resistive-plate chambers in the barrel, and thin-gap chambers in the endcap regions.

Recorded events are selected by the first-level trigger system implemented in custom hardware, followed by selections made by algorithms implemented in software in the high-level trigger [43]. The first-level trigger accepts events from the 40 MHz bunch crossings at a rate below 100 kHz, which the high-level trigger further reduces to record events to disk at about 1 kHz.

An extensive software suite [44] is used in data simulation, in the reconstruction and analysis of real and simulated data, in detector operations, and in the trigger and data acquisition systems of the experiment.

3 Samples of data and simulated events

Proton–proton (pp) collision data are used recorded with the ATLAS detector in the years 2015 to 2018 at a centre-of-mass energy of 13 TeV. After applying data-quality requirements [45], the data sample corresponds to an integrated luminosity of 140.1(12) fb^{-1} [46]. The LUCID-2 detector [47] was used for the primary luminosity measurements, complemented by measurements using the inner detector and calorimeters.

Events were selected online during data taking by single-electron or single-muon triggers [48,49]. Multiple unprescaled triggers were combined in a logical OR to increase the selection efficiency. The lowest-threshold triggers utilised isolation requirements to reduce the trigger rate. The higher-level lepton triggers had transverse momentum (p_T) thresholds of 20 GeV for muons and 24 GeV for electrons in 2015 data, and 26 GeV for both the lepton types in 2016, 2017 and 2018 data. They were complemented by other triggers with higher p_T thresholds but no isolation requirements to increase the trigger efficiency.

Large sets of simulated events from signal and background processes were produced with Monte Carlo (MC) event generator programs to model the selected data. After event simulation, the response of the ATLAS detector was simulated using the Geant4 toolkit [50] with a full detector model [51] or a fast simulation [51,52] which employed a parameterisation of the calorimeter response. Samples relying on fast simulation were used to evaluate systematic uncertainties in the event generators and for the modelling of $t\bar{t}$ production with two bosons.

To account for additional inelastic pp collisions in the same and neighbouring bunch crossings (pile-up), minimum-bias interactions were overlaid on the hard-scattering events at the level of energy depositions simulated using Geant4. The minimum-bias events were simulated using Pythia [8.186] [53] with the A3 [54] set of tuned parameters and the NNPDF[2.3lo] set of parton distribution functions (PDF) [55]. The resulting events were weighted to reproduce the observed pile-up distribution. The average number of interactions per bunch crossing during the entire data-taking period from 2015 to 2018 is 33.7.

Finally, the simulated events were reconstructed using the same software as applied to the collision data. The same event selection requirements were applied and the selected events were passed through the same analysis chain. Small corrections were applied to simulated events such that the efficiencies of the utilised reconstruction methods are in better agreement with the response observed in data. More details of the simulated event samples are provided in the following subsections. Except for the events simulated with the Sherpa generator [56,57], the EvtGen [58] program was used to simulate bottom and charm hadron decays. If not mentioned otherwise, the top-quark mass was set to $m_t = 172.5$ GeV and the Higgs-boson mass to $m_H = 125$ GeV. All processes for which the parton shower is simulated using Pythia[8] use the A14 set of tuned parameters [59] and the NNPDF[2.3lo] PDF set.

3.1 Simulation of tHq FCNC signal samples

Two different signal processes are studied: the $t\bar{t}(t \rightarrow Hq)$ decay and the $gq \rightarrow Ht$ production process. The EFT operators parametrising the FCNC coupling are implemented in the TopFCNC [60] model using the FeynRules[2.0] framework [61], allowing for next-to-leading-order (NLO) calculations of the postulated processes. The decay process events were simulated using the NLO matrix-element generator POWHEGBOX[v2] [62–68], with the NNPDF[3.0nlo] PDF set [69]. The production of a top quark–antiquark pair is performed according to SM calculations in the five-flavour scheme, setting the masses of all quarks except for the top quark to zero. One top quark is required to decay via the SM decay mode $t \rightarrow Wb$, while the other performs the FCNC decay $t \rightarrow Hq$. Both top-quark decays are modelled using MADSPIN [70,71]. Only leptonic final states for the SM decay of the top quark are considered. The Higgs-boson decay, and parton showers, hadronisation, and the underlying event, were modelled using PYTHIA[8.308] [72]. The matrix-element-to-parton-shower matching is steered by the h_{damp} parameter, which controls the p_{T} of the first additional gluon emission beyond the leading-order (LO) Feynman diagram in the parton shower and therefore regulates the high-p_{T} emission against which the $t\bar{t}$ system recoils. The event generation was performed with $h_{\text{damp}} = 1.5m_t$ [73]. Four separate samples are produced, modelling the tHu/ tHc coupling with either the top quark or the top antiquark decaying via the FCNC interaction. For consistency across searches, all tHq FCNC samples are normalised to the cross-section corresponding to a branching ratio of $\mathcal{B}(t \rightarrow Hq) = 0.1\,\%$. As explained previously, kinematic differences between the left- and right-handed couplings are negligible in the case of $t \rightarrow Hq$ decay process. Therefore, the same samples are used to model the left-handed and the right-handed FCNC couplings. The matrix element generator MGNLO[2.9.9] [74] was used to model the $gq \rightarrow Ht$ production signal using the TOPFCNC model with the NNPDF[3.0nlo] PDF set and the five-flavour scheme. Separate samples are produced, each with exactly one of the Wilson coefficients set to 1.0 and the others set to zero, all of them at NLO in QCD.

The SM top-quark and Higgs-boson decays are simulated using MADSPIN. The three relevant Higgs-boson decays ($H \rightarrow WW^*$, $H \rightarrow ZZ^*$, $H \rightarrow \tau^+\tau^-$) are modelled in separate samples. All Higgs-boson decays, parton shower, hadronisation, and the underlying event, were modelled using PYTHIA[8.307]. The samples are normalised to the cross-section calculated with MGNLO.

3.2 Simulation of background processes

Samples of simulated events from SM $t\bar{t}$ and single-top-quark production were simulated using the NLO matrix-element generator POWHEGBOX[v2]. For $t\bar{t}$ and tW production and s-channel single-top-quark production ($t\bar{b}$ production) the NNPDF[3.0nlo] PDF set was used with the five-flavour scheme. Following a recommendation given in Ref. [68], single top-quark production in the t-channel (tq production) was simulated with the NNPDF[3.0nlo_nf4] PDF set, which implements the four-flavour scheme. Parton showers, hadronisation, and the underlying event were modelled using PYTHIA[8.230]. The event simulation used a value of $h_{\text{damp}} = 1.5m_t$.

The $t\bar{t}$ production cross-section was scaled to $\sigma(t\bar{t}) =$ 832 pb, the value obtained from next-to-next-to-leading-order predictions from the TOP++2.0 program (see Ref. [75] and references therein), and it includes the resummation of next-to-next-to-leading logarithmic soft-gluon terms. The predicted cross-sections of tq and $\bar{t}q$ production used to scale the corresponding samples of simulated events are $\sigma(tq) = 136$ pb and $\sigma(\bar{t}q) = 81$ pb and were calculated at NLO in QCD with the HATHOR[2.1] program [76,77]. The total cross-section for $t\bar{b}$ production was also computed at NLO in QCD with the HATHOR[2.1] program and the corresponding sample of simulated events was scaled to $\sigma(t\bar{b} + \bar{t}b) = 10.32$ pb. The cross-section used for normalising the tW sample is $\sigma(tW + \bar{t}W) = 71.7$ pb [78].

The production of a vector boson in association with jets (V+jets, $V = W, Z$), including b- and c-jets, was simulated with the SHERPA[2.2.11] generator. NLO-accurate matrix elements for up to two partons and LO-accurate matrix elements for three to five partons are calculated in the five-flavour scheme using the COMIX [79] and OPENLOOPS [80–82] libraries. The default SHERPA parton shower [83] based on Catani–Seymour dipole factorisation and the cluster hadronisation model [84] are used. The samples are simulated using a dedicated set of tuned parameters developed by the SHERPA authors and use the NNPDF[3.0nnlo] PDF set.

The $t\bar{t}W$ process was simulated using the SHERPA[2.2.10] generator. The matrix elements were calculated for up to one additional parton at NLO and up to two partons at LO using COMIX and OPENLOOPS, and merged with the SHERPA parton shower using the MEPS@NLO prescription [85]. In addition to the nominal prediction at NLO in QCD, higher-order corrections related to electroweak (EWK) contributions are also included. Event-by-event correction factors are applied that provide virtual NLO EWK corrections to $\mathcal{O}(\alpha^2\alpha_s^2)$ and LO corrections to $\mathcal{O}(\alpha^3)$ [57,86,87]. An independent SHERPA[2.2.10] sample was produced at LO to account for the sub-leading EWK corrections to $\mathcal{O}(\alpha^3\alpha_s)$ [88]. The NLO QCD and NLO EWK contributions from SHERPA are combined following the method of Ref. [89]. The $t\bar{t}W$ samples are normalised using a cross-section of 722 fb computed at NLO including the hard non-logarithmically enhanced radiation at NLO in QCD [89].

The modelling of the production of a top quark–antiquark pair with a Z boson decaying leptonically is done using the MGNLO[2.8.1] generator. It provides matrix elements at NLO in QCD, employing the NNPDF[2.3lo] PDF set. The generated events are interfaced with PYTHIA[8.244] for the parton shower and hadronisation stages. The $t\bar{t}Z/\gamma^*(\rightarrow \ell^+\ell^-)$ prediction was normalised to the calculation at NLO QCD and NLO EWK accuracy based on Ref. [28] with the additional inclusion of off-shell effects, corresponding to 162 fb.

The production of $t\bar{t}H$ events was modelled using the POWHEGBOX[v2] generator at NLO in QCD with the NNPDF[3.0nlo] PDF set. The events were interfaced to PYTHIA[8.230]. The cross-section was calculated at NLO QCD and NLO EWK using MGNLO and amounts to 507 fb.

The production of two or three weak vector bosons (VV, VVV) in 2ℓ, 3ℓ and 4ℓ final states was simulated using the SHERPA[2.2.12] generator including the off-shell contributions. Matrix elements including additional partons were calculated at NLO in QCD for up to one parton and at LO accuracy for two or three additional partons using COMIX and OPENLOOPS. For the parton shower simulation, the same method as in the W+jets and Z+jets samples is used. The VV and VVV samples are normalised to the total cross-sections provided by SHERPA.

The tZq process was modelled at NLO with the MGNLO [2.9.5] generator and the NNPDF[3.0nlo] PDF. The generated events were interfaced with PYTHIA[8.230]. Matrix elements of the tWZ process were also calculated with MGNLO[2.2.2], using the same PDF set. The events were interfaced with PYTHIA[8.212] using the same tune and PDF set as used for tZq production. The samples were normalised to the theoretical cross-section at NLO QCD.

Some rare processes are considered: $t\bar{t}t$, $t\bar{t}t\bar{t}$, tHW, tHq, $t\bar{t}WW$, $t\bar{t}HH$, $t\bar{t}WH$, $t\bar{t}ZZ$, $t\bar{t}WZ$ and VH production. The processes involving at least one top quark were simulated with MGNLO, while VH was produced with POWHEGBOX[v2]. Simulated events of all processes were interfaced to PYTHIA[8] to simulate parton showers and hadronisation. The processes are normalised to their predicted NLO cross-sections. Their combined contribution is nearly negligible, ranging from 0.1 to 1 %, depending on the kinematic region considered.

4 Object reconstruction and event preselection

Events are required to have at least one vertex reconstructed from at least two ID tracks with transverse momenta of $p_T >$ 0.5 GeV. The primary vertex of an event is defined as the vertex with the highest p_T^2 summed over the ID tracks [90] matched to it.

Electron candidates are reconstructed by matching a track in the ID to clusters of energy deposits in the electromagnetic calorimeter [91]. The pseudorapidity of clusters, η_{cluster}, is required to be in the range of $|\eta_{\text{cluster}}| < 2.47$. However, clusters are excluded if they are in the transition region $1.37 < |\eta_{\text{cluster}}| < 1.52$ between the barrel and endcap electromagnetic calorimeters. Electron candidates must have $p_T > 10$ GeV. A likelihood-based discriminant is constructed to simultaneously evaluate several properties of electron candidates, including shower shapes in the electromagnetic calorimeter, track quality, and the detection of transition radiation produced in the TRT [92]. Applying a discriminant requirement enhances the selection of prompt electrons produced in W-, Z- or Higgs-boson decays and leptonic τ-lepton decays, while effectively rejecting photon conversions and hadrons misidentified as electrons. All selected electrons must meet the *Tight* selection criteria as defined in Ref. [92]. ig Muon candidates are reconstructed by combining tracks in the MS with tracks in the ID [93]. The tracks must be in the range of $|\eta| < 2.5$ and have $p_T > 10$ GeV. Similarly to electrons, likelihood-based identification criteria are applied [93]. Muons are required to satisfy the *Medium* selection defined in Ref. [93].

The tracks matched to electron and muon candidates must point to the primary vertex, which is ensured by requirements imposed on the transverse impact-parameter significance, $|d_0/\sigma(d_0)| < 5.0$ for electrons and $|d_0/\sigma(d_0)| < 3.0$ for muons, and on the longitudinal impact parameter, z_0, for which $|z_0 \sin(\theta)| < 0.5$ mm has to be satisfied for both lepton flavours. Non-prompt electrons and muons are leptons produced by mechanisms other than W-, Z- or Higgs-boson decays and leptonic τ-lepton decays. They are effectively rejected by using multivariate discriminants computed with boosted decision trees (BDT), which integrate electromagnetic shower shapes and track information from the ID [94]. Separate BDTs are trained for electrons in the barrel ($|\eta| < 1.37$) and endcap ($|\eta| > 1.37$) regions, while a single BDT is employed for muons. The efficiency for correctly identifying prompt muons (electrons) ranges from approximately 80 % to 95 % (65 % to 90 %) for p_T values between 20 GeV and 45 GeV, with the efficiency plateauing beyond 45 GeV. Overall, the BDTs achieve a 71 % (90 %) rejection rate for muons (electrons) from B-hadron decay. Additionally, the contribution of electrons reconstructed with an incorrectly reconstructed charge is significantly reduced by using an additional BDT [91], which consolidates information about an electron candidate's charge, impact parameter, energy, and ID track into a single discriminant. This achieves a 95 % efficiency for electrons with a correct charge assignment while rejecting 94 % of charge-misidentified electrons.

Scale factors are used to correct the efficiencies in simulation to match the efficiencies measured for the electron [48] and muon [49] triggers, and the reconstruction, identification and isolation criteria [91,93].

Jets are reconstructed from particle-flow objects [95] with the anti-k_t clustering algorithm [96,97] using a radius parameter of 0.4. This algorithm matches topological energy clusters [98] in the calorimeters to selected tracks in the ID. The energy of tracks is subtracted from the matched topological clusters and both the tracks and the energy-subtracted topological clusters are used as input to the jet reconstruction. The jet energy is calibrated by applying several simulation-based corrections and techniques correcting for differences between simulation and data [99]. The jets must satisfy $p_T > 20$ GeV and $|\eta| < 2.5$.

To suppress jets originating from pile-up collisions, several track-based variables are combined with a multivariate technique to form the jet-vertex-tagger (JVT) discriminant [100]. Jets with $p_T < 60$ GeV and $|\eta| < 2.4$ are required to have a JVT discriminant above 0.5, which corresponds to an efficiency of 92% for jets from the primary vertex, while 98 % of jets from pile-up events are rejected.

Identification of jets containing B hadrons (b-tagging) is performed with the DL1r algorithm, which uses a deep feed-forward neural network with several b-tagging algorithms as inputs [101]. These input algorithms exploit the impact parameters of charged-particle tracks, the properties of reconstructed secondary vertices and the topology of b- and c-hadron decays inside the jets. The requirement on the DL1r discriminant is chosen such that the average tagging efficiency of b-jets from simulated dileptonic $t\bar{t}$ events is 70 %. The corresponding p_T-dependent c-jet rejection factors range from 10 to 14, while those for light-flavour jets range from 100 to 900. Differences between the b-tagging efficiency between collision data and simulation are corrected using simulation-to-data scale factors derived from $t\bar{t}$ events. The scale factors depend on the p_T of the jets and are consistent with unity within the uncertainties. The obtained scale factors depend on the parton-shower generator used to produce the $t\bar{t}$ samples. When using samples produced with a different parton-shower generator, for example SHERPA, to model W+jets events, or when evaluating systematic uncertainties with a setup based on HERWIG, additional correction factors called MC-to-MC scale factors are applied. Since the DL1r algorithm uses measurements from the ID, the identification of b-jets is limited to the region with $|\eta| < 2.5$.

With the above definitions of physical objects it is possible for ambiguities to arise, since all objects are reconstructed independently of each other. To avoid the double-counting of candidates which satisfy more than one selection criterion, a procedure called *overlap removal* is applied. Reconstructed physical objects are removed in the following order: electrons sharing an ID track with a muon; jets within $\Delta R = 0.2$ of an electron, thereby avoiding double-counting electron energy deposits as jets; electrons within $\Delta R = 0.4$ of a remaining jet, for reducing the impact of non-prompt electrons; jets within $\Delta R = 0.2$ of a muon if they have two or fewer matched tracks; muons within $\Delta R = 0.4$ of a remaining jet, reducing the rate of non-prompt muons.

The missing transverse momentum $\vec{p}_T^{\,\text{miss}}$ is reconstructed as the negative vector sum of the transverse momentum of the reconstructed leptons and jets, and ID tracks that point to the primary vertex but are not matched to a reconstructed object [102]. The magnitude of $\vec{p}_T^{\,\text{miss}}$ is denoted by E_T^{miss}.

Events selected by this analysis are required to have at least one charged lepton with $p_T > 28$ GeV. Additional leptons must satisfy a p_T threshold of 10 GeV. In the 2ℓSS final state, exactly two leptons of the same charge are required, while in the 3ℓ final state the requirement is three leptons with a total charge of $\pm 1e$. The lepton with the highest p_T is referred to as ℓ_0. The lepton with the second highest p_T is denoted by ℓ_1 and, for events in the 3ℓ final state, the lepton with the lowest p_T is called ℓ_2. In the 3ℓ final state an alternative labelling of leptons is introduced based on their charge. In any given 3ℓ event two leptons have the same charge while the remaining lepton has an opposite charge. The latter is labelled ℓ_{OS}, the former $\ell_{\text{SS},0}$ and $\ell_{\text{SS},1}$ with the number indexing the lepton in order of decreasing p_T. In addition to the requirements on leptons, considered events need to contain at least one jet, at least one of which is b-tagged. A summary of the preselection applied to events is given in Table 1.

Table 1 Overview of the preselections applied in the analysis. These selections ensure jet and b-tag multiplicities, lepton momenta, and define the 2ℓSS and 3ℓ final states

Preselection		
N_{jets}	≥ 1	
$N_{b\text{-tags}}$	≥ 1	
$p_T(\text{jet})$	≥ 20 GeV	
$p_T(\ell)$	≥ 10 GeV	
$p_T(\ell_0)$	≥ 28 GeV	
	2ℓSS	3ℓ
N_ℓ	$= 2$	$= 3$
$\sum q(\ell_i)$	$= \pm 2e$	$= \pm 1e$

5 Background estimate

Several SM background processes are present in the signal regions. Many of these processes can be simulated by using MC, others require dedicated treatment. Particularly the modelling of background from non-prompt leptons must be validated and potentially corrected. This background is separated into various categories, encompassing electrons from prompt muon decay, electrons from photon conversion and leptons produced in a hadronic jet, where further differentiation depending on the jet primary particle are made. Jets initiated by b-quarks, by other quarks or gluons, and by τ-leptons are considered, where leptons from b-jets are further categorised into electrons and muons. The production of these non-prompt leptons is fully accounted for by the simulated SM samples. By navigating through the generator-level parent particles of a given lepton, this lepton is sorted into one of the previously discussed lepton-origin categories. Based on this, several MC templates are defined containing the events corresponding to exactly one non-prompt lepton-origin category. The remaining events include only prompt leptons and remain in their original SM background template. All background estimate methods discussed in the following are based on these prompt and non-prompt MC templates. Several of the processes discussed in this section are assigned unconstrained (*free-floating*) normalisation factors in the final maximum-likelihood fit. These normalisation factors are constrained in the fit through dedicated control regions, enriched in the respective processes. It should be noted that the QCD multijet background is negligible in this analysis, owing to the rarity of the considered 2ℓSS and 3ℓ final states.

5.1 Non-prompt lepton background

The primary source of non-prompt lepton background is the decay of B-hadrons. These particular objects are also referred to as *heavy-flavour (HF) decay leptons*. They mainly consist of events from $t\bar{t}$ production (75 %), while the remaining events are split evenly between V+jets and single-top-quark production. The *Template fit method* [103] is used to determine the rates of HF-decay electrons and HF-decay muons. It assumes the kinematic distributions of the corresponding processes are well described, while their normalisation may require corrections. The normalisation factors are determined in the final maximum-likelihood fit, which is performed simultaneously in the 2ℓSS and the 3ℓ final states.

As explained above, various other non-prompt lepton processes contribute to this analysis. Their contribution is minor compared with the HF-decay e and HF-decay μ processes. In the fit, they are assigned normalisation uncertainties of 50 %.

5.2 Charge misidentification

In addition to the processes discussed above, the phase space of the 2ℓSS final state is contaminated by events containing prompt electrons with a misidentified charge. The modelling of such objects is strongly dependent on their p_{T}. Furthermore, electrons can radiate hard bremsstrahlung through interaction with the detector material, which then undergoes asymmetric conversion into an electron-positron-pair. The probability for electrons to interact with the detector material increases with the absolute value of the pseudorapidity $|\eta|$. Both, charge misidentified electrons and electrons from bremsstrahlung, are considered as a single background labelled Q-misID, which is modelled using a data-driven method based on the one described in Ref. [103]. To avoid double-counting Q-misID events, MC events featuring an electron from any of the considered processes are identified using generator level information and are excluded from the analysis.

The data-driven Q-misID background estimate is performed as follows. Events containing two isolated electrons with an invariant mass around the mass of the Z boson are considered, where the electrons can have either an opposite-sign charge (OS) or the same-sign charge (SS). To maintain orthogonality to the kinematic regions of the main analysis, there is an $N_{b\text{-tags}} = 0$ requirement. The m_{ee} distribution in the vicinity of $m_Z = 91.19$ GeV [104] is fitted separately for OS and SS events using Breit–Wigner functions. The fitted centres m_{peak} and widths σ are used to define the Z-windows up to 4σ from the centres, and sideband regions $[m_{\text{peak}} - 8\sigma,\ m_{\text{peak}} - 4\sigma] \cup [m_{\text{peak}} + 4\sigma,\ m_{\text{peak}} + 8\sigma]$. The assumption is made, that events in the Z-window consist of prompt $Z \to e^+e^-$ events and a uniform background. The uniform background is estimated from the average yield in the sideband regions, separately for the OS and SS events, and are subtracted in the Z-window.

Q-misID efficiencies are extracted in bins of $|\eta|$ and p_{T}, corresponding to the probability for an electron in a given bin to be charge-misidentified. These relate the number of background-corrected SS and OS events in the Z-window and can thus be determined from the obtained event yields. The Q-misID events in a given region of the 2ℓSS phase space are then modelled by selecting data events with two opposite-charge leptons while keeping all other selection requirements of the region unmodified, and weighting these data events with the obtained efficiencies. It should be noted that due to the high accuracy of the ATLAS muon spectrometer, the muon charge misidentification is negligible in this analysis.

5.3 Prompt-lepton background

The $t\bar{t}W$ and $t\bar{t}Z$ processes represent the primary background sources from prompt leptons. While measurements of $t\bar{t}W$ production deviate from theoretical predictions by 1.4σ [105], measurements of $t\bar{t}Z$ production align closely with SM expectations. However, it's worth noting that the latest measurement of $t\bar{t}Z$ production is conducted in regions with a jet multiplicity of at least four [106]. This analysis extends to kinematic regions with fewer jets, which may not be adequately modelled by MC simulations. To address this discrepancy, the normalisation of $t\bar{t}W$ and $t\bar{t}Z$ production is left unconstrained in the maximum-likelihood fit. Similar to the non-prompt templates, a single normalisation factor is applied per process across the entire phase space, encompassing both the 2ℓSS and the 3ℓ final states.

The 2ℓSS and 3ℓ event selection requires at least one b-jet in the final state. In the VV MC samples used in the analysis these quarks must be produced by the shower generator. To account for potential mismodeling of the jet flavour composition, the VV background is split according to the number of leptons (2ℓ, 3ℓ, 4ℓ) and the generator-level flavour of additional jets. If the event contains at least one jet originating from the decay of either a bottom or a charm hadron is sorted into the b/c category. If it exclusively contains jets from light quarks or τ-leptons it is included in the l/τ category. The $VV3\ell + b/c$ template has the largest contribution in the phase space and its normalisation is left free-floating in the maximum-likelihood fit. The remaining templates ($VV2\ell + l/\tau$, $VV2\ell + b/c$, $VV3\ell + l/\tau$, $VV4\ell + b/c$ and $VV4\ell + l/\tau$) are assigned individual 50% normalisation uncertainties. These minor VV templates, alongside the minor non-prompt templates and several SM processes are combined into one *Others* category in the following. The rates of the majority of processes in this category are similar in the analysis phase space.

6 Event categorisation

Preselected events are categorised into several kinematic regions. These regions are either enriched in signal events, to improve the overall sensitivity of the analysis, or in certain background events, to control the normalisation of specific processes.

6.1 Definition of signal regions

After event preselection, four signal regions are defined in this analysis, two in the 2ℓSS final state and two in the 3ℓ final state. One region per final state is enriched in the $t \rightarrow Hq$ decay signal. These two regions are referred to as SR2ℓDec and SR3ℓDec. The other two signal regions contain a larger fraction of $gq \rightarrow tH$ production signal and are correspondingly named SR2ℓProd and SR3ℓProd.

Both the 2ℓSS signal regions require exactly one b-tagged jet. Given that a higher jet multiplicity is anticipated for the decay signal compared to the production signal, the SR2ℓDec is defined by requiring $N_{\text{jets}} \geq 4$. A cut of $N_{\text{jets}} \leq 3$ in the SR2ℓProd ensures the orthogonality of the two regions. To minimise the contribution from HF-decay leptons, the p_{T} of ℓ_1 is required to be larger than 12 GeV in the SR2ℓDec and 16 GeV in the SR2ℓProd. As Q-misID events strongly contaminate the 2ℓSS final state, a cut on the invariant mass of the two leptons is imposed in both the regions. If both the leptons are identified as electrons, $|m(e, e) - m_Z| \geq 10$ GeV must be satisfied.

Similar to the 2ℓSS final state, both the signal regions in the 3ℓ final state require exactly one b-tagged jet. The primary difference between the two regions is again the jet multiplicity. Overall fewer jets are expected for the signal in the 3ℓ final state. Hence, $N_{\text{jets}} \geq 3$ is required for the SR3ℓDec, while $N_{\text{jets}} \leq 2$ is required for the SR3ℓProd. To reduce the HF-decay contribution, the definition of both the regions require cuts on the p_{T} of the two sub-leading leptons: $p_{\text{T}}(\ell_1) \geq 20$ GeV and $p_{\text{T}}(\ell_2) \geq 16$ GeV. As the Q-misID process does not contribute to the 3ℓ final state, no further restrictions to the event selection are made. The definition of all signal regions is summarised in Table 2, while their respective composition in terms of background processes is shown in Fig. 3.

Table 2 Overview of the event selections applied to define the signal regions of the analysis

	SR2ℓDec	SR2ℓProd	SR3ℓDec	SR3ℓProd
N_{jets}	≥ 4	≤ 3	≥ 3	≤ 2
$N_{b\text{-tags}}$	$= 1$	$= 1$	$= 1$	$= 1$
$p_{\text{T}}(\ell_1)$	≥ 12 GeV	≥ 16 GeV	≥ 20 GeV	≥ 20 GeV
$p_{\text{T}}(\ell_2)$	–	–	≥ 16 GeV	≥ 16 GeV
$\|m(e, e) - m_Z\|$	≥ 10 GeV	≥ 10 GeV	–	–

6.2 Control regions for non-prompt-lepton backgrounds

The template-fit method assumes that corrective normalisation factors are applicable independently of the considered final state. To ensure this assumption is correct, two control regions are defined for each of the HF-decay processes: one in the 2ℓSS final state (CR2ℓHFe and CR2ℓHFμ) and one in the 3ℓ final state (CR3ℓHFe and CR3ℓHFμ).

Overall, the average p_{T} of leptons originating from a HF decay is smaller than that of prompt leptons. Thus, all HF-decay control regions are defined by imposing upper boundaries on the p_{T} of the lowest-p_{T} lepton. The boundaries are chosen such that an orthogonality to the signal regions of the respective final state is ensured. Requiring the flavour of the lowest-p_{T} lepton to be either e or μ ensures that the region is exclusively enriched in HF-decay e or HF-decay μ events. In the CR2ℓHFe and the CR2ℓHFμ the p_{T}-leading lepton is required to be a muon, reducing the contamination of Q-misID events. Due to high statistical uncertainty, only the event yields of the CR2ℓHFe and the CR2ℓHFμ enter the maximum-likelihood fit. For the CR3ℓHFe and the CR3ℓHFμ, the distributions of the $p_{\text{T}}(\ell_1)$ variable are included. A summary of the definition of all non-prompt control regions can be found in Table 3.

6.3 Control regions for $t\bar{t}W$ and $t\bar{t}Z$ backgrounds

Three additional control regions are defined to determine the normalisation of the background from $t\bar{t}W$ and $t\bar{t}Z$ production. Studies on various kinematic distributions in the signal regions of the 2ℓSS final state show a strong similarity between the two processes. Therefore, in this final state only one control region (denoted CR2$\ell t\bar{t}V$) is defined to constrain the sum of $t\bar{t}W$ and $t\bar{t}Z$. This region requires at least four jets, exactly two of which are b-tagged, because both the top quarks in the process are expected to produce a b-quark. An additional requirement of $p_{\text{T}}(\ell_1) \geq 18$ GeV further increases the purity of the region in $t\bar{t}V$ events by

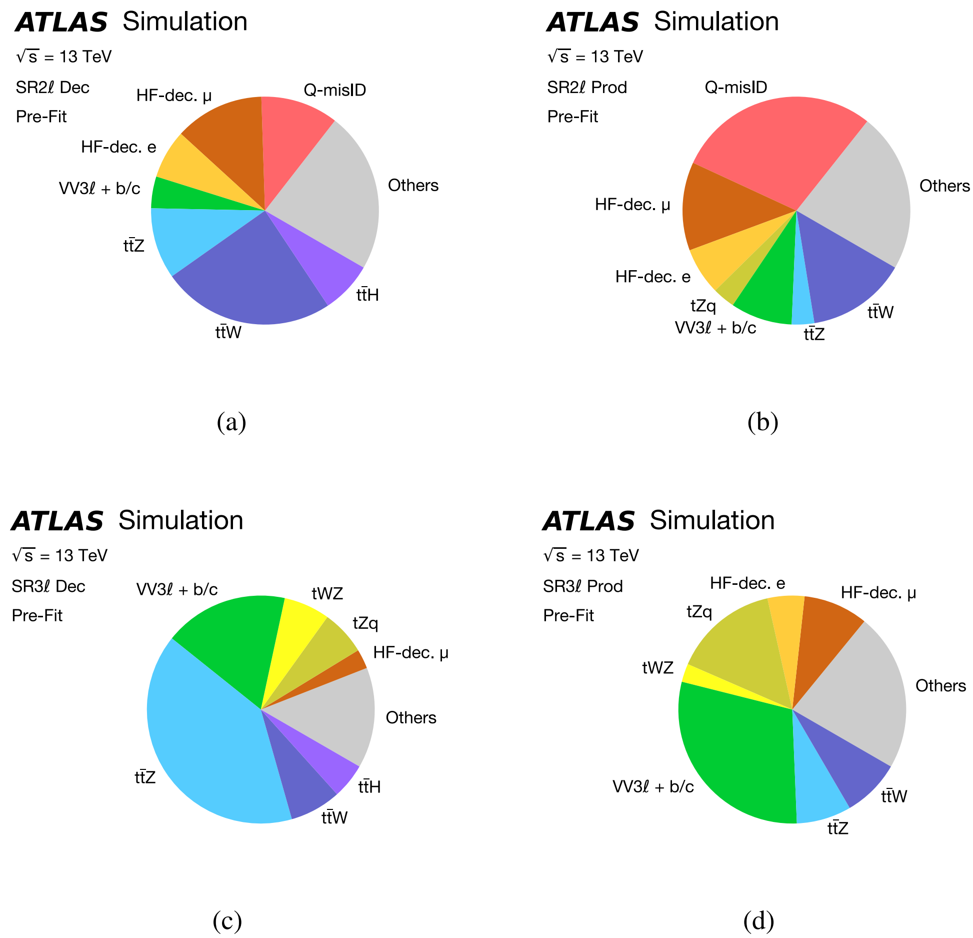

Fig. 3 The composition of background processes in the **a** SR2ℓDec, **b** SR2ℓProd, **c** SR3ℓDec and **d** SR3ℓProd. The *Others* template contains various minor processes, which individually only have small contributions. No correction to the normalisation of any process is applied

reducing contamination from HF-decay events. The $p_{\mathrm{T}}(\ell_1)$ variable is used as input for the maximum-likelihood fit.

In the 3ℓ final state, distinct shape differences between $t\bar{t}W$ and $t\bar{t}Z$ production are observed due to the absence of any requirement on the invariant mass of lepton pairs. Therefore, two control regions, CR3$\ell t\bar{t}W$ and CR3$\ell t\bar{t}Z$, are defined. Both the regions require at least two jets, two of which are b-tagged. Events are then assigned to the CR3$\ell t\bar{t}Z$ if at least one pair of leptons with the same flavour and opposite charge can be found satisfying $|m(\ell^+, \ell^-) - m_Z| < 10$ GeV. In cases where this criterion is not met, events are assigned to CR3$\ell t\bar{t}W$. In both the control regions, the transverse momentum of the p_{T}-leading b-tagged jet $p_{\mathrm{T}}(b\text{-jet}_0)$ is used as input for the maximum-likelihood fit. A summary of the definition of all $t\bar{t}V$ control regions can be found in Table 4.

Table 3 Overview of the event selections applied to define the non-prompt lepton background control regions of the analysis

	CR2ℓHFe	CR2ℓHFμ	CR3ℓHFe	CR3ℓHFμ
N_{jets}	≤ 3	≤ 3	≥ 1	≥ 1
$N_{b\text{-tags}}$	≥ 1	≥ 1	$= 1$	$= 1$
ℓ_0 flavour	μ	μ	–	–
ℓ_1 flavour	e	μ	–	–
$p_{\mathrm{T}}(\ell_1)$	< 16 GeV	< 16 GeV	≥ 20 GeV	≥ 20 GeV
ℓ_2 flavour	–	–	e	μ
$p_{\mathrm{T}}(\ell_2)$	–	–	< 16 GeV	< 16 GeV

7 Separation of signal and background

Artificial neural networks (NNs) are used to separate signal and background in all four signal regions combining several kinematic variables into optimised NN discriminants. In addition to variables derived from the reconstructed objects the NNs build on a diverse range of reconstructed kinematic variables. Detailed information regarding the reconstruction algorithms is provided in Sect. 7.1, while a comprehensive description of the NN training process can be found in Sect. 7.2.

7.1 Event reconstruction in signal regions

The reconstruction algorithms employed are described below. In tHq FCNC interactions, multiple decay modes of the Higgs boson that contribute to the 2ℓSS and 3ℓ final states are

Table 4 Overview of the event selections applied to define the $t\bar{t}W$ and $t\bar{t}Z$ control regions of the analysis

	CR2$\ell t\bar{t}V$	CR3$\ell t\bar{t}W$	CR3$\ell t\bar{t}Z$
N_{jets}	≥ 4	≥ 2	≥ 2
$N_{b\text{-tags}}$	$= 2$	$= 2$	$= 2$
ℓ_0 flavour	μ	–	–
$p_{\text{T}}(\ell_1)$	≥ 18 GeV	≥ 20 GeV	≥ 20 GeV
$p_{\text{T}}(\ell_2)$	–	≥ 16 GeV	≥ 16 GeV
$\lvert m(\ell^+, \ell^-) - m_Z \rvert$	–	≥ 10 GeV	< 10 GeV

considered. However, the $H \rightarrow WW^*$ decay mode has by far the largest contribution with $\geq 75\,\%$ in all signal regions. Thus, all reconstruction efforts presented here focus on this specific Higgs-boson decay mode. Most algorithms are customised to fit one of the two considered final states. The relevant final states for each algorithm are given in parentheses.

Recursive jigsaw reconstruction (2ℓSS **and** 3ℓ)
The Recursive Jigsaw Reconstruction (RJR) technique [107] is a method for resolving combinatorial and kinematic ambiguities which arise in hadron collider events. RJR relies on decay trees which describe the topologies of interest, and relates the reference frames of the intermediate particles in the decay. Lepton and jet assignment, along with the splitting of $E_{\text{T}}^{\text{miss}}$, is governed by a set of jigsaw rules which rely on known properties of the decay tree. For instance the top-quark and Higgs-boson masses can be used to constrain the assignment of the jets, or the W-boson mass can be used to facilitate $E_{\text{T}}^{\text{miss}}$ splitting and matching to leptons.

This process leads to the computation of four-vectors of the reconstructed intermediate states, accessible in any of the frames defined in the decay tree. For each of the four topologies ($2\ell 1b2j$, $2\ell 1b3j$, $3\ell 1b0j$, $3\ell 1b1j$, where b refers to $N_{b\text{-jets}}$ and j to N_{jets}) there are different intermediate states, split by production versus decay and again by final state. The particles that are reconstructed for each individual region are listed in Table 5. These include W and Higgs bosons, and top quarks. Figure 4 depicts the probability densities of two RJR reconstructed variables for the tHu signal and the combination of all background processes, showing clear shape differences between the two.

Neutrino independent combinatorics estimator (3ℓ) The considered decay scenario of a signal event in the 3ℓ final state involves one top quark decaying into a b-quark, a lepton and a neutrino, while the Higgs-boson decay is expected to yield two leptons and two neutrinos. Studies of the MC signal samples show that on average the two leptons from the Higgs-boson decay have the smallest angular separation out of any lepton pair in the event. Based on this information, the two leptons with the smallest angular separation ΔR are labelled $\ell_{H,0}$ and $\ell_{H,1}$, ordered by their transverse momentum. The remaining lepton is labelled ℓ_t, while the b-tagged jet is denoted b_t. Various kinematic parameters are calculated for these objects, two of which are shown as examples in Fig. 5 for the full tHu signal and the combination of all background processes, demonstrating their high separation power. However, these parameters are discarded, if the angular separation of b_t from either $\ell_{H,i}$ is smaller than the separation from ℓ_t. Conversely, when the angular separation of b_t from ℓ_t is found to be smaller than from any other lepton, and further, when $\ell_{H,0}$ and $\ell_{H,1}$ have opposite charges the *Neutrino independent combinatorics estimator* reconstruction (NICE Reco) condition is defined as satisfied. In this scenario, the calculated kinematic parameters have a particularly high separation power between signal and background processes. This information is provided as additional input to the NNs.

7.2 Training of feed-forward neural networks

The NNs are implemented using the NeuroBayes package [108,109], which combines a three-layer feed-forward NN with a complex and robust preprocessing of the input variables before they are presented to the NN. The preprocessing produces a ranking of the input variables based on an algorithm employing the total correlation of a set of variables to the target function which assumes the value 1 for signal and 0 for background events. The input variable selection is performed once per signal region.

The selected variables of all signal regions are listed in Tables 11, 12, 13, 14. Overall, invariant masses of reconstructed objects, including RJR objects, compose the largest fraction. The most significant variables in both the 3ℓ signal regions are the invariant mass of the opposite charge and either of the two same charge leptons $m(\ell_{\text{OS}}, \ell_{\text{SS},0})$ and $m(\ell_{\text{OS}}, \ell_{\text{SS},1})$. In the SR2$\ell$Prod, the invariant mass of the subleading-p_{T} lepton and the RJR Higgs boson $m(\ell_1, H)$ is the most important variable, followed by the number of jets N_{jets}. The most significant variable of the SR2ℓDec is the scalar p_{T} sum of all jets H_T(jets), a quantity that is also highly ranked in other trainings. The invariant mass of the leading-p_{T} lepton and the event's b-jet $m(\ell_0, b\text{-jet})$ is the second-highest ranked in the training.

Table 5 Particles from the tHq processes which are reconstructed using the Recursive Jigsaw Reconstruction (RJR) in the respective signal regions

Regions	Particle name	Description
	t_{SM}	The top quark decaying via $t \to Wb$
SR2ℓDec/	W_t	The W boson from the SM top-quark decay
SR3ℓDec	t_{FCNC}	The top quark decaying via $t \to Hq$
	H	The Higgs boson originating from th FCNC top-quark decay
SR2ℓDec	W_{had}	The hadronically decaying W boson from the $H \to WW^*$ decay
SR2ℓProd/	t_{SM}	The top quark produced in the $gq \to Ht$ process
SR3ℓProd	W_t	The W boson from the top-quark decay
	H	The Higgs boson produced in the $gq \to Ht$ process

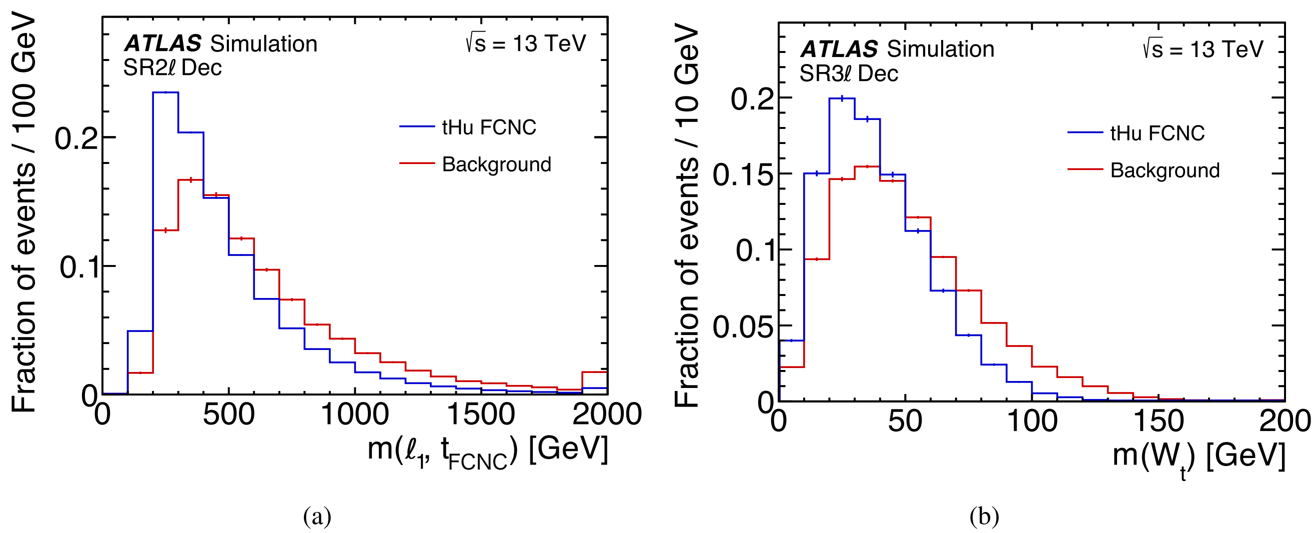

Fig. 4 Probability densities of **a** $m(\ell_1, t_{FCNC})$ in the SR2ℓDec and **b** $m(W_t)$ in the SR3ℓDec for the tHu signal process and the sum of all background processes. The vertical lines on bins represent MC-statistical uncertainties. The last bin includes the overflow

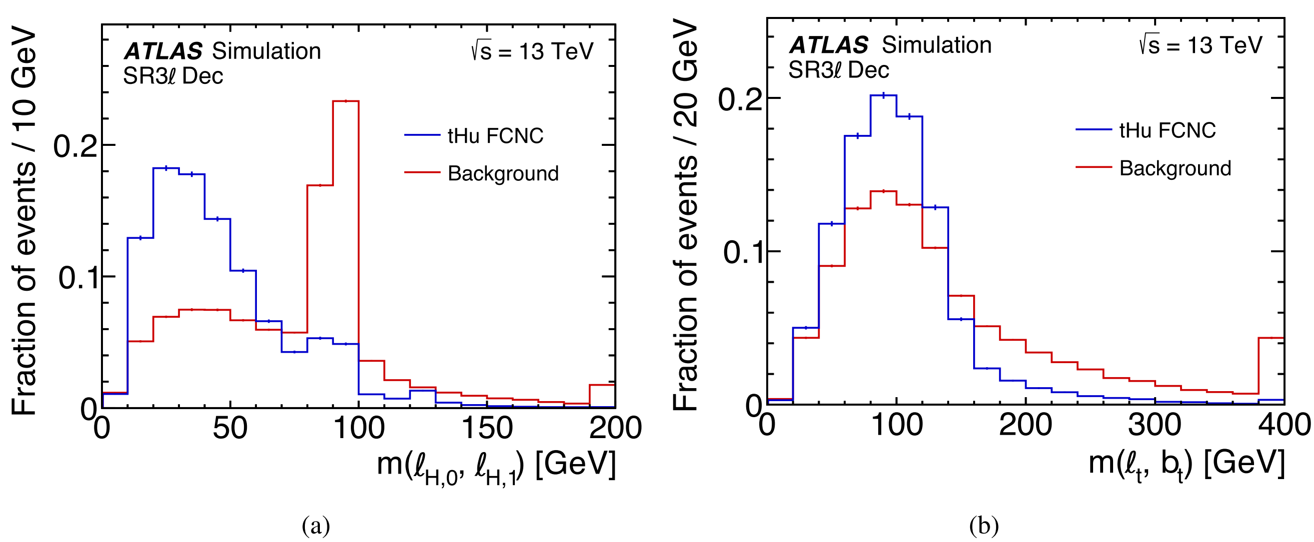

Fig. 5 Probability densities of **a** $m(\ell_{H,0}, \ell_{H,1})$ and **b** $m(\ell_t, b_t)$ in the SR3ℓDec for the tHu signal process and the sum of all background processes. The vertical lines on bins represent MC-statistical uncertainties. The last bin includes the overflow

Individual NNs are created for both the signal processes and every signal region, summing up to a total of eight NN architectures. The training uses the data-driven Q-misID estimate together with unmodified MC templates as input, before any corrections to their normalisation by the maximum-likelihood fit. Cross-training is employed to prevent overfitting, where the signal and background MC events are split into half. The splitting is performed in a pseudo-random way based on the parity of the unique event identification number. For each half, a separate NN model is trained, which is then applied to the other half of MC events in the final analysis.

During the training process of all the NNs, the signal is trained against all considered backgrounds with a fraction of 50 % signal events and 50 % background events. The different background processes are weighted relative to each other according to their expected number of events. NeuroBayes uses Bayesian regularisation techniques for the training process to improve the generalisation performance and to avoid overfitting. The network infrastructure consists of one input node for each input variable, a single hidden layer, and one output node giving a continuous output in the interval $(-1, +1)$. The number of nodes in the hidden layer is optimised individually for each NN model. As a non-linear activation function NeuroBayes uses the symmetric sigmoid function. In the region close to zero, the sigmoid function has a linear response. The final discriminant D_{NN} is obtained by linearly scaling the output of the NNs to the interval (0, 1).

8 Systematic uncertainties

Several sources of systematic uncertainty affect the expected event yield from signal and background processes and the shape of the NN discriminants used in the maximum-likelihood fits. The systematic uncertainties are divided into two major categories. There are experimental uncertainties in the reconstruction of the four-momenta of the final-state objects: electrons, muons, jets, b-tagged jets, and $E_{\text{T}}^{\text{miss}}$ as a sign of a high-p_{T} neutrino. The second category of uncertainties is related to the modelling of scattering processes with event generators and of the interaction of particles with the detector. All uncertainties are propagated through the analysis and their effects on the expected event yields and discriminant distributions are accounted for by including corresponding nuisance parameters in the fit. In the following, the estimate of experimental and modelling uncertainties is explained in more detail.

8.1 Experimental uncertainties

The uncertainty in the integrated luminosity of the combined 2015–2018 data set is 0.83% and is based on a calibration of the luminosity scale using x–y beam-separation scans [46]. The luminosity uncertainty is applied to the expected signal and background event yields.

Scale factors are applied to simulated events to correct for reconstruction, identification, isolation and trigger performance differences between data and detector simulation for electrons and muons. These scale factors and their systematic uncertainties, and the lepton momentum scale and resolution, were assessed using $Z \rightarrow e^+e^-$ and $Z \rightarrow \mu^+\mu^-$ events in simulation and data [91,93].

The jet energy scale (JES) was calibrated using a combination of test-beam data, simulation and in situ techniques [99]. The JES is parameterised in bins of jet p_{T} and η. Its uncertainty is decomposed into a set of 30 uncorrelated components, of which 29 are non-zero in a given event depending on the type of simulation used. Sources of uncertainty contributing to the JES uncertainties include the η intercalibration of forward jets in the range of $0.8 < |\eta_{\text{det}}| < 4.5$ with those in the central barrel region ($|\eta_{\text{det}}| < 0.8$), pile-up modelling, jet flavour composition and response, differences between jets induced by b-quarks and those from gluons or light-quarks, single-particle response, detector modelling, non-closure, and effects of jets not fully contained in the calorimeter.

The uncertainty of the jet energy resolution (JER) is evaluated by smearing jet energies according to a Gaussian function [99]. Thirteen orthogonal components account for jet-p_{T} and η-dependent differences between simulation and data which were determined using dijet events and noise measurements based on random cones. The smearing is applied to simulated events if the resolution in data is larger than in MC simulation, and to pseudo-data when the resolution is larger in simulation than in collision data. The JER uncertainties are defined by comparing both types of smearing and thereby taking the anti-correlation between different components into account. The nominal data remains unchanged. The uncertainty in the efficiency to satisfy the JVT requirement for pile-up suppression was derived in $Z(\rightarrow \mu^+\mu^-)$+jets events and is also considered [100]. The uncertainty in $E_{\text{T}}^{\text{miss}}$ due to a possible miscalibration of its soft-track component was derived from data–simulation comparisons of the p_{T} balance between the hard and soft $E_{\text{T}}^{\text{miss}}$ components [102].

The b-tagging requirement made in the measurement has uncertainties in the b-tagging efficiency of true b-jets and in the mistagging rates of light-quark jets and c-jets. The b-tagging efficiency is measured in dileptonic $t\bar{t}$ events. Differences between data and detector simulation are corrected by p_{T}-dependent scale factors applied to simulated events. The uncertainty in the scale factors is decomposed into 45 orthogonal components [110]. The uncertainties are propagated through the analysis as weights. The set of uncertainties used covers both the 70 % working point used in this analysis, as well as other working points of the `DL1r` discriminant. The rate of mistagging c-jets as b-jets was measured in semileptonic $t\bar{t}$ events, where one of the W bosons decays into an electron or a muon and a neutrino and the other decays into a quark–antiquark pair [111]. This event sample allows to utilise the relatively large and known $W \to cs$ contribution. The mistagging rate of c-jets depends on the jet p_{T} and has a total uncertainty in the range of 317%. The uncertainties are decomposed into 20 orthogonal components. The misidentification rate of light-quark jets was evaluated based on the techniques described in Ref. [112]. The resulting calibration factors are in the range of about 1.5–3.0 with uncertainties up to 50 %. The uncertainties are decomposed into 20 independent eigenvectors.

To account for differences between simulation and data in the pile-up distribution, the pile-up profile in the simulation is corrected to match the one in data. The uncertainty in the correction factor is applied in the measurement as a variation of the event weight.

8.2 Modelling uncertainties

Normalisation uncertainties are applied to all processes, except for the ones whose normalisation is a free parameter of the maximum-likelihood fit, specifically for the HF-decay templates, for $t\bar{t}W$ and $t\bar{t}Z$ production, and for the largest VV template $VV3\ell + b/c$. Thus, no normalisation uncertainty is applied to $t\bar{t}$, single-top-quark, Z+jets and W+jets production, all of which exclusively contribute to non-prompt templates. Minor non-prompt templates are assigned 50 % normalisation uncertainties. The same is true for the minor VV templates and all rare processes discussed in Sect. 3.2. For tZq and tWZ production, a respective uncertainty of 30 % is assigned based on a previous ATLAS measurement of the processes [113]. Asymmetric uncertainties of $^{+7\%}_{-10\%}$ are assigned to $t\bar{t}H$ production, estimated by varying the renormalisation and factorisation scales, and the combined PDF+α_{s} uncertainties [28].

Uncertainties in modelling parton showers and hadronisation are assigned to the tHq signal samples, and the background originating from $t\bar{t}$, $t\bar{t}H$, $t\bar{t}Z$ and $t\bar{t}W$ production. For the signal and $t\bar{t}$, $t\bar{t}H$ and $t\bar{t}Z$ production the nominal samples are compared with alternative samples, for which the individual matrix element generators were interfaced to HERWIG[7.1.3] [114,115] (for $t\bar{t}$ production), HERWIG[7.0.4] (for $t\bar{t}H$ production) and HERWIG[7.2.1] (for $t\bar{t}Z$ production) instead of the respective versions of PYTHIA[8]. For $t\bar{t}W$ production, two alternative samples are generated. The matrix element of both the samples is generated with POWHEG-BOX[v2], which is interfaced to PYTHIA[8] for one sample and to HERWIG[7] for the other. The relative differences between the two samples is determined for all bins in the analysis and applied to the nominal SHERPA[2.2.10] $t\bar{t}W$ sample.

The impact of the generator choice for $t\bar{t}W$ is evaluated using an alternative sample and is applied as systematic uncertainties for both the normalisation and shape. This alternative sample is generated with up to one additional parton in the final state at NLO accuracy using MGNLO[2.9.3], with different parton multiplicities being merged using the FxFx NLO matrix-element and parton-shower merging prescription [89] with a merging scale of 30 GeV. The events are interfaced with PYTHIA[8.245] using the A14 set of tuned parameters and the NNPDF[2.3lo] PDF set to simulate hadronisation and showering. The uncertainty is split into three components: a shape uncertainty in each region, a region migration uncertainty and a global normalisation uncertainty.

Uncertainties related to the choice of the renormalisation scale μ_{r} and the factorisation scale μ_{f} for the matrix-element calculations are evaluated by varying the scales independently by factors of 2 and 0.5, separately for VV production and each of the top-quark production processes, including production with an additional boson and the two signal processes. The scale variations are implemented as generator weights in the nominal sample. The uncertainties are treated as uncorrelated across individual processes.

The uncertainty in matching the NLO matrix elements to the parton shower when generating $t\bar{t}$ events is evaluated by comparing the nominal samples of simulated events to samples with an alternative setting of the $p_{\mathrm{T}}^{\mathrm{hard}}$ parameter in the matching code, using one instead of the default setting of zero. This parameter regulates the definition of the vetoed region of the parton shower, which is needed to avoid overlap in the phase space filled by POWHEG and PYTHIA. This estimate of the uncertainty follows the description in Ref. [116]. The uncertainty in the choice of the h_{damp} parameter for the $t\bar{t}$ event generation is estimated by using an additional $t\bar{t}$ sample produced with the h_{damp} parameter set to $3m_t$, while keeping all other generator settings the same as used for the nominal sample of events.

Three uncertainties are defined for the modelling of the Q-misID template. The statistical uncertainty in the Q-misID efficiencies obtained from the likelihood fit is taken into account. An uncertainty in the selection of the Z-window is calculated by redefining the Z-window with 3σ and 5σ, where σ corresponds to the width of the fitted Breit–Wigner distribution. The width of the Z-window is varied and the efficiencies are determined again, with the symmetrised difference to the nominal values comprising the uncertainty, which is then propagated through the analysis. Finally, a non-closure uncertainty is implemented by applying the Q-misID estimation method to a $Z \to ee$ MC sample and comparing the resulting misidentification rates to the MC prediction. The symmetrised difference applied to the nominal Q-misID rates constitutes the uncertainty.

Uncertainties in the amount of initial-state radiation are defined for the top-quark production processes $t\bar{t}$, $t\bar{t}Z$ and $t\bar{t}H$. They are assessed by varying the eigentune `Var3c` of the A14 PYTHIA[8] tune consistent with the uncertainties of

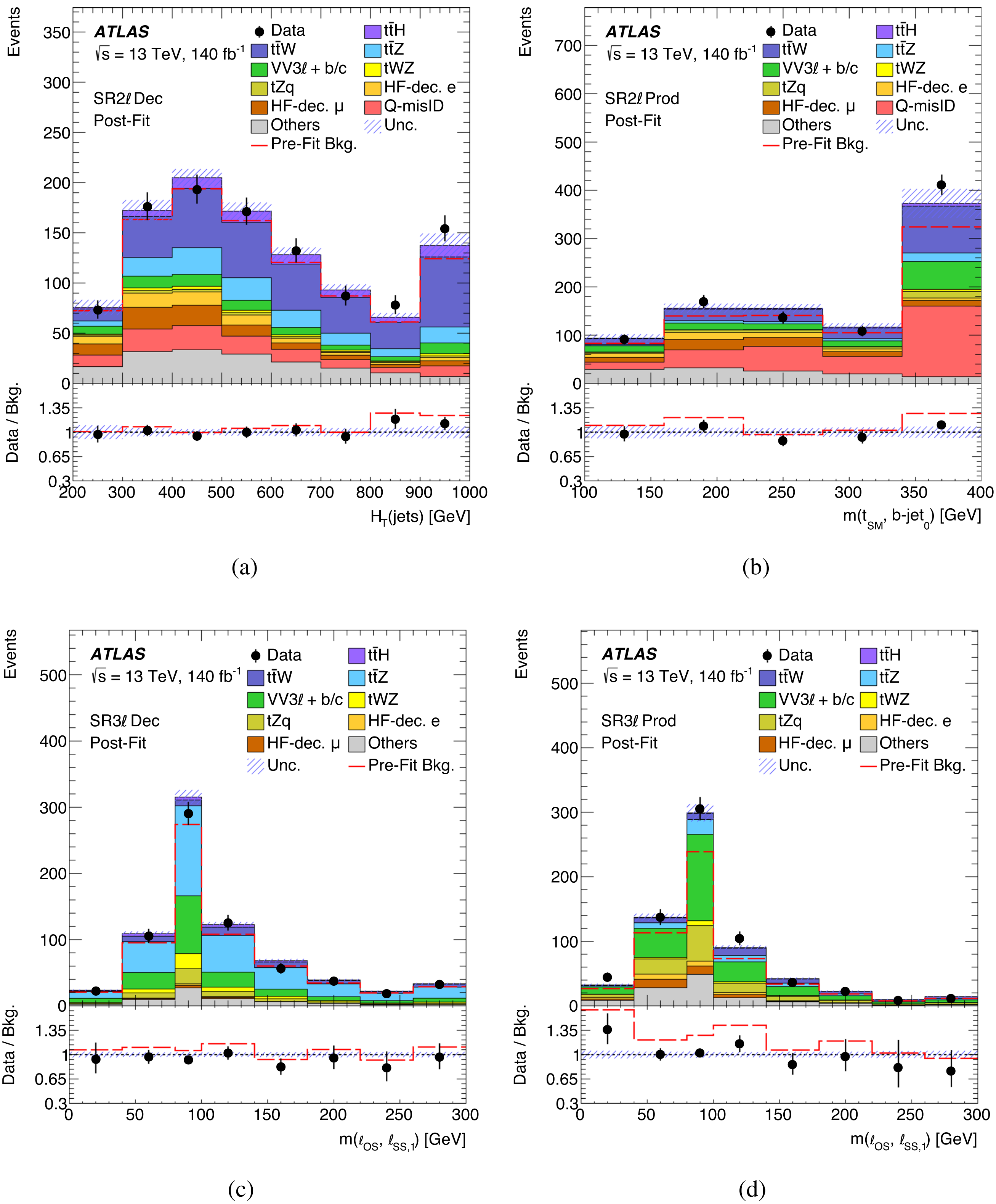

Fig. 6 Distributions of the most important NN input variable for the signal regions **a** SR2ℓDec, **b** SR2ℓProd, **c** SR3ℓDec and **d** SR3ℓProd. The corrections from a background-only fit are applied. Only events with $D_{\mathrm{NN}} < 0.5$ were used in the fit and in the plots. The first bin contains all events below its lower boundary, while the last bin contains all events falling above its upper boundary. The *Others* template contains various minor processes, which individually only have small contributions. The total statistical and systematic uncertainty is indicated by the hatched band. The dashed line depicts the sum of all background processes prior to the fit. The last bin includes the overflow

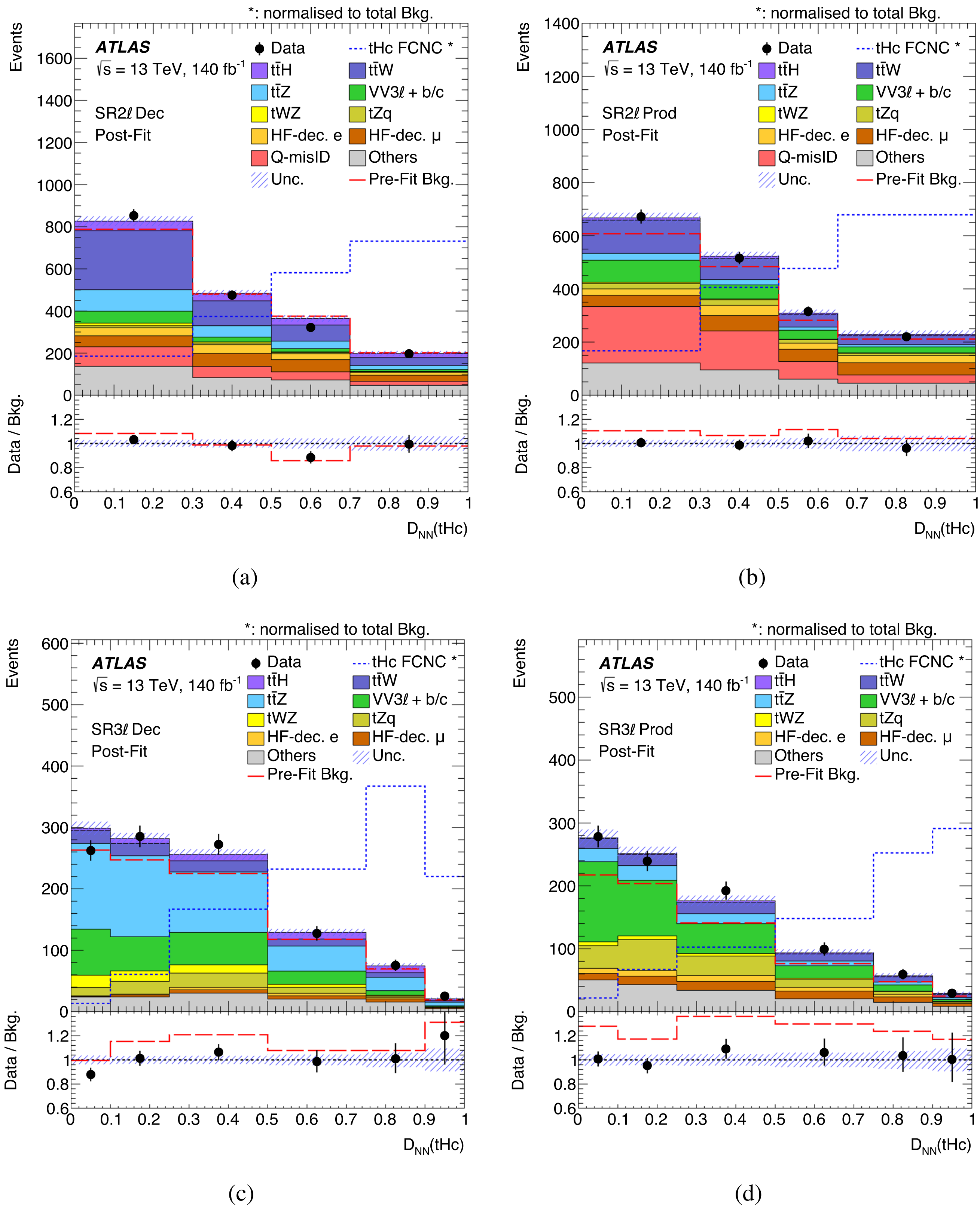

Fig. 7 The D_{NN} distributions in the **a** SR2ℓDec, **b** SR2ℓProd, **c** SR3ℓDec and **d** SR3ℓProd, obtained from the signal-plus-background fit to data in the tHc channel. The *Others* template contains various minor processes, which individually only have small contributions. The total statistical and systematic uncertainty is indicated by the hatched band. The dotted line represents the distribution of the signal, scaled to the number of background events. The dashed line depicts the sum of all background processes prior to the fit

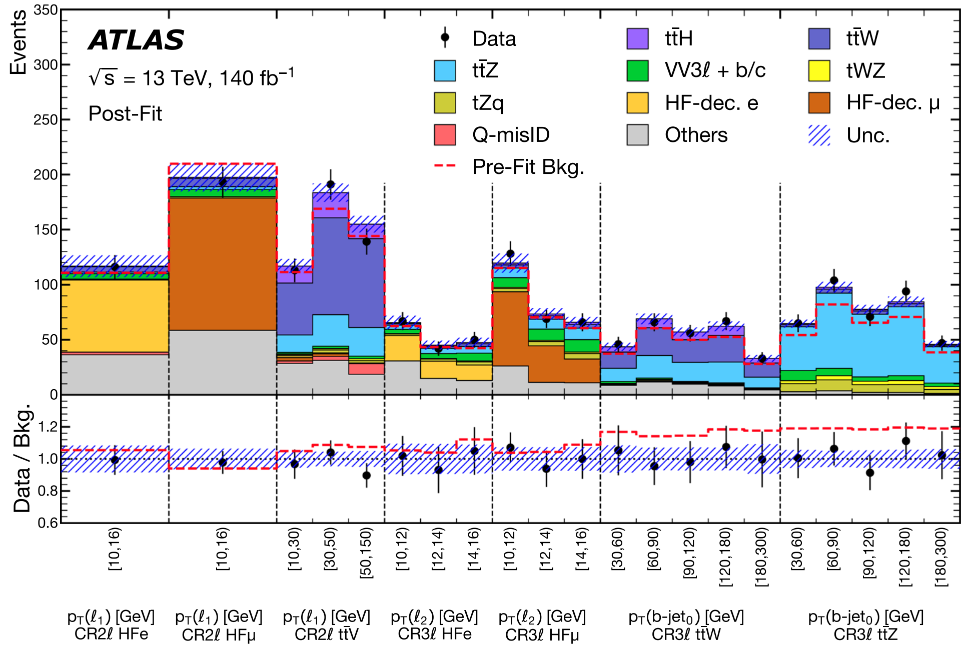

Fig. 8 Summary plot of the fitted distributions in all control regions obtained from the signal-plus-background fit to data in the tHc channel. The bin boundaries for each region are depicted by the parenthesised numbers. The *Others* template contains various minor processes, which individually only have small contributions. The total statistical and systematic uncertainty is indicated by the hatched band. The dashed line depicts the sum of all background processes prior to the fit

Table 6 The predicted and observed yields in all 2ℓSS regions of the analysis from the signal-plus-background fit to signal and control regions. The pre-fit predictions for the two signal components are presented also, scaled to a cross-section equivalent to a branching ratio $\mathcal{B}(t \rightarrow Hq) = 0.1\,\%$. The *Others* template contains various minor processes, which individually only have small contributions. The uncertainties in non-signal MC yields reflect the sum in quadrature of all post-fit systematic and statistical uncertainties. The row labelled *Post-fit BG* shows the sum of all above background (BG) processes with post-fit uncertainties, while the row labelled *Pre-fit BG* shows the total pre-fit background yield with the corresponding pre-fit uncertainties. Hyphens signify that the corresponding process does not contribute to the given region

Process	SR2ℓDec	SR2ℓProd	CR2ℓHFe	CR2ℓHFμ	CR$2\ell t\bar{t}V$
HF-decay e	122 ± 27	113 ± 25	66 ± 13	–	2.9 ± 0.9
HF-decay μ	201 ± 36	192 ± 35	0.1 ± 0.02	120 ± 22	5.6 ± 1.2
Q-misID	204 ± 16	457 ± 35	2.4 ± 0.2	–	15.5 ± 1.4
$t\bar{t}H$	132 ± 20	27 ± 5	0.6 ± 0.1	1.0 ± 0.2	51 ± 8
$t\bar{t}W$	512 ± 61	285 ± 42	4.8 ± 0.9	7.5 ± 1.4	216 ± 24
$t\bar{t}Z$	210 ± 21	66 ± 9	1.5 ± 0.2	2.4 ± 0.4	70 ± 6
VV 3ℓ+b/c	104 ± 20	192 ± 32	4.7 ± 1.0	6.6 ± 1.4	6.0 ± 1.2
tWZ	23 ± 7	12 ± 4	0.11 ± 0.04	0.17 ± 0.06	3.6 ± 1.1
tZq	26 ± 8	63 ± 18	0.7 ± 0.2	1.1 ± 0.3	5.8 ± 1.7
Others	340 ± 64	322 ± 46	36 ± 8	59 ± 20	79 ± 14
Pre-fit BG	1845 ± 91	1585 ± 70	111 ± 11	210 ± 32	424 ± 22
Post-fit BG	1874 ± 38	1729 ± 36	117 ± 10	198 ± 12	455 ± 17
$t\bar{t}(t \rightarrow Hu)$	207 ± 22	181 ± 10	3.4 ± 0.3	5.4 ± 0.7	6.8 ± 0.6
$ug \rightarrow Ht$	31 ± 4	68 ± 2	1.2 ± 0.1	2.1 ± 0.2	1.1 ± 0.1
$t\bar{t}(t \rightarrow Hc)$	196 ± 22	180 ± 10	3.5 ± 0.4	5.9 ± 0.7	13.4 ± 1.5
$cg \rightarrow Ht$	5 ± 1	11 ± 1	0.2 ± 0.1	0.4 ± 0.1	0.2 ± 0.1
Data	1847	1723	116	193	443

Table 7 The predicted and observed yields in all 3ℓ regions of the analysis from the signal-plus-background fit to signal and control regions. The pre-fit predictions for the two signal components are presented as well, scaled to a cross-section equivalent to a branching ratio $\mathcal{B}(t \to Hq) = 0.1\,\%$. The *Others* template contains various minor processes, which individually only have small contributions. The uncertainties in non-signal MC yields reflect the sum in quadrature of all post-fit systematic and statistical uncertainties. The row labelled *Post-fit BG* shows the sum of all above background (BG) processes with post-fit uncertainties, while the row labelled *Pre-fit BG* shows the total pre-fit background yield with the corresponding pre-fit uncertainties. Hyphens signify that the corresponding process does not contribute to the given region

Process	SR3ℓProd	SR3ℓDec	CR$3\ell t\bar{t}W$	CR$3\ell t\bar{t}Z$	CR3ℓHFe	CR3ℓHFμ
HF-decay e	38 ± 9	14 ± 3	1.3 ± 0.3	0.28 ± 0.09	53 ± 11	–
HF-decay μ	63 ± 11	22 ± 4	1.6 ± 0.3	0.37 ± 0.08	0.2 ± 0.1	122 ± 19
Q-misID	–	–	–	–	–	–
$t\bar{t}H$	10 ± 2	47 ± 7	32 ± 5	6.7 ± 1.1	3.0 ± 0.5	5.2 ± 0.9
$t\bar{t}W$	77 ± 12	80 ± 10	98 ± 16	12.5 ± 1.6	5.8 ± 1.0	9.5 ± 1.4
$t\bar{t}Z$	75 ± 11	438 ± 40	78 ± 7	261 ± 20	14.7 ± 1.8	28 ± 3
VV 3ℓ+b/c	296 ± 49	215 ± 39	4.8 ± 0.9	27 ± 5	15 ± 3	30 ± 5
tWZ	19 ± 6	57 ± 18	2.9 ± 0.9	16 ± 5	1.9 ± 0.6	3.6 ± 1.1
tZq	134 ± 38	69 ± 20	3.5 ± 1.0	35 ± 10	6.1 ± 1.8	12 ± 3
Others	171 ± 32	119 ± 23	43 ± 7	11.7 ± 1.5	59 ± 8	48 ± 9
Pre-fit BG	710 ± 48	941 ± 42	228 ± 17	312 ± 19	148 ± 11	248 ± 16
Post-fit BG	882 ± 28	1061 ± 28	265 ± 14	371 ± 17	159 ± 10	258 ± 14
$t\bar{t}(t \to Hu)$	26 ± 2	39 ± 3	1.2 ± 0.2	0.7 ± 0.1	4.6 ± 0.5	8.0 ± 0.8
$ug \to Ht$	14 ± 1	7 ± 1	0.4 ± 0.1	0.2 ± 0.1	1.2 ± 0.1	2.1 ± 0.2
$t\bar{t}(t \to Hc)$	27 ± 2	37 ± 3	4.3 ± 0.4	1.5 ± 0.1	4.4 ± 0.5	7.8 ± 0.7
$cg \to Ht$	2 ± 1	1 ± 1	0.1 ± 0.1	0.1 ± 0.1	0.2 ± 0.1	0.4 ± 0.1
Data	896	1046	268	381	159	263

Table 8 Normalisation factors for various backgrounds determined from the signal-plus-background fit to signal and control regions. The results for the tHu fit and the tHc fit are shown

Process	tHu fit	tHc fit
HF-decay e	1.05 ± 0.24	1.02 ± 0.23
HF-decay μ	0.94 ± 0.18	0.92 ± 0.18
$VV3\ell + b/c$	1.41 ± 0.23	1.37 ± 0.24
$t\bar{t}W$	1.15 ± 0.14	1.19 ± 0.14
$t\bar{t}Z$	1.16 ± 0.11	1.17 ± 0.11

the tune. An uncertainty in the final-state radiation is introduced by varying the renormalisation scale μ_r in the parton shower, at which the strong coupling constant α_s is evaluated, by factors of 0.5 and 2.0.

In all uncertainty evaluations mentioned above the alternative samples or reweighted samples are normalised to the total cross-section of the nominal samples.

Uncertainties in the PDFs are evaluated for the background processes simulated using POWHEGBOX, meaning $t\bar{t}$, single-t and $t\bar{t}H$ production, using the PDF4LHC15 prescription with 30 eigenvectors [117]. Simulated events are reweighted to the central value and the eigenvectors of the combined PDF set. Systematically varied templates are

Table 9 The expected 95 % upper limits on the branching ratio $\mathcal{B}(t \to Hq)$ for the nominal and alternative fit configurations. One fit is performed in the full phase space considering only statistical uncertainties. Two other fits are performed using the full set of uncertainties in only the 2ℓSS or 3ℓ final states. The $\pm 1\,\sigma$ interval of the expected limit is indicated by the upper and lower indices. For the tHu channel, the assumption of $\mathcal{B}(t \to Hc) = 0$ is made and vice versa

Fit configuration	Expected 95 % CL upper limits / 10^{-4}	
	$\mathcal{B}(t \to Hu)$	$\mathcal{B}(t \to Hc)$
Nominal fit	$3.0^{+1.2}_{-0.8}$	$3.8^{+1.5}_{-1.1}$
Statistical uncertainties only	$2.6^{+1.1}_{-0.7}$	$3.3^{+1.2}_{-1.0}$
2ℓSS final state only	$3.6^{+1.5}_{-1.0}$	$4.3^{+1.9}_{-1.2}$
3ℓ final state only	$6.5^{+2.7}_{-1.9}$	$8.9^{+3.7}_{-2.6}$

Table 10 The observed (expected) 95 % upper limits on the branching ratio $\mathcal{B}(t \to Hq)$ and the absolute value of the Wilson coefficient $|C_{u\phi}|$ under the assumption of a cutoff-scale of $\Lambda = 1$ TeV. For the tHu channel, the assumption of $\mathcal{B}(t \to Hc) = 0$ is made and vice versa

Signal	Observed (expected) 95 % CL upper limits	
	$\mathcal{B}(t \to Hq)$	$\lvert C_{u\phi}^{qt,tq}\rvert$
tHu	$2.8\ (3.0) \times 10^{-4}$	0.71 (0.73)
tHc	$3.3\ (3.8) \times 10^{-4}$	0.76 (0.82)

constructed by taking the differences between the samples reweighted to the central value and those reweighted to the eigenvectors. In the likelihood fit, the PDF uncertainties are treated as correlated across the top-quark production processes.

The uncertainties due to the finite number of simulated events, also called the MC statistical uncertainty, is accounted for by adding a nuisance parameter for each bin of the D_{NN} distributions and the distributions in the CRs, implementing the Barlow–Beeston approach [118].

9 Statistical analysis

The normalisation μ of the tHu and tHc signal couplings is determined in binned profile maximum-likelihood fits. The fits are performed simultaneously in all signal and control regions. In the signal regions, the respective D_{NN} distributions optimised for the considered signal coupling are used. For the CR2ℓHFe and CR2ℓHFμ only event yields are employed in the fit, whereas for the CR3ℓHFe and CR3ℓHFμ the transverse momentum of the third-leading-p_{T} lepton is fitted. In the CR2$\ell t\bar{t}V$, the distribution of the subleading-p_{T} lepton's transverse momentum is used, as it provides separation between prompt and non-prompt leptons. The CR3$\ell t\bar{t}W$ and CR3$\ell t\bar{t}Z$ are incorporated into the fit with the distribution of the transverse momentum of the leading-p_{T} b-tagged jet. This distribution separates the $t\bar{t}Z$ background from remaining VV events in the CR3$\ell t\bar{t}Z$ and is also adopted in the CR3$\ell t\bar{t}W$ for reasons of consistency. In the fits, each of the signal processes are treated as maximally anti-correlated, implying that the presence of one signal automatically precludes the presence of the other signal.

The likelihood function is constructed as a product of Poisson probability terms over all considered bins. The fitted event yields in the bins depend on nuisance parameters θ which include the effects of systematic uncertainties. Each nuisance parameter, except those representing the MC statistical uncertainties, is constrained by a Gaussian distribution term in the likelihood function. Some systematically varied discriminant distributions are smoothed and nuisance parameters of systematic uncertainties with negligible impact on the parameter of interest are entirely removed to reduce spurious effects in minimisation, improve convergence of the fit, and reduce the computing time. Normalisation and shape effects from a source of systematic uncertainty are treated separately in this removal process. Single-sided systematic variations are turned into symmetric variations by taking the difference between the nominal model and the alternative model and mirroring this difference in the opposite direction. This is done for the event yield and for the event shape, where the distributions are subtracted from the nominal one. For most sources with two variations, their effects are made symmetric by using the average deviation from the nominal prediction. Exceptions are the uncertainties in the JER, for which the asymmetric variations are kept because the underlying effects are known to be asymmetric. Free-floating normalisation factors are assigned to the templates modelling the HF-decay e and HF-decay μ background, as well as the $VV3\ell$+b/c, $t\bar{t}W$, and $t\bar{t}Z$ templates.

The test statistic q_μ is defined as the profile likelihood ratio

$$q_\mu = -2\ln\frac{\mathcal{L}(\mu,\hat{\hat{\theta}})}{\mathcal{L}(\hat{\mu},\hat{\theta})},$$

where $\hat{\mu}$ and $\hat{\theta}$ are the values of the parameters that maximise the likelihood function and $\hat{\hat{\theta}}$ are the values of the nuisance parameters that maximise the likelihood function for a given value of μ. The test statistic is evaluated with the RooFit package [119]. If the observed signal normalisation μ is compatible with the background hypothesis, that is $\mu = 0$, the test statistic q_μ is used in the $\mathrm{CL_S}$ method [120] to obtain exclusion limits on the signal normalisation. For a given signal scenario, values of μ yielding $\mathrm{CL_S} \leq 0.05$, where $\mathrm{CL_S}$ is computed using the asymptotic approximation [121], are excluded at $\geq 95\,\%$ CL. The obtained upper limits on the signal strength μ are then transformed into limits on the respective Wilson coefficient $C_{u\phi}$ and the corresponding branching ratio $\mathcal{B}(t \to Hq)$ through their dimension-6 operators [60].

10 Results

This section presents the results of the profile-likelihood fit. Prior to the full fit to extract the signal normalisation, a background-only fit using only regions with little signal contribution is performed to check the modelling of NN input variables. Once the modelling is checked and validity of the fit model is established, the signal normalisation is determined in a full fit to data using the entire phase space of the analysis.

10.1 Cross-checks on the modelling of the neural network input variables

Before the application of the NNs to the full collision data, modelling of the input variables is checked in parts of the signal regions. For this purpose, the events populating the respective signal regions up to a threshold value of $D_{\mathrm{NN}} = 0.5$ are selected. The threshold of $D_{\mathrm{NN}} = 0.5$ is chosen to maximise the available statistics while avoiding a signal contamination of more than 10 %. The full fit is performed with both statistical and systematic uncertainties considered in all control regions and the low-D_{NN} signal regions. The corrections made by the fit are then applied to the input variables of the various NNs, using only events with $D_{\text{NN}} < 0.5$, to check the variable modelling. The resulting distributions of the most important NN input variables in each signal region are shown in Fig. 6. Overall, no discrepancies between the post-fit distributions and data could be observed in any of the input variables.

10.2 Full fit to data

Figure 7 shows the $D_{\text{NN}}(tHc)$ distributions in all four signal regions after the fit. A summary plot of all 2ℓSS and 3ℓ control regions is shown in Fig. 8. Overall, a good agreement between MC and data is observed. The event yields shown in Tables 6, 7 confirm this. The best fit value of the normalisation of the tHu (tHc) signal is found to be $\mu_{tHq} = -0.03 \pm 0.15(-0.08 \pm 0.19)$. No pulls beyond 1σ or strong constraints are observed for any of the nuisance parameters. The observed post-fit values of all normalisation factors and nuisance parameters are in agreement with the background-only fit consistent with the statistical uncertainties, suggesting a good modelling of the most signal-sensitive D_{NN} bins. The obtained normalisation factors for free-floating background processes are listed in Table 8. For the HF-decay e and HF-decay μ processes they are compatible with one. A 40 % increase can be observed for the $VV3\ell{+}b/c$ template, owing to the poorer modelling of b-jets by the shower generator. The normalisations of the $t\bar{t}W$ and $t\bar{t}Z$ processes are increased by approximately 15 %, which is compatible at a 1σ level. The increased normalisation of $t\bar{t}W$ production is expected based on dedicated measurements of the process, while for $t\bar{t}Z$, the slightly higher normalisation comes from the inclusion of events with low jet multiplicity. Studies on the process confirm that for higher values of N_{jets} the normalisation is compatible with one.

As the best fit value of the signal strength is compatible with $\mu = 0$, upper limits are determined with the CL_S method. In addition to the nominal limits of the analysis, expected limits are determined for a fit considering only statistical uncertainties, as well as for fits in the 2ℓSS and 3ℓ channels separately. A comparison of the expected upper limits on the branching ratio $\mathcal{B}(t \to Hq)$ for each configuration is shown in Table 9. A degradation in the expected upper limit of approximately 20 % can be observed for both the signal processes when systematic uncertainties are included. This shows that the sensitivity of this analysis is primarily limited by available statistics. When comparing the two final states with each other, a clear dominance of the 2ℓSS final state can be observed. Including the 3ℓ final states yields an improvement of 20 % in the tHu channel and 13 % in the tHc channel.

The observed upper limits on the branching ratio $\mathcal{B}(t \to Hq)$ together with a reinterpretation as limits on the absolute value of the Wilson coefficient $|C_{u\phi}|$ for the EFT dimension-6 operators can be found in Table 10. The signal does not interfere with other SM processes, meaning that the signal normalisation is proportional to $|C_{u\phi}|^2$ and limits can only be set on the coefficient's absolute value. Additionally, owing to the averaging of the left-handed and the right-handed signal component, these limits are set on the average of the two respective coefficients $|C_{u\phi}^{tq}|$ and $|C_{u\phi}^{qt}|$. The final observed (expected) upper limits on the branching ratio are $\mathcal{B}(t \to Hu) < 2.8\,(3.0) \times 10^{-4}$ and $\mathcal{B}(t \to Hc) < 3.3\,(3.8) \times 10^{-4}$ for a cutoff scale $\Lambda = 1$ TeV. The limits on the Wilson coefficients amount to $|C_{u\phi}^{ut,tu}| < 0.71\,(0.73)$ and $|C_{u\phi}^{ct,tc}| < 0.76\,(0.82)$. Limits for each of the two signal couplings are determined with the assumption that the other signal coupling do not contribute.

Compared with a previous ATLAS search for tHq FCNC couplings in 2ℓSS/ 3ℓ final states using a partial Run 2 data sample of 36 fb^{-1} [32], a luminosity-adjusted improvement by a factor of two for the tHc channel and three for the tHu channel can be observed. This is determined by creating an Asimov-data sample, scaling its luminosity to that of the previous analysis, and comparing the resulting expected upper limits to the original analysis. This improvement primarily results from using improved analysis techniques such as new methods for event reconstruction and a more thorough multivariate analysis, and more precise detector calibrations. The additional improvement in the tHu channel is achieved because of the inclusion of the $gq \to Ht$ production process in the analysis. This process primarily plays a role in the tHu channel because the up quark is a valence quark of the proton.

11 Combination of results with other searches

The reported results are combined with the corresponding ATLAS searches that use $H \to \tau^+\tau^-$ decays with one or two hadronically decaying τ-leptons [33], and $H \to b\bar{b}$ [34] and $H \to \gamma\gamma$ [35] decays. For clarity, this analysis is referred to as the $H \to VV^*$ channel in the following, as the $H \to WW^*/ZZ^*$ decay modes are by far the most dominant ones contributing to 2ℓSS and 3ℓ final states. Orthogonality among all analyses is ensured by their respective event selections. The $H \to \tau^+\tau^-$ and the $H \to VV^*$ analysis, specifically, are orthogonal to each other, because the $H \to \tau^+\tau^-$ analysis exclusively uses events with exactly one or zero leptons. The combination is performed through a simultaneous profile-likelihood fit of all four analyses. The correlations between the uncertainties in the different channels are assessed. In each search, the dominant systematic uncertainties are different. In addition, the $H \to \tau^+\tau^-$, $H \to \gamma\gamma$ and $H \to VV^*$ channels are dominated by the statistical uncertainty in the data. Therefore, the combination exhibits minimal sensitivity to possible correlations of

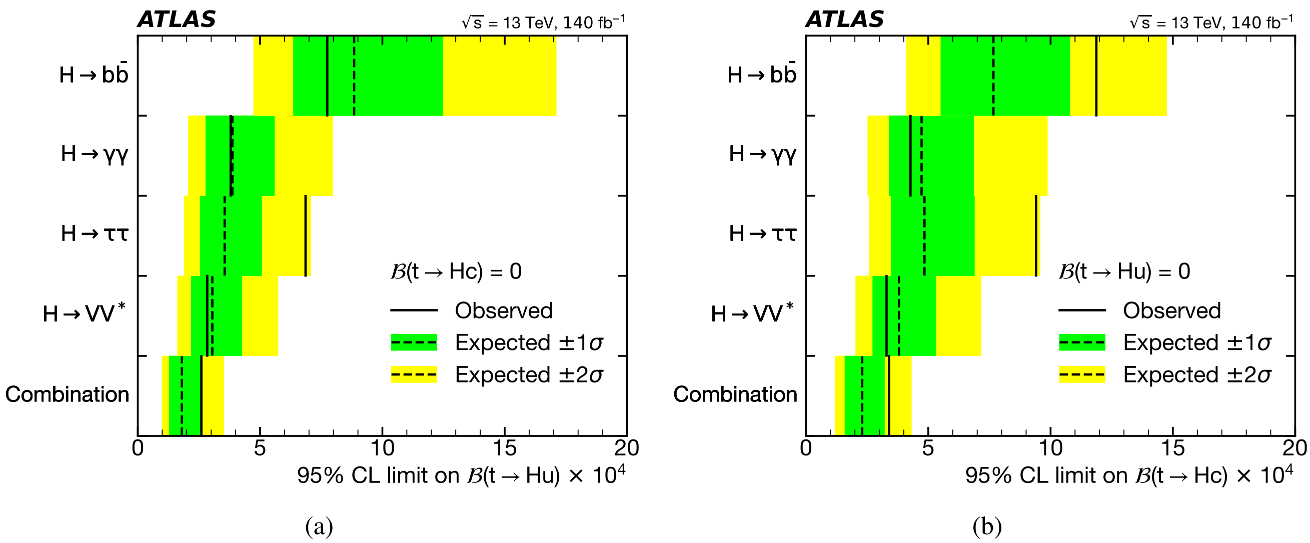

Fig. 9 The 95 % CL upper limits on **a** $\mathcal{B}(t \rightarrow Hu)$ assuming $\mathcal{B}(t \rightarrow Hc) = 0$ and **b** $\mathcal{B}(t \rightarrow Hc)$ assuming $\mathcal{B}(t \rightarrow Hu) = 0$ for the individual searches and their combination. The observed limits (solid lines) are compared with the expected (median) limits under the background-only hypothesis (dotted lines). The surrounding shaded bands correspond to the 68 % and 95 % CL intervals around the expected limits, denoted by $\pm 1\sigma$ and $\pm 2\sigma$, respectively. The $H \rightarrow VV^*$ also includes events from leptonic $H \rightarrow \tau^+\tau^-$ decays

uncertainties across channels. Specifically, uncertainties pertaining to luminosity, pile-up modelling, and jet energy scale and resolution are correlated among the four channels. The uncertainties related to b-tagging are correlated between the $H \rightarrow \tau^+\tau^-$, the $H \rightarrow b\bar{b}$ and the $H \rightarrow VV^*$ analyses, but uncorrelated with the $H \rightarrow \gamma\gamma$ analysis, which uses a simplified b-tagging scheme. The remaining uncertainties (mostly from experimental sources, and signal and background modelling) are taken as uncorrelated. Some of the sources of systematic uncertainties (especially related to electron and muon identification and signal modelling) are common to the three search channels, but are treated as uncorrelated due to slight differences in their treatment by individual analyses. The combined p-value for the tHu fit is 0.134, while that for the tHc fit it is 0.117, showing an overall good agreement among the four analyses.

The observed (expected) 95 % CL combined upper limits on the branching ratios are $\mathcal{B}(t \rightarrow Hu) < 2.6\,(1.8) \times 10^{-4}$ and $\mathcal{B}(t \rightarrow Hc) < 3.4\,(2.3) \times 10^{-4}$. For the tHc coupling the observed limit is larger than that of the individual $H \rightarrow VV^*$ analysis, because of the strong upward-fluctuation in the $H \rightarrow \tau^+\tau^-$ analysis. A summary of the upper limits on the branching ratios from the individual searches, and their combination, is given in Fig. 9. In the EFT framework, the limits observed for the respective branching ratios translate to a limit on the Wilson coefficients of the tHu dimension-6 operators of $|C_{u\phi}^{ut,tu}| < 0.68(0.56)$ at 95 % CL, assuming $C_{u\phi}^{ct,tc} = 0$, and for a mass scale $\Lambda = 1$ TeV. The analogous limit on the Wilson coefficient of the tHc dimension-6 operator amounts to $|C_{u\phi}^{ct,tc}| < 0.78(0.64)$ assuming $C_{u\phi}^{ut,tu} = 0$.

12 Conclusion

A search is reported for FCNC couplings between the top quark, the Higgs boson and a second up-type quark in final states containing either two leptons of the same charge or three leptons. This search uses 140 fb^{-1} of proton–proton collision data collected with the ATLAS detector at the LHC between 2015 and 2018. The FCNC processes are considered in $t\bar{t}$ production where either the top quark or the top anti-quark decays via $t \rightarrow Hq$, and in the production of a single top quark with a Higgs boson via the $q \rightarrow tH$ FCNC process. The results are compatible with the SM and no evidence of FCNC couplings is observed. Upper limits at 95 % CL are set on the branching ratio $\mathcal{B}(t \rightarrow Hq)$. The observed (expected) upper limits on the branching ratio are $\mathcal{B}(t \rightarrow Hu) < 2.8\,(3.0) \times 10^{-4}$ and $\mathcal{B}(t \rightarrow Hc) < 3.3\,(3.8) \times 10^{-4}$. They are reinterpreted as limits on the average of the Wilson coefficients for the left-handed and the right-handed dimension-6 operators modelling the effective tHq couplings with a new physics scale at $\Lambda = 1$ TeV. These limits amount to $|C_{u\phi}^{ut,tu}| < 0.71\,(0.73)$ and $|C_{u\phi}^{ct,tc}| < 0.76\,(0.82)$. These are the most stringent upper limits reported by any analysis searching for tHq FCNC couplings with the ATLAS detector. They are also lower than any other search for these couplings in 2ℓSS and 3ℓ final states.

The results are combined with three other searches for tHq FCNC couplings with the ATLAS detector. The combined observed (expected) limits set by all four analyses, considering correlations between the individual searches, are $\mathcal{B}(t \rightarrow Hu) < 2.6\,(1.8) \times 10^{-4}$ and $\mathcal{B}(t \rightarrow Hc) < 3.4\,(2.3) \times 10^{-4}$ on the branching ratios, and $|C_{u\phi}^{ut,tu}| <$

0.68(0.56) and $|C_{u\phi}^{ct,tc}| < 0.78(0.64)$ on the dimension-6 Wilson coefficients.

Acknowledgements We thank CERN for the very successful operation of the LHC and its injectors, as well as the support staff at CERN and at our institutions worldwide without whom ATLAS could not be operated efficiently.The crucial computing support from all WLCG partners is acknowledged gratefully, in particular from CERN, the ATLAS Tier-1 facilities at TRIUMF/SFU (Canada), NDGF (Denmark, Norway, Sweden), CC-IN2P3 (France), KIT/GridKA (Germany), INFN-CNAF (Italy), NL-T1 (Netherlands), PIC (Spain), RAL (UK) and BNL (USA), the Tier-2 facilities worldwide and large non-WLCG resource providers. Major contributors of computing resources are listed in Ref. [122]. We gratefully acknowledge the support of ANPCyT, Argentina; YerPhI, Armenia; ARC, Australia; BMWFW and FWF, Austria; ANAS, Azerbaijan; CNPq and FAPESP, Brazil; NSERC, NRC and CFI, Canada; CERN; ANID, Chile; CAS, MOST and NSFC, China; Minciencias, Colombia; MEYS CR, Czech Republic; DNRF and DNSRC, Denmark; IN2P3-CNRS and CEA-DRF/IRFU, France; SRNSFG, Georgia; BMBF, HGF and MPG, Germany; GSRI, Greece; RGC and Hong Kong SAR, China; ISF and Benoziyo Center, Israel; INFN, Italy; MEXT and JSPS, Japan; CNRST, Morocco; NWO, Netherlands; RCN, Norway; MEiN, Poland; FCT, Portugal; MNE/IFA, Romania; MESTD, Serbia; MSSR, Slovakia; ARRS and MIZŠ, Slovenia; DSI/NRF, South Africa; MICINN, Spain; SRC and Wallenberg Foundation, Sweden; SERI, SNSF and Cantons of Bern and Geneva, Switzerland; MOST, Taipei; TENMAK, Türkiye; STFC, United Kingdom; DOE and NSF, USA. Individual groups and members have received support from BCKDF, CANARIE, CRC and DRAC, Canada; CERN-CZ, PRIMUS 21/SCI/017 and UNCE SCI/013, Czech Republic; COST, ERC, ERDF, Horizon 2020, ICSC-NextGenerationEU and Marie Skłodowska-Curie Actions, European Union; Investissements d'Avenir Labex, Investissements d'Avenir Idex and ANR, France; DFG and AvH Foundation, Germany; Herakleitos, Thales and Aristeia programmes co-financed by EU-ESF and the Greek NSRF, Greece; BSF-NSF and MINERVA, Israel; Norwegian Financial Mechanism 2014-2021, Norway; NCN and NAWA, Poland; La Caixa Banking Foundation, CERCA Programme Generalitat de Catalunya and PROMETEO and GenT Programmes Generalitat Valenciana, Spain; Göran Gustafssons Stiftelse, Sweden; The Royal Society and Leverhulme Trust, UK. In addition, individual members wish to acknowledge support from CERN: European Organization for Nuclear Research (CERN PJAS); Chile: Agencia Nacional de Investigación y Desarrollo (FONDECYT 1190886, FONDECYT 1210400, FONDECYT 1230812, FONDECYT 1230987); China: National Natural Science Foundation of China (NSFC-12175119, NSFC 12275265, NSFC-12075060); Czech Republic: PRIMUS Research Programme (PRIMUS/21/SCI/017); European Union: European Research Council (ERC-948254, ERC 101089007), Horizon 2020 Framework Programme (MUCCA-CHIST-ERA-19-XAI-00), European Union, Future Artificial Intelligence Research (FAIR-NextGenerationEU PE00000013), Italian Center for High Performance Computing, Big Data and Quantum Computing (ICSC, NextGenerationEU); France: Agence Nationale de la Recherche (ANR-20-CE31-0013, ANR-21-CE31-0013, ANR-21-CE31-0022), Investissements d'Avenir Labex (ANR-11-LABX-0012); Germany: Baden-Württemberg Stiftung (BW Stiftung-Postdoc Eliteprogramme), Deutsche Forschungsgemeinschaft (DFG-469666862, DFG-CR 312/5-2); Italy: Istituto Nazionale di Fisica Nucleare (ICSC, NextGenerationEU); Japan: Japan Society for the Promotion of Science (JSPS KAKENHI JP21H05085, JSPS KAKENHI JP22H01227, JSPS KAKENHI JP22H04944, JSPS KAKENHI JP22KK0227); Netherlands: Netherlands Organisation for Scientific Research (NWO Veni 2020-VI.Veni.202.179); Norway: Research Council of Norway (RCN-314472); Poland: Polish National Agency for Academic Exchange (PPN/PPO/2020/1/00002/U/00001), Polish National Science Centre (NCN 2021/42/E/ST2/00350, NCN OPUS nr 2022/47/B/ST2/03059, NCN UMO-2019/34/E/ST2/00393, UMO-2020/37/B/ST2/01043, UMO-2021/40/C/ST2/00187, UMO-2022/47/O/ST2/00148); Slovenia: Slovenian Research Agency (ARIS grant J1-3010); Spain: BBVA Foundation (LEO22-1-603), Generalitat Valenciana (Artemisa, FEDER, IDIFEDER/2018/048), Ministry of Science and Innovation (MCIN and NextGenEU-PCI2022-135018-2, MICIN and FEDER-PID2021-125273NB, RYC2019-028510-I, RYC2020-030254-I, RYC2021-031273-I, RYC2022-038164-I), PROMETEO and GenT Programmes Generalitat Valenciana (CIDEGENT/2019/023, CIDEGENT/2019/027); Sweden: Swedish Research Council (VR 2018-00482, VR 2022-03845, VR 2022-04683, VR grant 2021-03651), Knut and Alice Wallenberg Foundation (KAW 2017.0100, KAW 2018.0157, KAW 2018.0458, KAW 2019.0447, KAW 2022.0358); Switzerland: Swiss National Science Foundation (SNSF-PCEFP2_194658); UK: Leverhulme Trust (Leverhulme Trust RPG-2020-004), Royal Society (NIF-R1-231091); United States of America: Neubauer Family Foundation.

Data Availability Statement This manuscript has no associated data. [Author's comment: "All ATLAS scientific output is published in journals, and preliminary results are made available in Conference Notes. All are openly available, without restriction on use by external parties beyond copyright law and the standard conditions agreed by CERN. Data associated with journal publications are also made available: tables and data from plots (e.g. cross section values, likelihood profiles, selection efficiencies, cross section limits, ...) are stored in appropriate repositories such as HEPDATA (http://hepdata.cedar.ac.uk/). ATLAS also strives to make additional material related to the paper available that allows a reinterpretation of the data in the context of new theoretical models. For example, an extended encapsulation of the analysis is often provided for measurements in the framework of RIVET (http://rivet.hepforge.org/)." This information is taken from the ATLAS Data Access Policy, which is a public document that can be downloaded from http://opendata.cern.ch/record/413 [opendata.cern.ch].]

Code Availability Statement This manuscript has no associated code/software. [Author's comment: Code/Software sharing not applicable to this article as no code/software was generated or analysed during the current study.]

Appendix

Tables 11, 12, 13, 14 list the input variables to the NNs used in the four signal regions, approximately ordered by the increase in significance provided by each variable. The exact order differs among the two signal processes.

Table 11 List of input variables to the NN in the SR3ℓProd, approximately ordered by the increase in significance provided by each variable. The exact order differs among the two signal processes

Variable	Description
$m(\ell_{\mathrm{OS}}, \ell_{\mathrm{SS},1})$	Invariant mass of the opposite-charge and the subleading-p_{T} same-charge lepton
$m(\ell_{\mathrm{OS}}, \ell_{\mathrm{SS},0})$	Invariant mass of the opposite-charge and the leading-p_{T} same-charge lepton
$m(\ell_t, b_t)$	Invariant mass of the b-tagged jet and the lepton assigned to the top-quark decay
N_{jets}	Number of jets
H_T (jets)	Scalar sum of the p_{T} of all jets
$m(t_{\mathrm{SM}}, H)$	Invariant mass of the RJR top quark decaying via $t \to Wb$ and the Higgs boson
$\Delta R(\ell_{\mathrm{SS},0}, \ell_{\mathrm{SS},1})$	Angular separation between the leading and subleading-p_{T} same-charge lepton
$m(\ell_{H,0}, \ell_{H,1})$	Invariant mass of the two leptons assigned to the Higgs-boson decay
$m(b\text{-jet}, \ell_{\mathrm{SS},0})$	Invariant mass of the b-tagged jet and the leading-p_{T} same-charge lepton
$\Delta R(\ell_t, b_t)$	Angular separation between the b-tagged jet and the lepton assigned to the top-quark decay
$p_{\mathrm{T}}(t_{\mathrm{SM}})$	Transverse momentum of the RJR top quark decaying via $t \to Wb$
$p_{\mathrm{T}}(b\text{-jet})$	Transverse momentum of the b-tagged jet
$\eta(\ell_{\mathrm{SS},1})$	Pseudorapidity of the subleading-p_{T} same-charge lepton
$p_{\mathrm{T}}(\ell_{\mathrm{SS},1})$	Transverse momentum of the subleading-p_{T} same-charge lepton
$m(H, \ell_{\mathrm{SS},1})$	Invariant mass of the RJR Higgs boson and the subleading-p_{T} same-charge lepton
$\Delta R(t_{\mathrm{SM}}, \ell_{\mathrm{OS}})$	Angular separation between the RJR top quark decaying via $t \to Wb$ and the opposite-charge lepton
$\Delta R(H, \ell_{\mathrm{OS}})$	Angular separation between the RJR Higgs boson and the opposite-charge lepton
$\Delta R(\ell_{\mathrm{OS}, \ell_{\mathrm{SS},1}})$	Angular separation between the opposite-charge and the subleading-p_{T} same-charge lepton

Table 12 List of input variables to the NN in the SR3ℓDec, approximately ordered by the increase in significance provided by each variable. The exact order differs among the two signal processes. Variables labelled NICE were reconstructed with a fulfilled NICE Reco condition

Variable	Description
$m(\ell_{\mathrm{OS}}, \ell_{\mathrm{SS},1})$	Invariant mass of the opposite-charge and the subleading-p_{T} same-charge lepton
$m(\ell_{\mathrm{OS}}, \ell_{\mathrm{SS},0})$	Invariant mass of the opposite-charge and the leading-p_{T} same-charge lepton
NICE $m(\ell_t, b_t)$	Invariant mass of the b-tagged jet and the lepton assigned to the top-quark decay with a fulfilled NICE Reco condition
H_T (jets)	Scalar sum of the p_{T} of all jets
$m(b\text{-jet}, \ell_{\mathrm{SS},0})$	Invariant mass of the b-tagged jet and the leading-p_{T} same-charge lepton
$m(t_{\mathrm{SM}}, H)$	Invariant mass of the RJR top quark decaying via $t \to Wb$ and the RJR Higgs boson
$m(\ell_{H,0}, \ell_{H,1})$	Invariant mass of the two leptons assigned to the Higgs-boson decay
$m(H, \ell_{\mathrm{SS},1})$	Invariant mass of the RJR Higgs boson and the subleading-p_{T} same-charge lepton
$\Delta R(b\text{-jet}, t_{\mathrm{SM}})$	Angular separation between the b-tagged jet and the RJR top quark decaying via $t \to Wb$
$m(\ell_0, t_{\mathrm{SM}})$	Invariant mass of the leading-p_{T} lepton and the RJR top quark decaying via $t \to Wb$
$p_{\mathrm{T}}(t_{\mathrm{SM}})$	Transverse momentum of the RJR top quark decaying via $t \to Wb$
$m(t_{\mathrm{SM}}, \ell_{\mathrm{SS},1})$	Invariant mass of the RJR top quark decaying via $t \to Wb$ and the subleading-p_{T} same-charge lepton
$\Delta R(\ell_{\mathrm{OS}}, \ell_{\mathrm{SS},0})$	Angular separation between the opposite-charge and the leading-p_{T} same-charge lepton
$p_{\mathrm{T}}(\ell_{\mathrm{OS}})$	Transverse momentum of the opposite-charge lepton
$m(b\text{-jet}, \ell_{\mathrm{OS}})$	Invariant mass of the b-tagged jet and the opposite-charge lepton
$m(b\text{-jet}, H)$	Invariant mass of the b-tagged jet and the RJR Higgs boson
$p_{\mathrm{T}}(\ell_2)$	Transverse momentum of the third-leading-p_{T} lepton
$\eta(\ell_0)$	Pseudorapidity of the leading-p_{T} lepton
$m(W_t)$	Mass of the RJR W boson from the top-quark decay
$m(\ell_t, b_t)$	Invariant mass of the b-tagged jet and the lepton assigned to the top-quark decay

Table 13 List of input variables to the NN in the SR2ℓProd, approximately ordered by the increase in significance provided by each variable. The exact order differs among the various signal processes

Variable	Description
$m(\ell_1, H)$	Invariant mass of the subleading-p_T lepton and the RJR Higgs boson
N_{jets}	Number of jets
$m(b\text{-jet}, t_{SM})$	Invariant mass of the b-tagged jet and the RJR top quark decaying via $t \to Wb$
$m(H, b\text{-jet})$	Invariant mass of the RJR Higgs boson and the b-tagged jet
$p_T(W_{had})$	Transverse momentum of the hadronically decaying RJR W boson
$\Delta R(\ell_1, H)$	Angular separation between the subleading-p_T lepton and the RJR Higgs boson
$m(W_{had})$	Mass of the hadronically decaying RJR W boson
$p_T(\ell_1)$	Transverse momentum of the subleading-p_T lepton
$\eta(\ell_1)$	Pseudorapidity of the subleading-p_T lepton
$\Delta R(H, W_t)$	Angular separation between the RJR Higgs boson and the RJR W boson from the top-quark decay
$\Delta R(\ell_0, \ell_1)$	Angular separation between leading and subleading-p_T lepton
$m(\ell_1, b\text{-jet})$	Invariant mass of the subleading-p_T lepton and the b-tagged jet
$\eta(b\text{-jet})$	Pseudorapidity of the b-tagged jet
$\Delta R(\ell_0, t_{SM})$	Angular separation between the leading-p_T lepton and the RJR top quark decaying via $t \to Wb$
E_T^{miss}	Missing transverse momentum
fl.(ℓ_0)	Flavour of the leading-p_T lepton
$\eta(\ell_0)$	Pseudorapidity of the leading-p_T lepton
$p_T(\ell_0)$	Transverse momentum of the leading-p_T lepton
$\Delta R(\ell_1, t_{SM})$	Angular separation between the subleading-p_T lepton and the RJR top quark decaying via $t \to Wb$
$m(H, W_t)$	Invariant mass of the RJR Higgs boson and the RJR W boson from the top-quark decay
$\Delta R(\ell_1, W_t)$	Angular separation between the subleading-p_T lepton and the RJR W boson from the top-quark decay
$m(\ell_0, H)$	Invariant mass of the leading-p_T lepton and the RJR Higgs boson
$p_T(b\text{-jet})$	Transverse momentum of the b-tagged jet

Table 14 List of input variables to the NN in the SR2ℓDec, approximately ordered by the increase in significance provided by each variable. The exact order differs among the various signal processes

Variable	Description
H_T(jets)	Scalar sum of the p_T of all jets
$m(\ell_0, b\text{-jet})$	Invariant mass of the leading-p_T lepton and the b-tagged jet
$\Delta R(\ell_1, H)$	Angular separation between the subleading-p_T lepton and the RJR Higgs boson
$p_T(\ell_1)$	Transverse momentum of the subleading-p_T lepton
$m(\text{jets}_{\min\Delta R})$	Invariant mass of the two non-b-tagged jets with the smallest ΔR
$m(t_{SM}, l\text{-jet}_0)$	Invariant mass of the RJR top quark decaying via $t \to Wb$ and the leading-p_T non-b-tagged jet
$\eta(\ell_1)$	Pseudorapidity of the subleading-p_T lepton
$\Delta R(\ell_0, l\text{-jet}_1)$	Angular separation between the leading-p_T lepton and the subleading-p_T non-b-tagged jet
$m(\ell_1, l\text{-jet}_0)$	Invariant mass of the subleading-p_T lepton and the leading-p_T non-b-tagged jet
$m(\ell_0, l\text{-jet}_0)$	Invariant mass of the leading-p_T lepton and the leading-p_T non-b-tagged jet
$\Delta R(\ell_0, l\text{-jet}_2)$	Angular separation between the leading-p_T lepton and the third-leading-p_T non-b-tagged jet
$\Delta R(\ell_1, l\text{-jet}_2)$	Angular separation between the subleading-p_T lepton and the third-leading-p_T non-b-tagged jet
$m(t_{FCNC}, l\text{-jet}_0)$	Invariant mass of the RJR top quark decaying via $t \to Hq$and the leading-p_T non-b-tagged jet
$m(\ell_1, l\text{-jet}_1)$	Invariant mass of the subleading-p_T lepton and the subleading-p_T non-b-tagged jet
$m(\ell_1, t_{FCNC})$	Invariant mass of the subleading-p_T lepton and the RJR top quark decaying via $t \to Hq$
$m(W_t, W_{had})$	Invariant mass of the RJR W boson from the top-quark decay and the hadronically decaying RJR W boson
$\Delta R(\ell_0, l\text{-jet}_0)$	Angular separation between the leading-p_T lepton and the leading-p_T non-b-tagged jet

Table 14 continued

Variable	Description
$m(\ell_1, b\text{-jet})$	Invariant mass of the subleading-p_T lepton and the b-tagged jet
N_{jets}	Number of jets
$m(H, b\text{-jet})$	Invariant mass of the RJR Higgs boson and the b-tagged jet
$H_T(\ell_0, \ell_1)$	Scalar sum of the p_T of all leptons
$p_T(\ell_0)$	Transverse momentum of the leading-p_T lepton
$m(W_t, t_{\text{FCNC}})$	Invariant mass of the RJR W boson from the top-quark decay and the RJR top quark decaying via $t \to Hq$

References

1. ATLAS Collaboration, Observation of a new particle in the search for the Standard Model Higgs boson with the ATLAS detector at the LHC. Phys. Lett. B **716**, 1 (2012). https://doi.org/10.1016/j.physletb.2012.08.020. arXiv:1207.7214 [hep-ex]
2. CMS Collaboration, Observation of a new boson at a mass of 125 GeV with the CMS experiment at the LHC. Phys. Lett. B **716**, 30 (2012). https://doi.org/10.1016/j.physletb.2012.08.021. arXiv:1207.7235 [hep-ex]
3. ATLAS Collaboration, A detailed map of Higgs boson interactions by the ATLAS experiment ten years after the discovery. Nature **607**, 52 (2022). https://doi.org/10.1038/s41586-022-04893-w. arXiv:2207.00092 [hep-ex] [Erratum: Nature 612 (2022) E24. https://doi.org/10.1038/s41586-022-05581-5]
4. CMS Collaboration, A portrait of the Higgs boson by the CMS experiment ten years after the discovery. Nature **607**, 60 (2022). https://doi.org/10.1038/s41586-022-04892-x. arXiv:2207.00043 [hep-ex] [Erratum: Nature 623 (2023) E4. https://doi.org/10.1038/s41586-023-06164-8]
5. S.L. Glashow, J. Iliopoulos, L. Maiani, Weak interactions with lepton-hadron symmetry. Phys. Rev. D **2**, 1285 (1970). https://doi.org/10.1103/PhysRevD.2.1285
6. G. Eilam, J.L. Hewett, A. Soni, Rare decays of the top quark in the standard and two-Higgs-doublet models. Phys. Rev. D **44**, 1473 (1991). https://doi.org/10.1103/PhysRevD.44.1473 [Erratum: Phys. Rev. D 59 (1998) 039901]
7. B. Mele, S. Petrarca, A. Soddu, A new evaluation of the $t \to cH$ decay width in the standard model. Phys. Lett. B **435**, 401 (1998). https://doi.org/10.1016/S0370-2693(98)00822-3. arXiv:hep-ph/9805498 [hep-ph]
8. J.A. Aguilar-Saavedra, Top flavor-changing neutral interactions: theoretical expectations and experimental detection. Acta Phys. Polon. B **35**, 2695 (2004). https://doi.org/10.48550/arXiv.hep-ph/0409342. arXiv:hep-ph/0409342 [hep-ph]
9. C. Zhang, F. Maltoni, Top-quark decay into Higgs boson and a light quark at next-to-leading order in QCD. Phys. Rev. D **88**, 054005 (2013). https://doi.org/10.1103/PhysRevD.88.054005. arXiv:1305.7386 [hep-ph]
10. W. Altmannshofer, B. Maddock, D. Tuckler, Rare top decays as probes of flavorful Higgs bosons. Phys. Rev. D **100**, 015003 (2019). https://doi.org/10.1103/PhysRevD.100.015003. arXiv:1904.10956 [hep-ph]
11. G.C. Branco et al., Theory and phenomenology of two-Higgs-doublet models. Phys. Rep. **516**, 1 (2012). https://doi.org/10.1016/j.physrep.2012.02.002. arXiv:1106.0034 [hep-ph]
12. S. Béjar, J. Guasch, J. Solà, Loop induced flavor changing neutral decays of the top quark in a general two-Higgs-doublet model. Nucl. Phys. B **600**, 21 (2001). https://doi.org/10.1016/S0550-3213(01)00044-X. arXiv:hep-ph/0011091 [hep-ph]
13. J. Guasch, J. Solà, FCNC top quark decays in the MSSM: a door to SUSY physics in high luminosity colliders? Nucl. Phys. B **562**, 3 (1999). https://doi.org/10.1016/S0550-3213(99)00579-9. arXiv:hep-ph/9906268 [hep-ph]
14. J.J. Cao et al., Supersymmetry-induced flavor-changing neutral-current top-quark processes at the CERN Large Hadron Collider. Phys. Rev. D **75**, 075021 (2007). https://doi.org/10.1103/PhysRevD.75.075021. arXiv:hep-ph/0702264 [hep-ph]
15. J. Cao, C. Han, L. Wu, J.M. Yang, M. Zhang, SUSY induced top quark FCNC decay $t \to ch$ after Run I of LHC. Eur. Phys. J. C **74**, 3058 (2014). https://doi.org/10.1140/epjc/s10052-014-3058-1. arXiv:1404.1241 [hep-ph]
16. G. Eilam, A. Gemintern, T. Han, J.M. Yang, X. Zhang, Top-quark rare decay $t \to ch$ in R-parity-violating SUSY. Phys. Lett. B **510**, 227 (2001). https://doi.org/10.1016/S0370-2693(01)00598-6. arXiv:hep-ph/0102037 [hep-ph]
17. J.A. Aguilar-Saavedra, Effects of mixing with quark singlets. Phys. Rev. D **67**, 035003 (2003). https://doi.org/10.1103/PhysRevD.67.035003. arXiv:hep-ph/0210112 [hep-ph] [Erratum: Phys. Rev. D 69 (2004) 099901]
18. A. Azatov, M. Toharia, L. Zhu, Higgs mediated flavor changing neutral currents in warped extra dimensions. Phys. Rev. D **80**, 035016 (2009). https://doi.org/10.1103/PhysRevD.80.035016. arXiv:0906.1990 [hep-ph]
19. T.P. Cheng, M. Sher, Mass-matrix ansatz and flavor nonconservation in models with multiple Higgs doublets. Phys. Rev. D **35**, 3484 (1987). https://doi.org/10.1103/PhysRevD.35.3484
20. I. Baum, G. Eilam, S. Bar-Shalom, Scalar flavor changing neutral currents and rare top quark decays in a two Higgs doublet model "for the top quark". Phys. Rev. D **77**, 113008 (2008). https://doi.org/10.1103/PhysRevD.77.113008. arXiv:0802.2622 [hep-ph]
21. K.-F. Chen, W.-S. Hou, C. Kao, M. Kohda, When the Higgs meets the top: search for $t \to ch^0$ at the LHC. Phys. Lett. B **725**, 378 (2013). https://doi.org/10.1016/j.physletb.2013.07.060. arXiv:1304.8037 [hep-ph]
22. C.-W. Chiang, H. Fukuda, M. Takeuchi, T.T. Yanagida, Flavor-changing neutral-current decays in top-specific variant axion model. JHEP **11**, 057 (2015). https://doi.org/10.1007/JHEP11(2015)057. arXiv:1507.04354 [hep-ph]
23. A. Crivellin, J. Heeck, P. Stoffer, Perturbed lepton-specific two-Higgs-doublet model facing experimental hints for physics beyond the standard model. Phys. Rev. Lett. **116**, 081801 (2016). https://doi.org/10.1103/PhysRevLett.116.081801. arXiv:1507.07567 [hep-ph]
24. F.J. Botella, G.C. Branco, M. Nebot, M.N. Rebelo, Flavour-changing Higgs couplings in a class of two Higgs doublet models. Eur. Phys. J. C **76**, 161 (2016). https://doi.org/10.1140/epjc/s10052-016-3993-0. arXiv:1508.05101 [hep-ph]
25. S. Gori, C. Grojean, A. Juste, A. Paul, Heavy Higgs searches: flavour matters. JHEP **01**, 108 (2018). https://doi.org/10.1007/JHEP01(2018)108. arXiv:1710.03752 [hep-ph]

26. C.-W. Chiang, H. Fukuda, M. Takeuchi, T.T. Yanagida, Current status of top-specific variant axion model. Phys. Rev. D **97**, 035015 (2018). https://doi.org/10.1103/PhysRevD.97.035015. arXiv:1711.02993 [hep-ph]
27. A. Greljo, J.F. Kamenik, J. Kopp, Disentangling flavor violation in the top-Higgs sector at the LHC. JHEP **07**, 046 (2014). https://doi.org/10.1007/JHEP07(2014)046. arXiv:1404.1278 [hep-ph]
28. D. de Florian et al., Handbook of LHC Higgs Cross Sections: 4. Deciphering the Nature of the Higgs Sector (2017). https://doi.org/10.23731/CYRM-2017-002. arXiv:1610.07922 [hep-ph]
29. G. Durieux, F. Maltoni, C. Zhang, Global approach to top-quark flavor-changing interactions. Phys. Rev. D **91**, 074017 (2015). https://doi.org/10.1103/PhysRevD.91.074017. arXiv:1412.7166 [hep-ph]
30. ATLAS Collaboration, Search for top-quark decays $t \to Hq$ with 36 fb^{-1} of pp collision data at $\sqrt{s} = 13$ TeV with the ATLAS detector. JHEP **05**, 123 (2019). https://doi.org/10.1007/JHEP05(2019)123. arXiv:1812.11568 [hep-ex]
31. ATLAS Collaboration, Search for top quark decays $t \to qH$, with $H \to \gamma\gamma$, in $\sqrt{s} = 13$ TeV pp collisions using the ATLAS detector. JHEP **10**, 129 (2017). https://doi.org/10.1007/JHEP10(2017)129. arXiv:1707.01404 [hep-ex]
32. ATLAS Collaboration, Search for flavor-changing neutral currents in top quark decays $t \to Hc$ and $t \to Hu$ in multilepton final states in proton–proton collisions at $\sqrt{s} = 13$ TeV with the ATLAS detector. Phys. Rev. D **98**, 032002 (2018). https://doi.org/10.1103/PhysRevD.98.032002. arXiv:1805.03483 [hep-ex]
33. ATLAS Collaboration, Search for flavour-changing neutral current interactions of the top quark and the Higgs boson in events with a pair of τ-leptons in pp collisions at $\sqrt{s} = 13$ TeV with the ATLAS detector. JHEP **06**, 155 (2023). https://doi.org/10.1007/JHEP06(2023)155. arXiv:2208.11415 [hep-ex]
34. ATLAS Collaboration, Search for a new scalar resonance in flavour-changing neutral-current top-quark decays $t \to qX$ ($q = u, c$), with $X \to b\bar{b}$, in proton–proton collisions at $\sqrt{s} = 13$ TeV with the ATLAS detector. JHEP **07**, 199 (2023). https://doi.org/10.1007/JHEP07(2023)199. arXiv:2301.03902 [hep-ex]
35. ATLAS Collaboration, Search for flavour-changing neutral tqH interactions with $H \to \gamma\gamma$ in pp collisions at $\sqrt{s} = 13$ TeV using the ATLAS detector. JHEP **12**, 195 (2023). https://doi.org/10.1007/jhep12(2023)195. arXiv:2309.12817 [hep-ex]
36. C.M.S. Collaboration, Search for the flavor-changing neutral current interactions of the top quark and the Higgs boson which decays into a pair of b quarks at $\sqrt{s} = 13$ TeV. JHEP **06**, 102 (2018). https://doi.org/10.1007/JHEP06(2018)102. arXiv:1712.02399 [hep-ex]
37. C.M.S. Collaboration, Search for flavor-changing neutral current interactions of the top quark and the Higgs boson decaying to a bottom quark-antiquark pair at $\sqrt{s}$ =13 TeV. JHEP **02**, 169 (2022). https://doi.org/10.1007/JHEP02(2022)169. arXiv:2112.09734 [hep-ex]
38. C.M.S. Collaboration, Search for flavor-changing neutral current interactions of the top quark and Higgs boson in final states with two photons in proton-proton collisions at $\sqrt{s} = 13$ TeV. JHEP **02**, 169 (2022). https://doi.org/10.1007/JHEP02(2022)169. arXiv:2111.02219 [hep-ex]
39. D.E. Rumelhart, G.E. Hinton, R.J. Williams, Learning Internal Representations by Error Propagation, in *Parallel Distributed Processing: Explorations in the Microstructure of Cognition, Volume 1: Foundations*. ed. by D.E. Rumelhart, J.L. Mcclelland (MIT Press, Cambridge, 1986)
40. ATLAS Collaboration, The ATLAS Experiment at the CERN Large Hadron Collider. JINST **3**, S08003 (2008). https://doi.org/10.1088/1748-0221/3/08/S08003
41. ATLAS Collaboration, ATLAS Insertable B-Layer: Technical Design Report, ATLAS-TDR-19; CERN-LHCC-2010-013 (2010). https://cds.cern.ch/record/1291633 [Addendum: ATLAS-TDR-19-ADD-1; CERN-LHCC-2012-009 (2012). https://cds.cern.ch/record/1451888]
42. B. Abbott et al., Production and integration of the ATLAS Insertable B-Layer. JINST **13**, T05008 (2018). https://doi.org/10.1088/1748-0221/13/05/T05008. arXiv:1803.00844 [physics.ins-det]
43. ATLAS Collaboration, Performance of the ATLAS trigger system in 2015. Eur. Phys. J. C **77**, 317 (2017). https://doi.org/10.1140/epjc/s10052-017-4852-3. arXiv:1611.09661 [hep-ex]
44. ATLAS Collaboration, The ATLAS Collaboration Software and Firmware, ATL-SOFT-PUB-2021-001 (2021). https://cds.cern.ch/record/2767187
45. ATLAS Collaboration, ATLAS data quality operations and performance for 2015–2018 data-taking. JINST **15**, P04003 (2020). https://doi.org/10.1088/1748-0221/15/04/P04003. arXiv:1911.04632 [physics.ins-det]
46. ATLAS Collaboration, Luminosity determination in pp collisions at $\sqrt{s} = 13$ TeV using the ATLAS detector at the LHC. Eur. Phys. J. C **83**, 982 (2023). https://doi.org/10.1140/epjc/s10052-023-11747-w. arXiv:2212.09379 [hep-ex]
47. G. Avoni et al., The new LUCID-2 detector for luminosity measurement and monitoring in ATLAS. JINST **13**, P07017 (2018). https://doi.org/10.1088/1748-0221/13/07/p07017
48. ATLAS Collaboration, Performance of electron and photon triggers in ATLAS during LHC Run2. Eur. Phys. J. C **80**, 47 (2020). https://doi.org/10.1140/epjc/s10052-019-7500-2. arXiv:1909.00761 [hep-ex]
49. ATLAS Collaboration, Performance of the ATLAS muon triggers in Run2. JINST **15**, P09015 (2020). https://doi.org/10.1088/1748-0221/15/09/p09015. arXiv:2004.13447 [physics.ins-det]
50. S. Agostinelli et al., Geant4—a simulation toolkit. Nucl. Instrum. Meth. A **506**, 250 (2003). https://doi.org/10.1016/S0168-9002(03)01368-8
51. ATLAS Collaboration, The ATLAS Simulation Infrastructure. Eur. Phys. J. C **70**, 823 (2010). https://doi.org/10.1140/epjc/s10052-010-1429-9. arXiv:1005.4568 [physics.ins-det]
52. ATLAS Collaboration, The simulation principle and performance of the ATLAS fast calorimeter simulation FastCaloSim, ATL-PHYS-PUB-2010-013 (2010). https://cds.cern.ch/record/1300517
53. T. Sjöstrand et al., An introduction to PYTHIA 8.2. Comput. Phys. Commun. **191**, 159 (2015). https://doi.org/10.1016/j.cpc.2015.01.024. arXiv:1410.3012 [hep-ph]
54. ATLAS Collaboration, The Pythia8 A3 tune description of ATLAS minimum bias and inelastic measurements incorporating the Donnachie–Landshoff diffractive model, ATL-PHYS-PUB-2016-017 (2016). https://cds.cern.ch/record/2206965
55. NNPDF Collaboration, R.D. Ball et al., Parton distributions with LHC data. Nucl. Phys. B **867**, 244 (2013). https://doi.org/10.1016/j.nuclphysb.2012.10.003. arXiv:1207.1303 [hep-ph]
56. T. Gleisberg et al., Event generation with SHERPA 1.1. JHEP **02**, 007 (2009). https://doi.org/10.1088/1126-6708/2009/02/007. arXiv:0811.4622 [hep-ph]
57. E. Bothmann et al., Event generation with Sherpa 2.2. SciPost Phys. **7**, 034 (2019). https://doi.org/10.21468/SciPostPhys.7.3.034. arXiv:1905.09127 [hep-ph]
58. D.J. Lange, The EvtGen particle decay simulation package. Nucl. Instrum. Meth. A **462**, 152 (2001). https://doi.org/10.1016/S0168-9002(01)00089-4
59. ATLAS Collaboration, ATLAS Pythia8 tunes to 7 TeV data, ATL-PHYS-PUB-2014-021 (2014). https://cds.cern.ch/record/1966419
60. C. Degrande, F. Maltoni, J. Wang, C. Zhang, Automatic computations at next-to-leading order in QCD for top-quark flavor-changing neutral processes. Phys. Rev. D **91**, 034024 (2015).

https://doi.org/10.1103/PhysRevD.91.034024. arXiv:1412.5594 [hep-ex]
61. A. Alloul, N.D. Christensen, C. Degrande, C. Duhr, B. Fuks, FeynRules 2.0—a complete toolbox for tree-level phenomenology. Comput. Phys. Commun. **185**, 2250 (2014). arXiv:1310.1921 [hep-ph]
62. P. Nason, A new method for combining NLO QCD with shower Monte Carlo algorithms. JHEP **11**, 040 (2004). https://doi.org/10.1088/1126-6708/2004/11/040. arXiv:hep-ph/0409146
63. S. Frixione, G. Ridolfi, P. Nason, A positive-weight next-to-leading-order Monte Carlo for heavy flavour hadroproduction. JHEP **09**, 126 (2007). https://doi.org/10.1088/1126-6708/2007/09/126. arXiv:0707.3088 [hep-ph]
64. S. Frixione, P. Nason, C. Oleari, Matching NLO QCD computations with parton shower simulations: the POWHEG method. JHEP **11**, 070 (2007). https://doi.org/10.1088/1126-6708/2007/11/070. arXiv:0709.2092 [hep-ph]
65. S. Alioli, P. Nason, C. Oleari, E. Re, NLO single-top production matched with shower in POWHEG: s- and t-channel contributions. JHEP **09**, 111 (2009). https://doi.org/10.1088/1126-6708/2009/09/111. arXiv:0907.4076 [hep-ph] [Erratum: JHEP 02 (2010) 011, https://doi.org/10.1007/JHEP02(2010)011]
66. S. Alioli, P. Nason, C. Oleari, E. Re, A general framework for implementing NLO calculations in shower Monte Carlo programs: the POWHEG BOX. JHEP **06**, 043 (2010). https://doi.org/10.1007/JHEP06(2010)043. arXiv:1002.2581 [hep-ph]
67. E. Re, Single-top Wt-channel production matched with parton showers using the POWHEG method. Eur. Phys. J. C **71**, 1547 (2011). https://doi.org/10.1140/epjc/s10052-011-1547-z. arXiv:1009.2450 [hep-ph]
68. R. Frederix, E. Re, P. Torrielli, Single-top t-channel hadroproduction in the four-flavour scheme with POWHEG and aMC@NLO. JHEP **09**, 130 (2012). https://doi.org/10.1007/JHEP09(2012)130. arXiv:1207.5391 [hep-ph]
69. NNPDF Collaboration, R.D. Ball et al., Parton distributions for the LHC run II. JHEP **04**, 040 (2015). https://doi.org/10.1007/JHEP04(2015)040. arXiv:1410.8849 [hep-ph]
70. S. Frixione, E. Laenen, P. Motylinski, B.R. Webber, Angular correlations of lepton pairs from vector boson and top quark decays in Monte Carlo simulations. JHEP **04**, 081 (2007). https://doi.org/10.1088/1126-6708/2007/04/081. arXiv:hep-ph/0702198
71. P. Artoisenet, R. Frederix, O. Mattelaer, R. Rietkerk, Automatic spin-entangled decays of heavy resonances in Monte Carlo simulations. JHEP **03**, 015 (2013). https://doi.org/10.1007/JHEP03(2013)015. arXiv:1212.3460 [hep-ph]
72. C. Bierlich et al., A comprehensive guide to the physics and usage of PYTHIA 8.3. SciPost Phys. Codeb. **2022**, 8 (2022). https://doi.org/10.21468/SciPostPhysCodeb.8. arXiv:2203.11601 [hep-ph]
73. ATLAS Collaboration, Studies on top-quark Monte Carlo modelling for Top2016, ATL-PHYS-PUB-2016-020 (2016). https://cds.cern.ch/record/2216168
74. J. Alwall et al., The automated computation of tree-level and next-to-leading order differential cross sections, and their matching to parton shower simulations. JHEP **07**, 079 (2014). https://doi.org/10.1007/JHEP07(2014)079. arXiv:1405.0301 [hep-ph]
75. M. Czakon, A. Mitov, Top++: a program for the calculation of the top-pair cross-section at hadron colliders. Comput. Phys. Commun. **185**, 2930 (2014). https://doi.org/10.1016/j.cpc.2014.06.021. arXiv:1112.5675 [hep-ph]
76. M. Aliev et al., HATHOR—HAdronic Top and Heavy quarks crOss section calculatoR. Comput. Phys. Commun. **182**, 1034 (2011). https://doi.org/10.1016/j.cpc.2010.12.040. arXiv:1007.1327 [hep-ph]
77. P. Kant et al., HatHor for single top-quark production: updated predictions and uncertainty estimates for single top-quark production in hadronic collisions. Comput. Phys. Commun. **191**, 74 (2015). https://doi.org/10.1016/j.cpc.2015.02.001. arXiv:1406.4403 [hep-ph]
78. N. Kidonakis, Theoretical results for electroweak boson and single-top production. PoS **DIS2015**, 170 (2016). https://doi.org/10.22323/1.247.0170. arXiv:1506.04072 [hep-ph]
79. T. Gleisberg, S. Höche, Comix, a new matrix element generator. JHEP **12**, 039 (2008). https://doi.org/10.1088/1126-6708/2008/12/039. arXiv:0808.3674 [hep-ph]
80. F. Buccioni et al., OpenLoops 2. Eur. Phys. J. C **79**, 866 (2019). https://doi.org/10.1140/epjc/s10052-019-7306-2. arXiv:1907.13071 [hep-ph]
81. F. Cascioli, P. Maierhöfer, S. Pozzorini, Scattering amplitudes with open loops. Phys. Rev. Lett. **108**, 111601 (2012). https://doi.org/10.1103/PhysRevLett.108.111601. arXiv:1111.5206 [hep-ph]
82. A. Denner, S. Dittmaier, L. Hofer, Collier: a fortran-based complex one-loop library in extended regularizations. Comput. Phys. Commun. **212**, 220 (2017). https://doi.org/10.1016/j.cpc.2016.10.013. arXiv:1604.06792 [hep-ph]
83. S. Schumann, F. Krauss, A parton shower algorithm based on Catani-Seymour dipole factorisation. JHEP **03**, 038 (2008). https://doi.org/10.1088/1126-6708/2008/03/038. arXiv:0709.1027 [hep-ph]
84. J.-C. Winter, F. Krauss, G. Soff, A modified cluster-hadronisation model. Eur. Phys. J. C **36**, 381 (2004). https://doi.org/10.1140/epjc/s2004-01960-8. arXiv:hep-ph/0311085
85. S. Höche, F. Krauss, M. Schönherr, F. Siegert, QCD matrix elements + parton showers. The NLO case. JHEP **04**, 027 (2013). https://doi.org/10.1007/JHEP04(2013)027. arXiv:1207.5030 [hep-ph]
86. S. Kallweit, J.M. Lindert, P. Maierhöfer, S. Pozzorini, M. Schönherr, NLO QCD+EW predictions for V + jets including off-shell vector-boson decays and multÄ³et merging. JHEP **04**, 021 (2016). https://doi.org/10.1007/JHEP04(2016)021. arXiv:1511.08692 [hep-ph]
87. C. Gütschow, J.M. Lindert, M. Schönherr, Multi-jet merged top-pair production including electroweak corrections. Eur. Phys. J. C **78**, 317 (2018). https://doi.org/10.1140/epjc/s10052-018-5804-2. arXiv:1803.00950 [hep-ph]
88. R. Frederix, D. Pagani, M. Zaro, Large NLO corrections in $t\bar{t}W>\pm$ and $t\bar{t}t\bar{t}$ hadroproduction from supposedly subleading EW contributions. JHEP **02**, 031 (2018). https://doi.org/10.1007/JHEP02(2018)031. arXiv:1711.02116 [hep-ph]
89. R. Frederix, I. Tsinikos, On improving NLO merging for t$\bar{\text{t}}$W production. JHEP **11**, 029 (2021). https://doi.org/10.1007/JHEP11(2021)029. arXiv:2108.07826 [hep-ph]
90. ATLAS Collaboration, Vertex Reconstruction Performance of the ATLAS Detector at $\sqrt{s}$ = 13 TeV, ATL-PHYS-PUB-2015-026 (2015). https://cds.cern.ch/record/2037717
91. ATLAS Collaboration, Electron and photon performance measurements with the ATLAS detector using the 2015–2017 LHC proton–proton collision data. JINST **14**, P12006 (2019). https://doi.org/10.1088/1748-0221/14/12/P12006. arXiv:1908.00005 [hep-ex]
92. ATLAS Collaboration, Electron and photon efficiencies in LHC Run2 with the ATLAS experiment (2023). arXiv:2308.13362 [hep-ex]
93. ATLAS Collaboration, Muon reconstruction and identification efficiency in ATLAS using the full Run2 pp collision data set at $\sqrt{s}$ = 13 TeV. Eur. Phys. J. C **81**, 578 (2021). https://doi.org/10.1140/epjc/s10052-021-09233-2. arXiv:2012.00578 [hep-ex]
94. ATLAS Collaboration, Evidence for the associated production of the Higgs boson and a top quark pair with the ATLAS detector. Phys. Rev. D **97**, 072003 (2018). https://doi.org/10.1103/PhysRevD.97.072003. arXiv:1712.08891 [hep-ex]

95. ATLAS Collaboration, Jet reconstruction and performance using particle flow with the ATLAS Detector. Eur. Phys. J. C **77**, 466 (2017). https://doi.org/10.1140/epjc/s10052-017-5031-2. arXiv:1703.10485 [hep-ex]
96. M. Cacciari, G.P. Salam, G. Soyez, The anti-k_t jet clustering algorithm. JHEP **04**, 063 (2008). https://doi.org/10.1088/1126-6708/2008/04/063. arXiv:0802.1189 [hep-ph]
97. M. Cacciari, G.P. Salam, G. Soyez, FastJet user manual. Eur. Phys. J. C **72**, 1896 (2012). https://doi.org/10.1140/epjc/s10052-012-1896-2. arXiv:1111.6097 [hep-ph]
98. ATLAS Collaboration, Topological cell clustering in the ATLAS calorimeters and its performance in LHC Run1. Eur. Phys. J. C **77**, 490 (2017). https://doi.org/10.1140/epjc/s10052-017-5004-5. arXiv:1603.02934 [hep-ex]
99. ATLAS Collaboration, Jet energy scale and resolution measured in proton–proton collisions at $\sqrt{s} = 13$ TeV with the ATLAS detector. Eur. Phys. J. C **81**, 689 (2021). https://doi.org/10.1140/epjc/s10052-021-09402-3. arXiv:2007.02645 [hep-ex]
100. ATLAS Collaboration, Performance of pile-up mitigation techniques for jets in pp collisions at $\sqrt{s} = 8$ TeV using the ATLAS detector. Eur. Phys. J. C **76**, 581 (2016). https://doi.org/10.1140/epjc/s10052-016-4395-z. arXiv:1510.03823 [hep-ex]
101. ATLAS Collaboration, ATLAS flavour-tagging algorithms for the LHC Run2 pp collision dataset. Eur. Phys. J. C **83**, 681 (2023). https://doi.org/10.1140/epjc/s10052-023-11699-1. arXiv:2211.16345 [physics.data-an]
102. ATLAS Collaboration, The performance of missing transverse momentum reconstruction and its significance with the ATLAS detector using 140 fb^{-1} of $\sqrt{s} = 13$ TeV pp collisions (2024). arXiv:2402.05858 [hep-ex]
103. ATLAS Collaboration, Observation of four-top-quark production in the multilepton final state with the ATLAS detector. Eur. Phys. J. C **83**, 496 (2023). https://doi.org/10.1140/epjc/s10052-023-11573-0. arXiv:2303.15061 [hep-ex]
104. Particle Data Group, M. Tanabashi et al., Review of Particle Physics. Phys. Rev. D **98**, 030001 (2018). https://doi.org/10.1103/PhysRevD.98.030001
105. ATLAS Collaboration, Measurement of the total and differential cross-sections of $t\bar{t}W$ production in pp collisions at $\sqrt{s} = 13$ TeV with the ATLAS detector (2024). arXiv:2401.05299 [hep-ex]
106. ATLAS Collaboration, Inclusive and differential cross-section measurements of $t\bar{t}Z$ production in pp collisions at $\sqrt{s} = 13$ TeV with the ATLAS detector, including EFT and spin-correlation interpretations (2023). arXiv:2312.04450 [hep-ex]
107. P. Jackson, C. Rogan, Recursive Jigsaw Reconstruction: HEP event analysis in the presence of kinematic and combinatoric ambiguities. Phys. Rev. D **96**, 112007 (2017). https://doi.org/10.1103/PhysRevD.96.112007. arXiv:1705.10733 [hep-ph]
108. M. Feindt, A Neural Bayesian Estimator for Conditional Probability Densities (2004). arXiv:physics/0402093 [physics.data-an]
109. M. Feindt, U. Kerzel, The NeuroBayes neural network package. Nucl. Instrum. Meth. A **559**, 190 (2006). https://doi.org/10.1016/j.nima.2005.11.166
110. ATLAS Collaboration, ATLAS b-jet identification performance and efficiency measurement with $t\bar{t}$ events in pp collisions at $\sqrt{s} = 13$ TeV. Eur. Phys. J. C **79**, 970 (2019). https://doi.org/10.1140/epjc/s10052-019-7450-8. arXiv:1907.05120 [hep-ex]
111. ATLAS Collaboration, Measurement of the c-jet mistagging efficiency in $t\bar{t}$ events using pp collision data at $\sqrt{s} = 13$ TeV collected with the ATLAS detector. Eur. Phys. J. C **82**, 95 (2022). https://doi.org/10.1140/epjc/s10052-021-09843-w. arXiv:2109.10627 [hep-ex]
112. ATLAS Collaboration, Calibration of the light-flavour jet mistagging efficiency of the b-tagging algorithms with Z+jets events using 139 fb^{-1} of ATLAS proton–proton collision data at $\sqrt{s} = 13$ TeV. Eur. Phys. J. C **83**, 728 (2023). https://doi.org/10.1140/epjc/s10052-023-11736-z. arXiv:2301.06319 [hep-ex]
113. ATLAS Collaboration, Measurement of the production cross-section of a single top quark in association with a Z boson in proton–proton collisions at 13 TeV with the ATLAS detector. Phys. Lett. B **780**, 557 (2018). https://doi.org/10.1016/j.physletb.2018.03.023. arXiv:1710.03659 [hep-ex]
114. M. Bähr et al., Herwig++ physics and manual. Eur. Phys. J. C **58**, 639 (2008). https://doi.org/10.1140/epjc/s10052-008-0798-9. arXiv:0803.0883 [hep-ph]
115. J. Bellm et al., Herwig 7.0/Herwig++ 3.0 release note. Eur. Phys. J. C **76**, 196 (2016). https://doi.org/10.1140/epjc/s10052-016-4018-8. arXiv:1512.01178 [hep-ph]
116. S. Höche, S. Mrenna, S. Payne, C.T. Preuss and P. Skands, A Study of QCD Radiation in VBF Higgs Production with Vincia and Pythia. SciPost Phys. **12**, 010 (2022). https://doi.org/10.21468/SciPostPhys.12.1.010. arXiv:2106.10987 [hep-ph]
117. J. Butterworth et al., PDF4LHC recommendations for LHC Run II. J. Phys. G **43**, 023001 (2016). https://doi.org/10.1088/0954-3899/43/2/023001. arXiv:1510.03865 [hep-ph]
118. R. Barlow, C. Beeston, Fitting using finite Monte Carlo samples. Comput. Phys. Commun. **77**, 219 (1993). https://doi.org/10.1016/0010-4655(93)90005-W
119. W. Verkerke, D. Kirkby, The RooFit toolkit for data modeling (2003). arXiv:physics/0306116 [physics.data-an]
120. A.L. Read, Presentation of search results: the CL_S technique. J. Phys. G **28**, 2693 (2002). https://doi.org/10.1088/0954-3899/28/10/313
121. G. Cowan, K. Cranmer, E. Gross, O. Vitells, Asymptotic formulae for likelihood-based tests of new physics. Eur. Phys. J. C **71**, 1554 (2011). https://doi.org/10.1140/epjc/s10052-011-1554-0. arXiv:1007.1727 [physics.data-an] [Erratum: Eur. Phys. J. C 73, 2501 (2013). https://doi.org/10.1140/epjc/s10052-013-2501-z]
122. ATLAS Collaboration, ATLAS Computing Acknowledgements, ATL-SOFT-PUB-2023-001 (2023). https://cds.cern.ch/record/2869272

ATLAS Collaboration★

G. Aad[103], E. Aakvaag[16], B. Abbott[121], K. Abeling[55], N. J. Abicht[49], S. H. Abidi[29], M. Aboelela[44], A. Aboulhorma[35e], H. Abramowicz[152], H. Abreu[151], Y. Abulaiti[118], B. S. Acharya[69a,69b,l], A. Ackermann[63a], C. Adam Bourdarios[4], L. Adamczyk[86a], S. V. Addepalli[26], M. J. Addison[102], J. Adelman[116], A. Adiguzel[21c], T. Adye[135], A. A. Affolder[137], Y. Afik[39], M. N. Agaras[13], J. Agarwala[73a,73b], A. Aggarwal[101], C. Agheorghiesei[27c], A. Ahmad[36], F. Ahmadov[38,y], W. S. Ahmed[105], S. Ahuja[96], X. Ai[62e], G. Aielli[76a,76b], A. Aikot[164], M. Ait Tamlihat[35e], B. Aitbenchikh[35a], I. Aizenberg[170], M. Akbiyik[101], T. P. A. Åkesson[99], A. V. Akimov[37], D. Akiyama[169], N. N. Akolkar[24], S. Aktas[21a], K. Al Khoury[41], G. L. Alberghi[23b], J. Albert[166], P. Albicocco[53], G. L. Albouy[60], S. Alderweireldt[52], Z. L. Alegria[122], M. Aleksa[36], I. N. Aleksandrov[38], C. Alexa[27b], T. Alexopoulos[10], F. Alfonsi[23b], M. Algren[56], M. Alhroob[142], B. Ali[133], H. M. J. Ali[92], S. Ali[149], S. W. Alibocus[93], M. Aliev[33c], G. Alimonti[71a], W. Alkakhi[55], C. Allaire[66], B. M. M. Allbrooke[147], J. F. Allen[52], C. A. Allendes Flores[138f], P. P. Allport[20], A. Aloisio[72a,72b], F. Alonso[91], C. Alpigiani[139], M. Alvarez Estevez[100], A. Alvarez Fernandez[101], M. Alves Cardoso[56], M. G. Alviggi[72a,72b], M. Aly[102], Y. Amaral Coutinho[83b], A. Ambler[105], C. Amelung[36], M. Amerl[102], C. G. Ames[110], D. Amidei[107], K. J. Amirie[156], S. P. Amor Dos Santos[131a], K. R. Amos[164], S. An[84], V. Ananiev[126], C. Anastopoulos[140], T. Andeen[11], J. K. Anders[36], S. Y. Andrean[47a,47b], A. Andreazza[71a,71b], S. Angelidakis[9], A. Angerami[41,aa], A. V. Anisenkov[37], A. Annovi[74a], C. Antel[56], M. T. Anthony[140], E. Antipov[146], M. Antonelli[53], F. Anulli[75a], M. Aoki[84], T. Aoki[154], J. A. Aparisi Pozo[164], M. A. Aparo[147], L. Aperio Bella[48], C. Appelt[18], A. Apyan[26], S. J. Arbiol Val[87], C. Arcangeletti[53], A. T. H. Arce[51], E. Arena[93], J.-F. Arguin[109], S. Argyropoulos[54], J. -H. Arling[48], O. Arnaez[4], H. Arnold[115], G. Artoni[75a,75b], H. Asada[112], K. Asai[119], S. Asai[154], N. A. Asbah[36], K. Assamagan[29], R. Astalos[28a], K. S. V. Astrand[99], S. Atashi[160], R. J. Atkin[33a], M. Atkinson[163], H. Atmani[35f], P. A. Atmasiddha[129], K. Augsten[133], S. Auricchio[72a,72b], A. D. Auriol[20], V. A. Austrup[102], G. Avolio[36], K. Axiotis[56], G. Azuelos[109,ae], D. Babal[28b], H. Bachacou[136], K. Bachas[153,p], A. Bachiu[34], F. Backman[47a,47b], A. Badea[39], T. M. Baer[107], P. Bagnaia[75a,75b], M. Bahmani[18], D. Bahner[54], K. Bai[124], J. T. Baines[135], L. Baines[95], O. K. Baker[173], E. Bakos[15], D. Bakshi Gupta[8], V. Balakrishnan[121], R. Balasubramanian[115], E. M. Baldin[37], P. Balek[86a], E. Ballabene[23a,23b], F. Balli[136], L. M. Baltes[63a], W. K. Balunas[32], J. Balz[101], E. Banas[87], M. Bandieramonte[130], A. Bandyopadhyay[24], S. Bansal[24], L. Barak[152], M. Barakat[48], E. L. Barberio[106], D. Barberis[57a,57b], M. Barbero[103], M. Z. Barel[115], K. N. Barends[33a], T. Barillari[111], M.-S. Barisits[36], T. Barklow[144], P. Baron[123], D. A. Baron Moreno[102], A. Baroncelli[62a], G. Barone[29], A. J. Barr[127], J. D. Barr[97], F. Barreiro[100], J. Barreiro Guimarães da Costa[14a], U. Barron[152], M. G. Barros Teixeira[131a], S. Barsov[37], F. Bartels[63a], R. Bartoldus[144], A. E. Barton[92], P. Bartos[28a], A. Basan[101], M. Baselga[49], A. Bassalat[66,b], M. J. Basso[157a], R. Bate[165], R. L. Bates[59], S. Batlamous[35e], B. Batool[142], M. Battaglia[137], D. Battulga[18], M. Bauce[75a,75b], M. Bauer[36], P. Bauer[24], L. T. Bazzano Hurrell[30], J. B. Beacham[51], T. Beau[128], J. Y. Beaucamp[91], P. H. Beauchemin[159], P. Bechtle[24], H. P. Beck[19,o], K. Becker[168], A. J. Beddall[82], V. A. Bednyakov[38], C. P. Bee[146], L. J. Beemster[15], T. A. Beermann[36], M. Begalli[83d], M. Begel[29], A. Behera[146], J. K. Behr[48], J. F. Beirer[36], F. Beisiegel[24], M. Belfkir[117b], G. Bella[152], L. Bellagamba[23b], A. Bellerive[34], P. Bellos[20], K. Beloborodov[37], D. Benchekroun[35a], F. Bendebba[35a], Y. Benhammou[152], K. C. Benkendorfer[61], L. Beresford[48], M. Beretta[53], E. Bergeaas Kuutmann[162], N. Berger[4], B. Bergmann[133], J. Beringer[17a], G. Bernardi[5], C. Bernius[144], F. U. Bernlochner[24], F. Bernon[36,103], A. Berrocal Guardia[13], T. Berry[96], P. Berta[134], A. Berthold[50], S. Bethke[111], A. Betti[75a,75b], A. J. Bevan[95], N. K. Bhalla[54], M. Bhamjee[33c], S. Bhatta[146], D. S. Bhattacharya[167], P. Bhattarai[144], K. D. Bhide[54], V. S. Bhopatkar[122], R. M. Bianchi[130], G. Bianco[23a,23b], O. Biebel[110], R. Bielski[124], M. Biglietti[77a], C. S. Billingsley[44], M. Bindi[55], A. Bingul[21b], C. Bini[75a,75b], A. Biondini[93], C. J. Birch-sykes[102], G. A. Bird[32], M. Birman[170], M. Biros[134], S. Biryukov[147], T. Bisanz[49], E. Bisceglie[43a,43b], J. P. Biswal[135], D. Biswas[142], K. Bjørke[126], I. Bloch[48], A. Blue[59], U. Blumenschein[95], J. Blumenthal[101], V. S. Bobrovnikov[37], M. Boehler[54], B. Boehm[167], D. Bogavac[36], A. G. Bogdanchikov[37], C. Bohm[47a], V. Boisvert[96], P. Bokan[36], T. Bold[86a], M. Bomben[5], M. Bona[95], M. Boonekamp[136], C. D. Booth[96], A. G. Borbély[59], I. S. Bordulev[37], H. M. Borecka-Bielska[109], G. Borissov[92], D. Bortoletto[127], D. Boscherini[23b], M. Bosman[13], J. D. Bossio Sola[36], K. Bouaouda[35a], N. Bouchhar[164], J. Boudreau[130], E. V. Bouhova-Thacker[92], D. Boumediene[40], R. Bouquet[57a,57b], A. Boveia[120], J. Boyd[36], D. Boye[29], I. R. Boyko[38], J. Bracinik[20], N. Brahimi[4], G. Brandt[172], O. Brandt[32], F. Braren[48], B. Brau[104], J. E. Brau[124], R. Brener[170], L. Brenner[115], R. Brenner[162],

S. Bressler[170], D. Britton[59], D. Britzger[111], I. Brock[24], G. Brooijmans[41], E. Brost[29], L. M. Brown[166], L. E. Bruce[61], T. L. Bruckler[127], P. A. Bruckman de Renstrom[87], B. Brüers[48], A. Bruni[23b], G. Bruni[23b], M. Bruschi[23b], N. Bruscino[75a,75b], T. Buanes[16], Q. Buat[139], D. Buchin[111], A. G. Buckley[59], O. Bulekov[37], B. A. Bullard[144], S. Burdin[93], C. D. Burgard[49], A. M. Burger[36], B. Burghgrave[8], O. Burlayenko[54], J. T. P. Burr[32], C. D. Burton[11], J. C. Burzynski[143], E. L. Busch[41], V. Büscher[101], P. J. Bussey[59], J. M. Butler[25], C. M. Buttar[59], J. M. Butterworth[97], W. Buttinger[135], C. J. Buxo Vazquez[108], A. R. Buzykaev[37], S. Cabrera Urbán[164], L. Cadamuro[66], D. Caforio[58], H. Cai[130], Y. Cai[14a,14e], Y. Cai[14c], V. M. M. Cairo[36], O. Cakir[3a], N. Calace[36], P. Calafiura[17a], G. Calderini[128], P. Calfayan[68], G. Callea[59], L. P. Caloba[83b], D. Calvet[40], S. Calvet[40], M. Calvetti[74a,74b], R. Camacho Toro[128], S. Camarda[36], D. Camarero Munoz[26], P. Camarri[76a,76b], M. T. Camerlingo[72a,72b], D. Cameron[36], C. Camincher[166], M. Campanelli[97], A. Camplani[42], V. Canale[72a,72b], A. C. Canbay[3a], E. Canonero[96], J. Cantero[164], Y. Cao[163], F. Capocasa[26], M. Capua[43a,43b], A. Carbone[71a,71b], R. Cardarelli[76a], J. C. J. Cardenas[8], F. Cardillo[164], G. Carducci[43a,43b], T. Carli[36], G. Carlino[72a], J. I. Carlotto[13], B. T. Carlson[130,q], E. M. Carlson[157a,166], L. Carminati[71a,71b], A. Carnelli[136], M. Carnesale[75a,75b], S. Caron[114], E. Carquin[138f], S. Carrá[71a], G. Carratta[23a,23b], A. M. Carroll[124], T. M. Carter[52], M. P. Casado[13,i], M. Caspar[48], F. L. Castillo[4], L. Castillo Garcia[13], V. Castillo Gimenez[164], N. F. Castro[131a,131e], A. Catinaccio[36], J. R. Catmore[126], T. Cavaliere[4], V. Cavaliere[29], N. Cavalli[23a,23b], Y. C. Cekmecelioglu[48], E. Celebi[21a], S. Cella[36], F. Celli[127], M. S. Centonze[70a,70b], V. Cepaitis[56], K. Cerny[123], A. S. Cerqueira[83a], A. Cerri[147], L. Cerrito[76a,76b], F. Cerutti[17a], B. Cervato[142], A. Cervelli[23b], G. Cesarini[53], S. A. Cetin[82], D. Chakraborty[116], J. Chan[17a], W. Y. Chan[154], J. D. Chapman[32], E. Chapon[136], B. Chargeishvili[150b], D. G. Charlton[20], M. Chatterjee[19], C. Chauhan[134], Y. Che[14c], S. Chekanov[6], S. V. Chekulaev[157a], G. A. Chelkov[38,a], A. Chen[107], B. Chen[152], B. Chen[166], H. Chen[14c], H. Chen[29], J. Chen[62c], J. Chen[143], M. Chen[127], S. Chen[154], S. J. Chen[14c], X. Chen[62c,136], X. Chen[14b,ad], Y. Chen[62a], C. L. Cheng[171], H. C. Cheng[64a], S. Cheong[144], A. Cheplakov[38], E. Cheremushkina[48], E. Cherepanova[115], R. Cherkaoui El Moursli[35e], E. Cheu[7], K. Cheung[65], L. Chevalier[136], V. Chiarella[53], G. Chiarelli[74a], N. Chiedde[103], G. Chiodini[70a], A. S. Chisholm[20], A. Chitan[27b], M. Chitishvili[164], M. V. Chizhov[38], K. Choi[11], Y. Chou[139], E. Y. S. Chow[114], K. L. Chu[170], M. C. Chu[64a], X. Chu[14a,14e], J. Chudoba[132], J. J. Chwastowski[87], D. Cieri[111], K. M. Ciesla[86a], V. Cindro[94], A. Ciocio[17a], F. Cirotto[72a,72b], Z. H. Citron[170], M. Citterio[71a], D. A. Ciubotaru[27b], A. Clark[56], P. J. Clark[52], C. Clarry[156], J. M. Clavijo Columbie[48], S. E. Clawson[48], C. Clement[47a,47b], J. Clercx[48], Y. Coadou[103], M. Cobal[69a,69c], A. Coccaro[57b], R. F. Coelho Barrue[131a], R. Coelho Lopes De Sa[104], S. Coelli[71a], B. Cole[41], J. Collot[60], P. Conde Muiño[131a,131g], M. P. Connell[33c], S. H. Connell[33c], E. I. Conroy[127], F. Conventi[72a,af], H. G. Cooke[20], A. M. Cooper-Sarkar[127], F. A. Corchia[23a,23b], A. Cordeiro Oudot Choi[128], L. D. Corpe[40], M. Corradi[75a,75b], F. Corriveau[105,w], A. Cortes-Gonzalez[18], M. J. Costa[164], F. Costanza[4], D. Costanzo[140], B. M. Cote[120], G. Cowan[96], K. Cranmer[171], D. Cremonini[23a,23b], S. Crépé-Renaudin[60], F. Crescioli[128], M. Cristinziani[142], M. Cristoforetti[78a,78b], V. Croft[115], J. E. Crosby[122], G. Crosetti[43a,43b], A. Cueto[100], H. Cui[14a,14e], Z. Cui[7], W. R. Cunningham[59], F. Curcio[164], J. R. Curran[52], P. Czodrowski[36], M. M. Czurylo[36], M. J. Da Cunha Sargedas De Sousa[57a,57b], J. V. Da Fonseca Pinto[83b], C. Da Via[102], W. Dabrowski[86a], T. Dado[49], S. Dahbi[149], T. Dai[107], D. Dal Santo[19], C. Dallapiccola[104], M. Dam[42], G. D'amen[29], V. D'Amico[110], J. Damp[101], J. R. Dandoy[34], M. Danninger[143], V. Dao[36], G. Darbo[57b], S. J. Das[29,ag], F. Dattola[48], S. D'Auria[71a,71b], A. D'avanzo[72a,72b], C. David[33a], T. Davidek[134], B. Davis-Purcell[34], I. Dawson[95], H. A. Day-hall[133], K. De[8], R. De Asmundis[72a], N. De Biase[48], S. De Castro[23a,23b], N. De Groot[114], P. de Jong[115], H. De la Torre[116], A. De Maria[14c], A. De Salvo[75a], U. De Sanctis[76a,76b], F. De Santis[70a,70b], A. De Santo[147], J. B. De Vivie De Regie[60], D. V. Dedovich[38], J. Degens[93], A. M. Deiana[44], F. Del Corso[23a,23b], J. Del Peso[100], F. Del Rio[63a], L. Delagrange[128], F. Deliot[136], C. M. Delitzsch[49], M. Della Pietra[72a,72b], D. Della Volpe[56], A. Dell'Acqua[36], L. Dell'Asta[71a,71b], M. Delmastro[4], P. A. Delsart[60], S. Demers[173], M. Demichev[38], S. P. Denisov[37], L. D'Eramo[40], D. Derendarz[87], F. Derue[128], P. Dervan[93], K. Desch[24], C. Deutsch[24], F. A. Di Bello[57a,57b], A. Di Ciaccio[76a,76b], L. Di Ciaccio[4], A. Di Domenico[75a,75b], C. Di Donato[72a,72b], A. Di Girolamo[36], G. Di Gregorio[36], A. Di Luca[78a,78b], B. Di Micco[77a,77b], R. Di Nardo[77a,77b], M. Diamantopoulou[34], F. A. Dias[115], T. Dias Do Vale[143], M. A. Diaz[138a,138b], F. G. Diaz Capriles[24], M. Didenko[164], E. B. Diehl[107], S. Díez Cornell[48], C. Diez Pardos[142], C. Dimitriadi[24,162], A. Dimitrievska[20], J. Dingfelder[24], I.-M. Dinu[27b], S. J. Dittmeier[63b], F. Dittus[36], M. Divisek[134], F. Djama[103], T. Djobava[150b], C. Doglioni[99,102], A. Dohnalova[28a], J. Dolejsi[134], Z. Dolezal[134], K. M. Dona[39], M. Donadelli[83c], B. Dong[108], J. Donini[40],

A. D'Onofrio[72a,72b], M. D'Onofrio[93], J. Dopke[135], A. Doria[72a], N. Dos Santos Fernandes[131a], P. Dougan[102], M. T. Dova[91], A. T. Doyle[59], M. A. Draguet[127], E. Dreyer[170], I. Drivas-koulouris[10], M. Drnevich[118], M. Drozdova[56], D. Du[62a], T. A. du Pree[115], F. Dubinin[37], M. Dubovsky[28a], E. Duchovni[170], G. Duckeck[110], O. A. Ducu[27b], D. Duda[52], A. Dudarev[36], E. R. Duden[26], M. D'uffizi[102], L. Duflot[66], M. Dührssen[36], I. Duminica[27g], A. E. Dumitriu[27b], M. Dunford[63a], S. Dungs[49], K. Dunne[47a,47b], A. Duperrin[103], H. Duran Yildiz[3a], M. Düren[58], A. Durglishvili[150b], B. L. Dwyer[116], G. I. Dyckes[17a], M. Dyndal[86a], B. S. Dziedzic[87], Z. O. Earnshaw[147], G. H. Eberwein[127], B. Eckerova[28a], S. Eggebrecht[55], E. Egidio Purcino De Souza[128], L. F. Ehrke[56], G. Eigen[16], K. Einsweiler[17a], T. Ekelof[162], P. A. Ekman[99], S. El Farkh[35b], Y. El Ghazali[35b], H. El Jarrari[36], A. El Moussaouy[109], V. Ellajosyula[162], M. Ellert[162], F. Ellinghaus[172], N. Ellis[36], J. Elmsheuser[29], M. Elsawy[117a], M. Elsing[36], D. Emeliyanov[135], Y. Enari[154], I. Ene[17a], S. Epari[13], P. A. Erland[87], M. Errenst[172], M. Escalier[66], C. Escobar[164], E. Etzion[152], G. Evans[131a], H. Evans[68], L. S. Evans[96], A. Ezhilov[37], S. Ezzarqtouni[35a], F. Fabbri[23a,23b], L. Fabbri[23a,23b], G. Facini[97], V. Fadeyev[137], R. M. Fakhrutdinov[37], D. Fakoudis[101], S. Falciano[75a], L. F. Falda Ulhoa Coelho[36], P. J. Falke[24], F. Fallavollita[111], J. Faltova[134], C. Fan[163], Y. Fan[14a], Y. Fang[14a,14e], M. Fanti[71a,71b], M. Faraj[69a,69b], Z. Farazpay[98], A. Farbin[8], A. Farilla[77a], T. Farooque[108], S. M. Farrington[52], F. Fassi[35e], D. Fassouliotis[9], M. Faucci Giannelli[76a,76b], W. J. Fawcett[32], L. Fayard[66], P. Federic[134], P. Federicova[132], O. L. Fedin[37,a], M. Feickert[171], L. Feligioni[103], D. E. Fellers[124], C. Feng[62b], M. Feng[14b], Z. Feng[115], M. J. Fenton[160], L. Ferencz[48], R. A. M. Ferguson[92], S. I. Fernandez Luengo[138f], P. Fernandez Martinez[13], M. J. V. Fernoux[103], J. Ferrando[92], A. Ferrari[162], P. Ferrari[114,115], R. Ferrari[73a], D. Ferrere[56], C. Ferretti[107], F. Fiedler[101], P. Fiedler[133], A. Filipčič[94], E. K. Filmer[1], F. Filthaut[114], M. C. N. Fiolhais[131a,131c,c], L. Fiorini[164], W. C. Fisher[108], T. Fitschen[102], P. M. Fitzhugh[136], I. Fleck[142], P. Fleischmann[107], T. Flick[172], M. Flores[33d,ab], L. R. Flores Castillo[64a], L. Flores Sanz De Acedo[36], F. M. Follega[78a,78b], N. Fomin[16], J. H. Foo[156], A. Formica[136], A. C. Forti[102], E. Fortin[36], A. W. Fortman[17a], M. G. Foti[17a], L. Fountas[9,j], D. Fournier[66], H. Fox[92], P. Francavilla[74a,74b], S. Francescato[61], S. Franchellucci[56], M. Franchini[23a,23b], S. Franchino[63a], D. Francis[36], L. Franco[114], V. Franco Lima[36], L. Franconi[48], M. Franklin[61], G. Frattari[26], W. S. Freund[83b], Y. Y. Frid[152], J. Friend[59], N. Fritzsche[50], A. Froch[54], D. Froidevaux[36], J. A. Frost[127], Y. Fu[62a], S. Fuenzalida Garrido[138f], M. Fujimoto[103], K. Y. Fung[64a], E. Furtado De Simas Filho[83e], M. Furukawa[154], J. Fuster[164], A. Gabrielli[23a,23b], A. Gabrielli[156], P. Gadow[36], G. Gagliardi[57a,57b], L. G. Gagnon[17a], S. Gaid[161], S. Galantzan[152], E. J. Gallas[127], B. J. Gallop[135], K. K. Gan[120], S. Ganguly[154], Y. Gao[52], F. M. Garay Walls[138a,138b], B. Garcia[29], C. García[164], A. Garcia Alonso[115], A. G. Garcia Caffaro[173], J. E. García Navarro[164], M. Garcia-Sciveres[17a], G. L. Gardner[129], R. W. Gardner[39], N. Garelli[159], D. Garg[80], R. B. Garg[144,m], J. M. Gargan[52], C. A. Garner[156], C. M. Garvey[33a], P. Gaspar[83b], V. K. Gassmann[159], G. Gaudio[73a], V. Gautam[13], P. Gauzzi[75a,75b], I. L. Gavrilenko[37], A. Gavrilyuk[37], C. Gay[165], G. Gaycken[48], E. N. Gazis[10], A. A. Geanta[27b], C. M. Gee[137], A. Gekow[120], C. Gemme[57b], M. H. Genest[60], A. D. Gentry[113], S. George[96], W. F. George[20], T. Geralis[46], P. Gessinger-Befurt[36], M. E. Geyik[172], M. Ghani[168], K. Ghorbanian[95], A. Ghosal[142], A. Ghosh[160], A. Ghosh[7], B. Giacobbe[23b], S. Giagu[75a,75b], T. Giani[115], P. Giannetti[74a], A. Giannini[62a], S. M. Gibson[96], M. Gignac[137], D. T. Gil[86b], A. K. Gilbert[86a], B. J. Gilbert[41], D. Gillberg[34], G. Gilles[115], L. Ginabat[128], D. M. Gingrich[2,ae], M. P. Giordani[69a,69c], P. F. Giraud[136], G. Giugliarelli[69a,69c], D. Giugni[71a], F. Giuli[36], I. Gkialas[9,j], L. K. Gladilin[37], C. Glasman[100], G. R. Gledhill[124], G. Glemža[48], M. Glisic[124], I. Gnesi[43b,f], Y. Go[29], M. Goblirsch-Kolb[36], B. Gocke[49], D. Godin[109], B. Gokturk[21a], S. Goldfarb[106], T. Golling[56], M. G. D. Gololo[33g], D. Golubkov[37], J. P. Gombas[108], A. Gomes[131a,131b], G. Gomes Da Silva[142], A. J. Gomez Delegido[164], R. Gonçalo[131a,131c], L. Gonella[20], A. Gongadze[150c], F. Gonnella[20], J. L. Gonski[144], R. Y. González Andana[52], S. González de la Hoz[164], R. Gonzalez Lopez[93], C. Gonzalez Renteria[17a], M. V. Gonzalez Rodrigues[48], R. Gonzalez Suarez[162], S. Gonzalez-Sevilla[56], L. Goossens[36], B. Gorini[36], E. Gorini[70a,70b], A. Gorišek[94], T. C. Gosart[129], A. T. Goshaw[51], M. I. Gostkin[38], S. Goswami[122], C. A. Gottardo[36], S. A. Gotz[110], M. Gouighri[35b], V. Goumarre[48], A. G. Goussiou[139], N. Govender[33c], I. Grabowska-Bold[86a], K. Graham[34], E. Gramstad[126], S. Grancagnolo[70a,70b], C. M. Grant[1,136], P. M. Gravila[27f], F. G. Gravili[70a,70b], H. M. Gray[17a], M. Greco[70a,70b], C. Grefe[24], I. M. Gregor[48], K. T. Greif[160], P. Grenier[144], S. G. Grewe[111], A. A. Grillo[137], K. Grimm[31], S. Grinstein[13,s], J. -F. Grivaz[66], E. Gross[170], J. Grosse-Knetter[55], J. C. Grundy[127], L. Guan[107], C. Gubbels[165], J. G. R. Guerrero Rojas[164], G. Guerrieri[69a,69c], F. Guescini[111], R. Gugel[101], J. A. M. Guhit[107], A. Guida[18], E. Guilloton[168], S. Guindon[36], F. Guo[14a,14e], J. Guo[62c], L. Guo[48], Y. Guo[107], R. Gupta[48], R. Gupta[130], S. Gurbuz[24], S. S. Gurdasani[54], G. Gustavino[36], M. Guth[56],

P. Gutierrez[121], L. F. Gutierrez Zagazeta[129], M. Gutsche[50], C. Gutschow[97], C. Gwenlan[127], C. B. Gwilliam[93], E. S. Haaland[126], A. Haas[118], M. Habedank[48], C. Haber[17a], H. K. Hadavand[8], A. Hadef[50], S. Hadzic[111], A. I. Hagan[92], J. J. Hahn[142], E. H. Haines[97], M. Haleem[167], J. Haley[122], J. J. Hall[140], G. D. Hallewell[103], L. Halser[19], K. Hamano[166], M. Hamer[24], G. N. Hamity[52], E. J. Hampshire[96], J. Han[62b], K. Han[62a], L. Han[14c], L. Han[62a], S. Han[17a], Y. F. Han[156], K. Hanagaki[84], M. Hance[137], D. A. Hangal[41], H. Hanif[143], M. D. Hank[129], J. B. Hansen[42], P. H. Hansen[42], K. Hara[158], D. Harada[56], T. Harenberg[172], S. Harkusha[37], M. L. Harris[104], Y. T. Harris[127], J. Harrison[13], N. M. Harrison[120], P. F. Harrison[168], N. M. Hartman[111], N. M. Hartmann[110], Y. Hasegawa[141], S. Hassan[16], R. Hauser[108], C. M. Hawkes[20], R. J. Hawkings[36], Y. Hayashi[154], S. Hayashida[112], D. Hayden[108], C. Hayes[107], R. L. Hayes[115], C. P. Hays[127], J. M. Hays[95], H. S. Hayward[93], F. He[62a], M. He[14a,14e], Y. He[155], Y. He[48], Y. He[97], N. B. Heatley[95], V. Hedberg[99], A. L. Heggelund[126], N. D. Hehir[95,*], C. Heidegger[54], K. K. Heidegger[54], W. D. Heidorn[81], J. Heilman[34], S. Heim[48], T. Heim[17a], J. G. Heinlein[129], J. J. Heinrich[124], L. Heinrich[111,ac], J. Hejbal[132], A. Held[171], S. Hellesund[16], C. M. Helling[165], S. Hellman[47a,47b], R. C. W. Henderson[92], L. Henkelmann[32], A. M. Henriques Correia[36], H. Herde[99], Y. Hernández Jiménez[146], L. M. Herrmann[24], T. Herrmann[50], G. Herten[54], R. Hertenberger[110], L. Hervas[36], M. E. Hesping[101], N. P. Hessey[157a], E. Hill[156], S. J. Hillier[20], J. R. Hinds[108], F. Hinterkeuser[24], M. Hirose[125], S. Hirose[158], D. Hirschbuehl[172], T. G. Hitchings[102], B. Hiti[94], J. Hobbs[146], R. Hobincu[27e], N. Hod[170], M. C. Hodgkinson[140], B. H. Hodkinson[127], A. Hoecker[36], D. D. Hofer[107], J. Hofer[48], T. Holm[24], M. Holzbock[111], L. B. A. H. Hommels[32], B. P. Honan[102], J. Hong[62c], T. M. Hong[130], B. H. Hooberman[163], W. H. Hopkins[6], Y. Horii[112], S. Hou[149], A. S. Howard[94], J. Howarth[59], J. Hoya[6], M. Hrabovsky[123], A. Hrynevich[48], T. Hryn'ova[4], P. J. Hsu[65], S. -C. Hsu[139], T. Hsu[66], M. Hu[17a], Q. Hu[62a], S. Huang[64b], X. Huang[14a,14e], Y. Huang[140], Y. Huang[101], Y. Huang[14a], Z. Huang[102], Z. Hubacek[133], M. Huebner[24], F. Huegging[24], T. B. Huffman[127], C. A. Hugli[48], M. Huhtinen[36], S. K. Huiberts[16], R. Hulsken[105], N. Huseynov[12], J. Huston[108], J. Huth[61], R. Hyneman[144], G. Iacobucci[56], G. Iakovidis[29], I. Ibragimov[142], L. Iconomidou-Fayard[66], J. P. Iddon[36], P. Iengo[72a,72b], R. Iguchi[154], T. Iizawa[127], Y. Ikegami[84], N. Ilic[156], H. Imam[35a], M. Ince Lezki[56], T. Ingebretsen Carlson[47a,47b], G. Introzzi[73a,73b], M. Iodice[77a], V. Ippolito[75a,75b], R. K. Irwin[93], M. Ishino[154], W. Islam[171], C. Issever[18,48], S. Istin[21a,ai], H. Ito[169], R. Iuppa[78a,78b], A. Ivina[170], J. M. Izen[45], V. Izzo[72a], P. Jacka[132,133], P. Jackson[1], B. P. Jaeger[143], C. S. Jagfeld[110], G. Jain[157a], P. Jain[54], K. Jakobs[54], T. Jakoubek[170], J. Jamieson[59], K. W. Janas[86a], M. Javurkova[104], L. Jeanty[124], J. Jejelava[150a,z], P. Jenni[54,g], C. E. Jessiman[34], C. Jia[62b], J. Jia[146], X. Jia[61], X. Jia[14a,14e], Z. Jia[14c], C. Jiang[52], S. Jiggins[48], J. Jimenez Pena[13], S. Jin[14c], A. Jinaru[27b], O. Jinnouchi[155], P. Johansson[140], K. A. Johns[7], J. W. Johnson[137], D. M. Jones[147], E. Jones[48], P. Jones[32], R. W. L. Jones[92], T. J. Jones[93], H. L. Joos[36,55], R. Joshi[120], J. Jovicevic[15], X. Ju[17a], J. J. Junggeburth[104], T. Junkermann[63a], A. Juste Rozas[13,s], M. K. Juzek[87], S. Kabana[138e], A. Kaczmarska[87], M. Kado[111], H. Kagan[120], M. Kagan[144], A. Kahn[41], A. Kahn[129], C. Kahra[101], T. Kaji[154], E. Kajomovitz[151], N. Kakati[170], I. Kalaitzidou[54], C. W. Kalderon[29], N. J. Kang[137], D. Kar[33g], K. Karava[127], M. J. Kareem[157b], E. Karentzos[54], I. Karkanias[153], O. Karkout[115], S. N. Karpov[38], Z. M. Karpova[38], V. Kartvelishvili[92], A. N. Karyukhin[37], E. Kasimi[153], J. Katzy[48], S. Kaur[34], K. Kawade[141], M. P. Kawale[121], C. Kawamoto[88], T. Kawamoto[62a], E. F. Kay[36], F. I. Kaya[159], S. Kazakos[108], V. F. Kazanin[37], Y. Ke[146], J. M. Keaveney[33a], R. Keeler[166], G. V. Kehris[61], J. S. Keller[34], A. S. Kelly[97], J. J. Kempster[147], P. D. Kennedy[101], O. Kepka[132], B. P. Kerridge[135], S. Kersten[172], B. P. Kerševan[94], L. Keszeghova[28a], S. Ketabchi Haghighat[156], R. A. Khan[130], A. Khanov[122], A. G. Kharlamov[37], T. Kharlamova[37], E. E. Khoda[139], M. Kholodenko[37], T. J. Khoo[18], G. Khoriauli[167], J. Khubua[150b], Y. A. R. Khwaira[66], B. Kibirige[33g], A. Kilgallon[124], D. W. Kim[47a,47b], Y. K. Kim[39], N. Kimura[97], M. K. Kingston[55], A. Kirchhoff[55], C. Kirfel[24], F. Kirfel[24], J. Kirk[135], A. E. Kiryunin[111], C. Kitsaki[10], O. Kivernyk[24], M. Klassen[159], C. Klein[34], L. Klein[167], M. H. Klein[44], S. B. Klein[56], U. Klein[93], P. Klimek[36], A. Klimentov[29], T. Klioutchnikova[36], P. Kluit[115], S. Kluth[111], E. Kneringer[79], T. M. Knight[156], A. Knue[49], R. Kobayashi[88], D. Kobylianskii[170], S. F. Koch[127], M. Kocian[144], P. Kodyš[134], D. M. Koeck[124], P. T. Koenig[24], T. Koffas[34], O. Kolay[50], I. Koletsou[4], T. Komarek[123], K. Köneke[54], A. X. Y. Kong[1], T. Kono[119], N. Konstantinidis[97], P. Kontaxakis[56], B. Konya[99], R. Kopeliansky[41], S. Koperny[86a], K. Korcyl[87], K. Kordas[153,e], A. Korn[97], S. Korn[55], I. Korolkov[13], N. Korotkova[37], B. Kortman[115], O. Kortner[111], S. Kortner[111], W. H. Kostecka[116], V. V. Kostyukhin[142], A. Kotsokechagia[136], A. Kotwal[51], A. Koulouris[36], A. Kourkoumeli-Charalampidi[73a,73b], C. Kourkoumelis[9], E. Kourlitis[111,ac], O. Kovanda[124], R. Kowalewski[166], W. Kozanecki[136], A. S. Kozhin[37], V. A. Kramarenko[37], G. Kramberger[94], P. Kramer[101],

M. W. Krasny[128], A. Krasznahorkay[36], J. W. Kraus[172], J. A. Kremer[48], T. Kresse[50], J. Kretzschmar[93], K. Kreul[18], P. Krieger[156], S. Krishnamurthy[104], M. Krivos[134], K. Krizka[20], K. Kroeninger[49], H. Kroha[111], J. Kroll[132], J. Kroll[129], K. S. Krowpman[108], U. Kruchonak[38], H. Krüger[24], N. Krumnack[81], M. C. Kruse[51], O. Kuchinskaia[37], S. Kuday[3a], S. Kuehn[36], R. Kuesters[54], T. Kuhl[48], V. Kukhtin[38], Y. Kulchitsky[37,a], S. Kuleshov[138b,138d], M. Kumar[33g], N. Kumari[48], P. Kumari[157b], A. Kupco[132], T. Kupfer[49], A. Kupich[37], O. Kuprash[54], H. Kurashige[85], L. L. Kurchaninov[157a], O. Kurdysh[66], Y. A. Kurochkin[37], A. Kurova[37], M. Kuze[155], A. K. Kvam[104], J. Kvita[123], T. Kwan[105], N. G. Kyriacou[107], L. A. O. Laatu[103], C. Lacasta[164], F. Lacava[75a,75b], H. Lacker[18], D. Lacour[128], N. N. Lad[97], E. Ladygin[38], A. Lafarge[40], B. Laforge[128], T. Lagouri[173], F. Z. Lahbabi[35a], S. Lai[55], I. K. Lakomiec[86a], J. E. Lambert[166], S. Lammers[68], W. Lampl[7], C. Lampoudis[153,e], G. Lamprinoudis[101], A. N. Lancaster[116], E. Lançon[29], U. Landgraf[54], M. P. J. Landon[95], V. S. Lang[54], O. K. B. Langrekken[126], A. J. Lankford[160], F. Lanni[36], K. Lantzsch[24], A. Lanza[73a], A. Lapertosa[57a,57b], J. F. Laporte[136], T. Lari[71a], F. Lasagni Manghi[23b], M. Lassnig[36], V. Latonova[132], A. Laudrain[101], A. Laurier[151], S. D. Lawlor[140], Z. Lawrence[102], R. Lazaridou[168], M. Lazzaroni[71a,71b], B. Le[102], E. M. Le Boulicaut[51], L. T. Le Pottier[17a], B. Leban[23a,23b], A. Lebedev[81], M. LeBlanc[102], F. Ledroit-Guillon[60], A. C. A. Lee[97], S. C. Lee[149], S. Lee[47a,47b], T. F. Lee[93], L. L. Leeuw[33c], H. P. Lefebvre[96], M. Lefebvre[166], C. Leggett[17a], G. Lehmann Miotto[36], M. Leigh[56], W. A. Leight[104], W. Leinonen[114], A. Leisos[153,r], M. A. L. Leite[83c], C. E. Leitgeb[18], R. Leitner[134], K. J. C. Leney[44], T. Lenz[24], S. Leone[74a], C. Leonidopoulos[52], A. Leopold[145], C. Leroy[109], R. Les[108], C. G. Lester[32], M. Levchenko[37], J. Levêque[4], L. J. Levinson[170], G. Levrini[23a,23b], M. P. Lewicki[87], C. Lewis[139], D. J. Lewis[4], A. Li[5], B. Li[62b], C. Li[62a], C.-Q. Li[111], H. Li[62a], H. Li[62b], H. Li[14c], H. Li[14b], H. Li[62b], J. Li[62c], K. Li[139], L. Li[62c], M. Li[14a,14e], Q. Y. Li[62a], S. Li[14a,14e], S. Li[62c,62d,d], T. Li[5], X. Li[105], Z. Li[127], Z. Li[154], Z. Li[14a,14e], S. Liang[14a,14e], Z. Liang[14a], M. Liberatore[136], B. Liberti[76a], K. Lie[64c], J. Lieber Marin[83e], H. Lien[68], K. Lin[108], R. E. Lindley[7], J. H. Lindon[2], E. Lipeles[129], A. Lipniacka[16], A. Lister[165], J. D. Little[4], B. Liu[14a], B. X. Liu[143], D. Liu[62c,62d], E. H. L. Liu[20], J. B. Liu[62a], J. K. K. Liu[32], K. Liu[62d], K. Liu[62c,62d], M. Liu[62a], M. Y. Liu[62a], P. Liu[14a], Q. Liu[62c,62d,139], X. Liu[62a], X. Liu[62b], Y. Liu[14d,14e], Y. L. Liu[62b], Y. W. Liu[62a], J. Llorente Merino[143], S. L. Lloyd[95], E. M. Lobodzinska[48], P. Loch[7], T. Lohse[18], K. Lohwasser[140], E. Loiacono[48], M. Lokajicek[132,*], J. D. Lomas[20], J. D. Long[163], I. Longarini[160], L. Longo[70a,70b], R. Longo[163], I. Lopez Paz[67], A. Lopez Solis[48], N. Lorenzo Martinez[4], A. M. Lory[110], G. Löschcke Centeno[147], O. Loseva[37], X. Lou[47a,47b], X. Lou[14a,14e], A. Lounis[66], P. A. Love[92], G. Lu[14a,14e], M. Lu[66], S. Lu[129], Y. J. Lu[65], H. J. Lubatti[139], C. Luci[75a,75b], F. L. Lucio Alves[14c], F. Luehring[68], I. Luise[146], O. Lukianchuk[66], O. Lundberg[145], B. Lund-Jensen[145,*], N. A. Luongo[6], M. S. Lutz[36], A. B. Lux[25], D. Lynn[29], R. Lysak[132], E. Lytken[99], V. Lyubushkin[38], T. Lyubushkina[38], M. M. Lyukova[146], M. Firdaus M. Soberi[52], H. Ma[29], K. Ma[62a], L. L. Ma[62b], W. Ma[62a], Y. Ma[122], D. M. Mac Donell[166], G. Maccarrone[53], J. C. MacDonald[101], P. C. Machado De Abreu Farias[83e], R. Madar[40], T. Madula[97], J. Maeda[85], T. Maeno[29], H. Maguire[140], V. Maiboroda[136], A. Maio[131a,131b,131d], K. Maj[86a], O. Majersky[48], S. Majewski[124], N. Makovec[66], V. Maksimovic[15], B. Malaescu[128], Pa. Malecki[87], V. P. Maleev[37], F. Malek[60,n], M. Mali[94], D. Malito[96], U. Mallik[80], S. Maltezos[10], S. Malyukov[38], J. Mamuzic[13], G. Mancini[53], M. N. Mancini[26], G. Manco[73a,73b], J. P. Mandalia[95], I. Mandić[94], L. Manhaes de Andrade Filho[83a], I. M. Maniatis[170], J. Manjarres Ramos[90], D. C. Mankad[170], A. Mann[110], S. Manzoni[36], L. Mao[62c], X. Mapekula[33c], A. Marantis[153,r], G. Marchiori[5], M. Marcisovsky[132], C. Marcon[71a], M. Marinescu[20], S. Marium[48], M. Marjanovic[121], A. Markhoos[54], M. Markovitch[66], E. J. Marshall[92], Z. Marshall[17a], S. Marti-Garcia[164], T. A. Martin[168], V. J. Martin[52], B. Martin dit Latour[16], L. Martinelli[75a,75b], M. Martinez[13,s], P. Martinez Agullo[164], V. I. Martinez Outschoorn[104], P. Martinez Suarez[13], S. Martin-Haugh[135], G. Martinovicova[134], V. S. Martoiu[27b], A. C. Martyniuk[97], A. Marzin[36], D. Mascione[78a,78b], L. Masetti[101], T. Mashimo[154], J. Masik[102], A. L. Maslennikov[37], P. Massarotti[72a,72b], P. Mastrandrea[74a,74b], A. Mastroberardino[43a,43b], T. Masubuchi[154], T. Mathisen[162], J. Matousek[134], N. Matsuzawa[154], J. Maurer[27b], A. J. Maury[66], B. Maček[94], D. A. Maximov[37], A. E. May[102], R. Mazini[149], I. Maznas[116], M. Mazza[108], S. M. Mazza[137], E. Mazzeo[71a,71b], C. Mc Ginn[29], J. P. Mc Gowan[166], S. P. Mc Kee[107], C. C. McCracken[165], E. F. McDonald[106], A. E. McDougall[115], J. A. Mcfayden[147], R. P. McGovern[129], G. Mchedlidze[150b], R. P. Mckenzie[33g], T. C. Mclachlan[48], D. J. Mclaughlin[97], S. J. McMahon[135], C. M. Mcpartland[93], R. A. McPherson[166,w], S. Mehlhase[110], A. Mehta[93], D. Melini[164], B. R. Mellado Garcia[33g], A. H. Melo[55], F. Meloni[48], A. M. Mendes Jacques Da Costa[102], H. Y. Meng[156], L. Meng[92], S. Menke[111], M. Mentink[36], E. Meoni[43a,43b], G. Mercado[116], C. Merlassino[69a,69c], L. Merola[72a,72b], C. Meroni[71a,71b], J. Metcalfe[6],

A. S. Mete[6], C. Meyer[68], J.-P. Meyer[136], R. P. Middleton[135], L. Mijović[52], G. Mikenberg[170], M. Mikestikova[132], M. Mikuž[94], H. Mildner[101], A. Milic[36], D. W. Miller[39], E. H. Miller[144], L. S. Miller[34], A. Milov[170], D. A. Milstead[47a,47b], T. Min[14c], A. A. Minaenko[37], I. A. Minashvili[150b], L. Mince[59], A. I. Mincer[118], B. Mindur[86a], M. Mineev[38], Y. Mino[88], L. M. Mir[13], M. Miralles Lopez[59], M. Mironova[17a], A. Mishima[154], M. C. Missio[114], A. Mitra[168], V. A. Mitsou[164], Y. Mitsumori[112], O. Miu[156], P. S. Miyagawa[95], T. Mkrtchyan[63a], M. Mlinarevic[97], T. Mlinarevic[97], M. Mlynarikova[36], S. Mobius[19], P. Mogg[110], M. H. Mohamed Farook[113], A. F. Mohammed[14a,14e], S. Mohapatra[41], G. Mokgatitswane[33g], L. Moleri[170], B. Mondal[142], S. Mondal[133], K. Mönig[48], E. Monnier[103], L. Monsonis Romero[164], J. Montejo Berlingen[13], M. Montella[120], F. Montereali[77a,77b], F. Monticelli[91], S. Monzani[69a,69c], N. Morange[66], A. L. Moreira De Carvalho[48], M. Moreno Llácer[164], C. Moreno Martinez[56], P. Morettini[57b], S. Morgenstern[36], M. Morii[61], M. Morinaga[154], F. Morodei[75a,75b], L. Morvaj[36], P. Moschovakos[36], B. Moser[36], M. Mosidze[150b], T. Moskalets[54], P. Moskvitina[114], J. Moss[31,k], A. Moussa[35d], E. J. W. Moyse[104], O. Mtintsilana[33g], S. Muanza[103], J. Mueller[130], D. Muenstermann[92], R. Müller[19], G. A. Mullier[162], A. J. Mullin[32], J. J. Mullin[129], D. P. Mungo[156], D. Munoz Perez[164], F. J. Munoz Sanchez[102], M. Murin[102], W. J. Murray[135,168], M. Muškinja[94], C. Mwewa[29], A. G. Myagkov[37,a], A. J. Myers[8], G. Myers[107], M. Myska[133], B. P. Nachman[17a], O. Nackenhorst[49], K. Nagai[127], K. Nagano[84], J. L. Nagle[29,ag], E. Nagy[103], A. M. Nairz[36], Y. Nakahama[84], K. Nakamura[84], K. Nakkalil[5], H. Nanjo[125], R. Narayan[44], E. A. Narayanan[113], I. Naryshkin[37], M. Naseri[34], S. Nasri[117b], C. Nass[24], G. Navarro[22a], J. Navarro-Gonzalez[164], R. Nayak[152], A. Nayaz[18], P. Y. Nechaeva[37], S. Nechaeva[23a,23b], F. Nechansky[48], L. Nedic[127], T. J. Neep[20], A. Negri[73a,73b], M. Negrini[23b], C. Nellist[115], C. Nelson[105], K. Nelson[107], S. Nemecek[132], M. Nessi[36,h], M. S. Neubauer[163], F. Neuhaus[101], J. Neundorf[48], R. Newhouse[165], P. R. Newman[20], C. W. Ng[130], Y. W. Y. Ng[48], B. Ngair[117a], H. D. N. Nguyen[109], R. B. Nickerson[127], R. Nicolaidou[136], J. Nielsen[137], M. Niemeyer[55], J. Niermann[55], N. Nikiforou[36], V. Nikolaenko[37,a], I. Nikolic-Audit[128], K. Nikolopoulos[20], P. Nilsson[29], I. Ninca[48], H. R. Nindhito[56], G. Ninio[152], A. Nisati[75a], N. Nishu[2], R. Nisius[111], J.-E. Nitschke[50], E. K. Nkadimeng[33g], T. Nobe[154], D. L. Noel[32], T. Nommensen[148], M. B. Norfolk[140], R. R. B. Norisam[97], B. J. Norman[34], M. Noury[35a], J. Novak[94], T. Novak[48], L. Novotny[133], R. Novotny[113], L. Nozka[123], K. Ntekas[160], N. M. J. Nunes De Moura Junior[83b], J. Ocariz[128], A. Ochi[85], I. Ochoa[131a], S. Oerdek[48,t], J. T. Offermann[39], A. Ogrodnik[134], A. Oh[102], C. C. Ohm[145], H. Oide[84], R. Oishi[154], M. L. Ojeda[48], Y. Okumura[154], L. F. Oleiro Seabra[131a], S. A. Olivares Pino[138d], G. Oliveira Correa[13], D. Oliveira Damazio[29], D. Oliveira Goncalves[83a], J. L. Oliver[160], Ö. O. Öncel[54], A. P. O'Neill[19], A. Onofre[131a,131e], P. U. E. Onyisi[11], M. J. Oreglia[39], G. E. Orellana[91], D. Orestano[77a,77b], N. Orlando[13], R. S. Orr[156], V. O'Shea[59], L. M. Osojnak[129], R. Ospanov[62a], G. Otero y Garzon[30], H. Otono[89], P. S. Ott[63a], G. J. Ottino[17a], M. Ouchrif[35d], F. Ould-Saada[126], T. Ovsiannikova[139], M. Owen[59], R. E. Owen[135], K. Y. Oyulmaz[21a], V. E. Ozcan[21a], F. Ozturk[87], N. Ozturk[8], S. Ozturk[82], H. A. Pacey[127], A. Pacheco Pages[13], C. Padilla Aranda[13], G. Padovano[75a,75b], S. Pagan Griso[17a], G. Palacino[68], A. Palazzo[70a,70b], J. Pampel[24], J. Pan[173], T. Pan[64a], D. K. Panchal[11], C. E. Pandini[115], J. G. Panduro Vazquez[96], H. D. Pandya[1], H. Pang[14b], P. Pani[48], G. Panizzo[69a,69c], L. Panwar[128], L. Paolozzi[56], S. Parajuli[163], A. Paramonov[6], C. Paraskevopoulos[53], D. Paredes Hernandez[64b], A. Pareti[73a,73b], K. R. Park[41], T. H. Park[156], M. A. Parker[32], F. Parodi[57a,57b], E. W. Parrish[116], V. A. Parrish[52], J. A. Parsons[41], U. Parzefall[54], B. Pascual Dias[109], L. Pascual Dominguez[152], E. Pasqualucci[75a], S. Passaggio[57b], F. Pastore[96], P. Patel[87], U. M. Patel[51], J. R. Pater[102], T. Pauly[36], C. I. Pazos[159], J. Pearkes[144], M. Pedersen[126], R. Pedro[131a], S. V. Peleganchuk[37], O. Penc[36], E. A. Pender[52], G. D. Penn[173], K. E. Penski[110], M. Penzin[37], B. S. Peralva[83d], A. P. Pereira Peixoto[139], L. Pereira Sanchez[144], D. V. Perepelitsa[29,ag], E. Perez Codina[157a], M. Perganti[10], H. Pernegger[36], O. Perrin[40], K. Peters[48], R. F. Y. Peters[102], B. A. Petersen[36], T. C. Petersen[42], E. Petit[103], V. Petousis[133], C. Petridou[153,e], T. Petru[134], A. Petrukhin[142], M. Pettee[17a], N. E. Pettersson[36], A. Petukhov[37], K. Petukhova[134], R. Pezoa[138f], L. Pezzotti[36], G. Pezzullo[173], T. M. Pham[171], T. Pham[106], P. W. Phillips[135], G. Piacquadio[146], E. Pianori[17a], F. Piazza[124], R. Piegaia[30], D. Pietreanu[27b], A. D. Pilkington[102], M. Pinamonti[69a,69c], J. L. Pinfold[2], B. C. Pinheiro Pereira[131a], A. E. Pinto Pinoargote[101,136], L. Pintucci[69a,69c], K. M. Piper[147], A. Pirttikoski[56], D. A. Pizzi[34], L. Pizzimento[64b], A. Pizzini[115], M. -A. Pleier[29], V. Plesanovs[54], V. Pleskot[134], E. Plotnikova[38], G. Poddar[95], R. Poettgen[99], L. Poggioli[128], I. Pokharel[55], S. Polacek[134], G. Polesello[73a], A. Poley[143,157a], A. Polini[23b], C. S. Pollard[168], Z. B. Pollock[120], E. Pompa Pacchi[75a,75b], D. Ponomarenko[114], L. Pontecorvo[36], S. Popa[27a], G. A. Popeneciu[27d], A. Poreba[36],

D. M. Portillo Quintero[157a], S. Pospisil[133], M. A. Postill[140], P. Postolache[27c], K. Potamianos[168], P. A. Potepa[86a], I. N. Potrap[38], C. J. Potter[32], H. Potti[1], J. Poveda[164], M. E. Pozo Astigarraga[36], A. Prades Ibanez[164], J. Pretel[54], D. Price[102], M. Primavera[70a], M. A. Principe Martin[100], R. Privara[123], T. Procter[59], M. L. Proffitt[139], N. Proklova[129], K. Prokofiev[64c], G. Proto[111], J. Proudfoot[6], M. Przybycien[86a], W. W. Przygoda[86b], A. Psallidas[46], J. E. Puddefoot[140], D. Pudzha[37], D. Pyatiizbyantseva[37], J. Qian[107], D. Qichen[102], Y. Qin[13], T. Qiu[52], A. Quadt[55], M. Queitsch-Maitland[102], G. Quetant[56], R. P. Quinn[165], G. Rabanal Bolanos[61], D. Rafanoharana[54], F. Ragusa[71a,71b], J. L. Rainbolt[39], J. A. Raine[56], S. Rajagopalan[29], E. Ramakoti[37], I. A. Ramirez-Berend[34], K. Ran[14e,48], N. P. Rapheeha[33g], H. Rasheed[27b], V. Raskina[128], D. F. Rassloff[63a], A. Rastogi[17a], S. Rave[101], B. Ravina[55], I. Ravinovich[170], M. Raymond[36], A. L. Read[126], N. P. Readioff[140], D. M. Rebuzzi[73a,73b], G. Redlinger[29], A. S. Reed[111], K. Reeves[26], J. A. Reidelsturz[172], D. Reikher[152], A. Rej[49], C. Rembser[36], M. Renda[27b], M. B. Rendel[111], F. Renner[48], A. G. Rennie[160], A. L. Rescia[48], S. Resconi[71a], M. Ressegotti[57a,57b], S. Rettie[36], J. G. Reyes Rivera[108], E. Reynolds[17a], O. L. Rezanova[37], P. Reznicek[134], H. Riani[35d], N. Ribaric[92], E. Ricci[78a,78b], R. Richter[111], S. Richter[47a,47b], E. Richter-Was[86b], M. Ridel[128], S. Ridouani[35d], P. Rieck[118], P. Riedler[36], E. M. Riefel[47a,47b], J. O. Rieger[115], M. Rijssenbeek[146], M. Rimoldi[36], L. Rinaldi[23a,23b], T. T. Rinn[29], M. P. Rinnagel[110], G. Ripellino[162], I. Riu[13], J. C. Rivera Vergara[166], F. Rizatdinova[122], E. Rizvi[95], B. R. Roberts[17a], S. H. Robertson[105,w], D. Robinson[32], C. M. Robles Gajardo[138f], M. Robles Manzano[101], A. Robson[59], A. Rocchi[76a,76b], C. Roda[74a,74b], S. Rodriguez Bosca[36], Y. Rodriguez Garcia[22a], A. Rodriguez Rodriguez[54], A. M. Rodríguez Vera[116], S. Roe[36], J. T. Roemer[160], A. R. Roepe-Gier[137], J. Roggel[172], O. Røhne[126], R. A. Rojas[104], C. P. A. Roland[128], J. Roloff[29], A. Romaniouk[37], E. Romano[73a,73b], M. Romano[23b], A. C. Romero Hernandez[163], N. Rompotis[93], L. Roos[128], S. Rosati[75a], B. J. Rosser[39], E. Rossi[127], E. Rossi[72a,72b], L. P. Rossi[61], L. Rossini[54], R. Rosten[120], M. Rotaru[27b], B. Rottler[54], C. Rougier[90], D. Rousseau[66], D. Rousso[48], A. Roy[163], S. Roy-Garand[156], A. Rozanov[103], Z. M. A. Rozario[59], Y. Rozen[151], A. Rubio Jimenez[164], A. J. Ruby[93], V. H. Ruelas Rivera[18], T. A. Ruggeri[1], A. Ruggiero[127], A. Ruiz-Martinez[164], A. Rummler[36], Z. Rurikova[54], N. A. Rusakovich[38], H. L. Russell[166], G. Russo[75a,75b], J. P. Rutherfoord[7], S. Rutherford Colmenares[32], K. Rybacki[92], M. Rybar[134], E. B. Rye[126], A. Ryzhov[44], J. A. Sabater Iglesias[56], P. Sabatini[164], H. F.-W. Sadrozinski[137], F. Safai Tehrani[75a], B. Safarzadeh Samani[135], S. Saha[1], M. Sahinsoy[111], A. Saibel[164], M. Saimpert[136], M. Saito[154], T. Saito[154], A. Sala[71a,71b], D. Salamani[36], A. Salnikov[144], J. Salt[164], A. Salvador Salas[152], D. Salvatore[43a,43b], F. Salvatore[147], A. Salzburger[36], D. Sammel[54], E. Sampson[92], D. Sampsonidis[153,e], D. Sampsonidou[124], J. Sánchez[164], V. Sanchez Sebastian[164], H. Sandaker[126], C. O. Sander[48], J. A. Sandesara[104], M. Sandhoff[172], C. Sandoval[22b], D. P. C. Sankey[135], T. Sano[88], A. Sansoni[53], L. Santi[75a,75b], C. Santoni[40], H. Santos[131a,131b], A. Santra[170], K. A. Saoucha[161], J. G. Saraiva[131a,131d], J. Sardain[7], O. Sasaki[84], K. Sato[158], C. Sauer[63b], F. Sauerburger[54], E. Sauvan[4], P. Savard[156,ae], R. Sawada[154], C. Sawyer[135], L. Sawyer[98], I. Sayago Galvan[164], C. Sbarra[23b], A. Sbrizzi[23a,23b], T. Scanlon[97], J. Schaarschmidt[139], U. Schäfer[101], A. C. Schaffer[44,66], D. Schaile[110], R. D. Schamberger[146], C. Scharf[18], M. M. Schefer[19], V. A. Schegelsky[37], D. Scheirich[134], F. Schenck[18], M. Schernau[160], C. Scheulen[55], C. Schiavi[57a,57b], M. Schioppa[43a,43b], B. Schlag[144,m], K. E. Schleicher[54], S. Schlenker[36], J. Schmeing[172], M. A. Schmidt[172], K. Schmieden[101], C. Schmitt[101], N. Schmitt[101], S. Schmitt[48], L. Schoeffel[136], A. Schoening[63b], P. G. Scholer[34], E. Schopf[127], M. Schott[101], J. Schovancova[36], S. Schramm[56], T. Schroer[56], H.-C. Schultz-Coulon[63a], M. Schumacher[54], B. A. Schumm[137], Ph. Schune[136], A. J. Schuy[139], H. R. Schwartz[137], A. Schwartzman[144], T. A. Schwarz[107], Ph. Schwemling[136], R. Schwienhorst[108], A. Sciandra[29], G. Sciolla[26], F. Scuri[74a], C. D. Sebastiani[93], K. Sedlaczek[116], P. Seema[18], S. C. Seidel[113], A. Seiden[137], B. D. Seidlitz[41], C. Seitz[48], J. M. Seixas[83b], G. Sekhniaidze[72a], L. Selem[60], N. Semprini-Cesari[23a,23b], D. Sengupta[56], V. Senthilkumar[164], L. Serin[66], L. Serkin[69a,69b], M. Sessa[76a,76b], H. Severini[121], F. Sforza[57a,57b], A. Sfyrla[56], Q. Sha[14a], E. Shabalina[55], A. H. Shah[32], R. Shaheen[145], J. D. Shahinian[129], D. Shaked Renous[170], L. Y. Shan[14a], M. Shapiro[17a], A. Sharma[36], A. S. Sharma[165], P. Sharma[80], P. B. Shatalov[37], K. Shaw[147], S. M. Shaw[102], A. Shcherbakova[37], Q. Shen[5,62c], D. J. Sheppard[143], P. Sherwood[97], L. Shi[97], X. Shi[14a], C. O. Shimmin[173], J. D. Shinner[96], I. P. J. Shipsey[127], S. Shirabe[89], M. Shiyakova[38,u], J. Shlomi[170], M. J. Shochet[39], J. Shojaii[106], D. R. Shope[126], B. Shrestha[121], S. Shrestha[120,ah], E. M. Shrif[33g], M. J. Shroff[166], P. Sicho[132], A. M. Sickles[163], E. Sideras Haddad[33g], A. C. Sidley[115], A. Sidoti[23b], F. Siegert[50], Dj. Sijacki[15], F. Sili[91], J. M. Silva[52], M. V. Silva Oliveira[29], S. B. Silverstein[47a], S. Simion[66], R. Simoniello[36], E. L. Simpson[102], H. Simpson[147], L. R. Simpson[107], N. D. Simpson[99], S. Simsek[82], S. Sindhu[55], P. Sinervo[156],

S. Singh[156], S. Sinha[48], S. Sinha[102], M. Sioli[23a,23b], I. Siral[36], E. Sitnikova[48], J. Sjölin[47a,47b], A. Skaf[55], E. Skorda[20], P. Skubic[121], M. Slawinska[87], V. Smakhtin[170], B. H. Smart[135], S. Yu. Smirnov[37], Y. Smirnov[37], L. N. Smirnova[37,a], O. Smirnova[99], A. C. Smith[41], D. R. Smith[160], E. A. Smith[39], H. A. Smith[127], J. L. Smith[102], R. Smith[144], M. Smizanska[92], K. Smolek[133], A. A. Snesarev[37], S. R. Snider[156], H. L. Snoek[115], S. Snyder[29], R. Sobie[166,w], A. Soffer[152], C. A. Solans Sanchez[36], E. Yu. Soldatov[37], U. Soldevila[164], A. A. Solodkov[37], S. Solomon[26], A. Soloshenko[38], K. Solovieva[54], O. V. Solovyanov[40], P. Sommer[36], A. Sonay[13], W. Y. Song[157b], A. Sopczak[133], A. L. Sopio[97], F. Sopkova[28b], J. D. Sorenson[113], I. R. Sotarriva Alvarez[155], V. Sothilingam[63a], O. J. Soto Sandoval[138b,138c], S. Sottocornola[68], R. Soualah[161], Z. Soumaimi[35e], D. South[48], N. Soybelman[170], S. Spagnolo[70a,70b], M. Spalla[111], D. Sperlich[54], G. Spigo[36], S. Spinali[92], D. P. Spiteri[59], M. Spousta[134], E. J. Staats[34], R. Stamen[63a], A. Stampekis[20], M. Standke[24], E. Stanecka[87], W. Stanek-Maslouska[48], M. V. Stange[50], B. Stanislaus[17a], M. M. Stanitzki[48], B. Stapf[48], E. A. Starchenko[37], G. H. Stark[137], J. Stark[90], P. Staroba[132], P. Starovoitov[63a], S. Stärz[105], R. Staszewski[87], G. Stavropoulos[46], J. Steentoft[162], P. Steinberg[29], B. Stelzer[143,157a], H. J. Stelzer[130], O. Stelzer-Chilton[157a], H. Stenzel[58], T. J. Stevenson[147], G. A. Stewart[36], J. R. Stewart[122], M. C. Stockton[36], G. Stoicea[27b], M. Stolarski[131a], S. Stonjek[111], A. Straessner[50], J. Strandberg[145], S. Strandberg[47a,47b], M. Stratmann[172], M. Strauss[121], T. Strebler[103], P. Strizenec[28b], R. Ströhmer[167], D. M. Strom[124], R. Stroynowski[44], A. Strubig[47a,47b], S. A. Stucci[29], B. Stugu[16], J. Stupak[121], N. A. Styles[48], D. Su[144], S. Su[62a], W. Su[62d], X. Su[62a], D. Suchy[28a], K. Sugizaki[154], V. V. Sulin[37], M. J. Sullivan[93], D. M. S. Sultan[127], L. Sultanaliyeva[37], S. Sultansoy[3b], T. Sumida[88], S. Sun[107], S. Sun[171], O. Sunneborn Gudnadottir[162], N. Sur[103], M. R. Sutton[147], H. Suzuki[158], M. Svatos[132], M. Swiatlowski[157a], T. Swirski[167], I. Sykora[28a], M. Sykora[134], T. Sykora[134], D. Ta[101], K. Tackmann[48,t], A. Taffard[160], R. Tafirout[157a], J. S. Tafoya Vargas[66], Y. Takubo[84], M. Talby[103], A. A. Talyshev[37], K. C. Tam[64b], N. M. Tamir[152], A. Tanaka[154], J. Tanaka[154], R. Tanaka[66], M. Tanasini[57a,57b], Z. Tao[165], S. Tapia Araya[138f], S. Tapprogge[101], A. Tarek Abouelfadl Mohamed[108], S. Tarem[151], K. Tariq[14a], G. Tarna[27b], G. F. Tartarelli[71a], M. J. Tartarin[90], P. Tas[134], M. Tasevsky[132], E. Tassi[43a,43b], A. C. Tate[163], G. Tateno[154], Y. Tayalati[35e,v], G. N. Taylor[106], W. Taylor[157b], A. S. Tee[171], R. Teixeira De Lima[144], P. Teixeira-Dias[96], J. J. Teoh[156], K. Terashi[154], J. Terron[100], S. Terzo[13], M. Testa[53], R. J. Teuscher[156,w], A. Thaler[79], O. Theiner[56], N. Themistokleous[52], T. Theveneaux-Pelzer[103], O. Thielmann[172], D. W. Thomas[96], J. P. Thomas[20], E. A. Thompson[17a], P. D. Thompson[20], E. Thomson[129], R. E. Thornberry[44], Y. Tian[55], V. Tikhomirov[37,a], Yu. A. Tikhonov[37], S. Timoshenko[37], D. Timoshyn[134], E. X. L. Ting[1], P. Tipton[173], S. H. Tlou[33g], K. Todome[155], S. Todorova-Nova[134], S. Todt[50], M. Togawa[84], J. Tojo[89], S. Tokár[28a], K. Tokushuku[84], O. Toldaiev[68], R. Tombs[32], M. Tomoto[84,112], L. Tompkins[144,m], K. W. Topolnicki[86b], E. Torrence[124], H. Torres[90], E. Torró Pastor[164], M. Toscani[30], C. Tosciri[39], M. Tost[11], D. R. Tovey[140], A. Traeet[16], I. S. Trandafir[27b], T. Trefzger[167], A. Tricoli[29], I. M. Trigger[157a], S. Trincaz-Duvoid[128], D. A. Trischuk[26], B. Trocmé[60], L. Truong[33c], M. Trzebinski[87], A. Trzupek[87], F. Tsai[146], M. Tsai[107], A. Tsiamis[153,e], P. V. Tsiareshka[37], S. Tsigaridas[157a], A. Tsirigotis[153,r], V. Tsiskaridze[156], E. G. Tskhadadze[150a], M. Tsopoulou[153], Y. Tsujikawa[88], I. I. Tsukerman[37], V. Tsulaia[17a], S. Tsuno[84], K. Tsuri[119], D. Tsybychev[146], Y. Tu[64b], A. Tudorache[27b], V. Tudorache[27b], A. N. Tuna[61], S. Turchikhin[57a,57b], I. Turk Cakir[3a], R. Turra[71a], T. Turtuvshin[38,x], P. M. Tuts[41], S. Tzamarias[153,e], E. Tzovara[101], F. Ukegawa[158], P. A. Ulloa Poblete[138b,138c], E. N. Umaka[29], G. Unal[36], A. Undrus[29], G. Unel[160], J. Urban[28b], P. Urquijo[106], P. Urrejola[138a], G. Usai[8], R. Ushioda[155], M. Usman[109], Z. Uysal[82], V. Vacek[133], B. Vachon[105], K. O. H. Vadla[126], T. Vafeiadis[36], A. Vaitkus[97], C. Valderanis[110], E. Valdes Santurio[47a,47b], M. Valente[157a], S. Valentinetti[23a,23b], A. Valero[164], E. Valiente Moreno[164], A. Vallier[90], J. A. Valls Ferrer[164], D. R. Van Arneman[115], T. R. Van Daalen[139], A. Van Der Graaf[49], P. Van Gemmeren[6], M. Van Rijnbach[126], S. Van Stroud[97], I. Van Vulpen[115], P. Vana[134], M. Vanadia[76a,76b], W. Vandelli[36], E. R. Vandewall[122], D. Vannicola[152], L. Vannoli[53], R. Vari[75a], E. W. Varnes[7], C. Varni[17b], T. Varol[149], D. Varouchas[66], L. Varriale[164], K. E. Varvell[148], M. E. Vasile[27b], L. Vaslin[84], G. A. Vasquez[166], A. Vasyukov[38], R. Vavricka[101], F. Vazeille[40], T. Vazquez Schroeder[36], J. Veatch[31], V. Vecchio[102], M. J. Veen[104], I. Veliscek[29], L. M. Veloce[156], F. Veloso[131a,131c], S. Veneziano[75a], A. Ventura[70a,70b], S. Ventura Gonzalez[136], A. Verbytskyi[111], M. Verducci[74a,74b], C. Vergis[95], M. Verissimo De Araujo[83b], W. Verkerke[115], J. C. Vermeulen[115], C. Vernieri[144], M. Vessella[104], M. C. Vetterli[143,ae], A. Vgenopoulos[153,e], N. Viaux Maira[138f], T. Vickey[140], O. E. Vickey Boeriu[140], G. H. A. Viehhauser[127], L. Vigani[63b], M. Villa[23a,23b], M. Villaplana Perez[164], E. M. Villhauer[52], E. Vilucchi[53], M. G. Vincter[34], G. S. Virdee[20], A. Visibile[115], C. Vittori[36], I. Vivarelli[23a,23b], E. Voevodina[111], F. Vogel[110], J. C. Voigt[50], P. Vokac[133], Yu. Volkotrub[86b], J. Von Ahnen[48], E. Von Toerne[24], B. Vormwald[36], V. Vorobel[134], K. Vorobev[37], M. Vos[164], K. Voss[142], M. Vozak[115], L. Vozdecky[121], N. Vranjes[15], M. Vranjes Milosavljevic[15], M. Vreeswijk[115], N. K. Vu[62c,62d], R. Vuillermet[36], O. Vujinovic[101], I. Vukotic[39], S. Wada[158], C. Wagner[104], J. M. Wagner[17a], W. Wagner[172], S. Wahdan[172], H. Wahlberg[91], M. Wakida[112], J. Walder[135], R. Walker[110], W. Walkowiak[142], A. Wall[129], E. J. Wallin[99], T. Wamorkar[6], A. Z. Wang[137], C. Wang[101], C. Wang[11], H. Wang[17a], J. Wang[64c], R. -J. Wang[101], R. Wang[61], R. Wang[6], S. M. Wang[149], S. Wang[62b], S. Wang[14a], T. Wang[62a], W. T. Wang[80], W. Wang[14a], X. Wang[14c], X. Wang[163], X. Wang[62c], Y. Wang[62d], Y. Wang[14c], Z. Wang[107], Z. Wang[51,62c,62d], Z. Wang[107], A. Warburton[105], R. J. Ward[20], N. Warrack[59], S. Waterhouse[96], A. T. Watson[20], H. Watson[59], M. F. Watson[20], E. Watton[59,135], G. Watts[139], B. M. Waugh[97], J. M. Webb[54], C. Weber[29], H. A. Weber[18], M. S. Weber[19], S. M. Weber[63a], C. Wei[62a], Y. Wei[127], A. R. Weidberg[127], E. J. Weik[118], J. Weingarten[49], M. Weirich[101], C. Weiser[54], C. J. Wells[48], T. Wenaus[29], B. Wendland[49], T. Wengler[36], N. S. Wenke[111], N. Wermes[24], M. Wessels[63a], A. M. Wharton[92], A. S. White[61], A. White[8], M. J. White[1], D. Whiteson[160], L. Wickremasinghe[125], W. Wiedenmann[171], M. Wielers[135], C. Wiglesworth[42], D. J. Wilbern[121], H. G. Wilkens[36], J. J. H. Wilkinson[32], D. M. Williams[41], H. H. Williams[129], S. Williams[32], S. Willocq[104], B. J. Wilson[102], P. J. Windischhofer[39], F. I. Winkel[30], F. Winklmeier[124], B. T. Winter[54], J. K. Winter[102], M. Wittgen[144], M. Wobisch[98], T. Wojtkowski[60], Z. Wolffs[115], J. Wollrath[160], M. W. Wolter[87], H. Wolters[131a,131c], M. C. Wong[137], E. L. Woodward[41], S. D. Worm[48], B. K. Wosiek[87], K. W. Woźniak[87], S. Wozniewski[55], K. Wraight[59], C. Wu[20], M. Wu[14d], M. Wu[114], S. L. Wu[171], X. Wu[56], Y. Wu[62a], Z. Wu[4], J. Wuerzinger[111,ac], T. R. Wyatt[102], B. M. Wynne[52], S. Xella[42], L. Xia[14c], M. Xia[14b], J. Xiang[64c], M. Xie[62a], X. Xie[62a], S. Xin[14a,14e], A. Xiong[124], J. Xiong[17a], D. Xu[14a], H. Xu[62a], L. Xu[62a], R. Xu[129], T. Xu[107], Y. Xu[14b], Z. Xu[52], Z. Xu[14c], B. Yabsley[148], S. Yacoob[33a], Y. Yamaguchi[155], E. Yamashita[154], H. Yamauchi[158], T. Yamazaki[17a], Y. Yamazaki[85], J. Yan[62c], S. Yan[59], Z. Yan[104], H. J. Yang[62c,62d], H. T. Yang[62a], S. Yang[62a], T. Yang[64c], X. Yang[36], X. Yang[14a], Y. Yang[44], Y. Yang[62a], Z. Yang[62a], W.-M. Yao[17a], H. Ye[14c], H. Ye[55], J. Ye[14a], S. Ye[29], X. Ye[62a], Y. Yeh[97], I. Yeletskikh[38], B. K. Yeo[17b], M. R. Yexley[97], T. P. Yildirim[127], P. Yin[41], K. Yorita[169], S. Younas[27b], C. J. S. Young[36], C. Young[144], C. Yu[14a,14e], Y. Yu[62a], M. Yuan[107], R. Yuan[62d], L. Yue[97], M. Zaazoua[62a], B. Zabinski[87], E. Zaid[52], Z. K. Zak[87], T. Zakareishvili[164], N. Zakharchuk[34], S. Zambito[56], J. A. Zamora Saa[138b,138d], J. Zang[154], D. Zanzi[54], O. Zaplatilek[133], C. Zeitnitz[172], H. Zeng[14a], J. C. Zeng[163], D. T. Zenger Jr[26], O. Zenin[37], T. Ženiš[28a], S. Zenz[95], S. Zerradi[35a], D. Zerwas[66], M. Zhai[14a,14e], D. F. Zhang[140], J. Zhang[62b], J. Zhang[6], K. Zhang[14a,14e], L. Zhang[62a], L. Zhang[14c], P. Zhang[14a,14e], R. Zhang[171], S. Zhang[107], S. Zhang[44], T. Zhang[154], X. Zhang[62c], X. Zhang[62b], Y. Zhang[5,62c], Y. Zhang[97], Y. Zhang[14c], Z. Zhang[17a], Z. Zhang[66], H. Zhao[139], T. Zhao[62b], Y. Zhao[137], Z. Zhao[62a], Z. Zhao[62a], A. Zhemchugov[38], J. Zheng[14c], K. Zheng[163], X. Zheng[62a], Z. Zheng[144], D. Zhong[163], B. Zhou[107], H. Zhou[7], N. Zhou[62c], Y. Zhou[14c], Y. Zhou[7], C. G. Zhu[62b], J. Zhu[107], Y. Zhu[62c], Y. Zhu[62a], X. Zhuang[14a], K. Zhukov[37], N. I. Zimine[38], J. Zinsser[63b], M. Ziolkowski[142], L. Živković[15], A. Zoccoli[23a,23b], K. Zoch[61], T. G. Zorbas[140], O. Zormpa[46], W. Zou[41], L. Zwalinski[36]

[1] Department of Physics, University of Adelaide, Adelaide, Australia
[2] Department of Physics, University of Alberta, Edmonton, AB, Canada
[3] [(a)]Department of Physics, Ankara University, Ankara, Türkiye; [(b)]Division of Physics, TOBB University of Economics and Technology, Ankara, Türkiye
[4] LAPP, Université Savoie Mont Blanc, CNRS/IN2P3, Annecy, France
[5] APC, Université Paris Cité, CNRS/IN2P3, Paris, France
[6] High Energy Physics Division, Argonne National Laboratory, Argonne, IL, USA
[7] Department of Physics, University of Arizona, Tucson, AZ, USA
[8] Department of Physics, University of Texas at Arlington, Arlington, TX, USA
[9] Physics Department, National and Kapodistrian University of Athens, Athens, Greece
[10] Physics Department, National Technical University of Athens, Zografou, Greece
[11] Department of Physics, University of Texas at Austin, Austin, TX, USA
[12] Institute of Physics, Azerbaijan Academy of Sciences, Baku, Azerbaijan
[13] Institut de Física d'Altes Energies (IFAE), Barcelona Institute of Science and Technology, Barcelona, Spain
[14] [(a)]Institute of High Energy Physics, Chinese Academy of Sciences, Beijing, China; [(b)]Physics Department, Tsinghua University, Beijing, China; [(c)]Department of Physics, Nanjing University, Nanjing, China; [(d)]School of Science,

Shenzhen Campus of Sun Yat-sen University, Shenzhen, China; [e]University of Chinese Academy of Science (UCAS), Beijing, China
[15] Institute of Physics, University of Belgrade, Belgrade, Serbia
[16] Department for Physics and Technology, University of Bergen, Bergen, Norway
[17] [a]Physics Division, Lawrence Berkeley National Laboratory, Berkeley, CA, USA; [b]University of California, Berkeley, CA, USA
[18] Institut für Physik, Humboldt Universität zu Berlin, Berlin, Germany
[19] Albert Einstein Center for Fundamental Physics and Laboratory for High Energy Physics, University of Bern, Bern, Switzerland
[20] School of Physics and Astronomy, University of Birmingham, Birmingham, UK
[21] [a]Department of Physics, Bogazici University, Istanbul, Türkiye; [b]Department of Physics Engineering, Gaziantep University, Gaziantep, Türkiye; [c]Department of Physics, Istanbul University, Istanbul, Türkiye
[22] [a]Facultad de Ciencias y Centro de Investigaciónes, Universidad Antonio Nariño, Bogotá, Colombia; [b]Departamento de Física, Universidad Nacional de Colombia, Bogotá, Colombia
[23] [a]Dipartimento di Fisica e Astronomia A. Righi, Università di Bologna, Bologna, Italy; [b]INFN Sezione di Bologna, Bologna, Italy
[24] Physikalisches Institut, Universität Bonn, Bonn, Germany
[25] Department of Physics, Boston University, Boston, MA, USA
[26] Department of Physics, Brandeis University, Waltham, MA, USA
[27] [a]Transilvania University of Brasov, Brasov, Romania; [b]Horia Hulubei National Institute of Physics and Nuclear Engineering, Bucharest, Romania; [c]Department of Physics, Alexandru Ioan Cuza University of Iasi, Iasi, Romania ; [d]Physics Department, National Institute for Research and Development of Isotopic and Molecular Technologies, Cluj-Napoca, Romania; [e]National University of Science and Technology Politechnica, Bucharest, Romania; [f]West University in Timisoara, Timisoara, Romania; [g]Faculty of Physics, University of Bucharest, Bucharest, Romania
[28] [a]Faculty of Mathematics, Physics and Informatics, Comenius University, Bratislava, Slovak Republic; [b]Department of Subnuclear Physics, Institute of Experimental Physics of the Slovak Academy of Sciences, Kosice, Slovak Republic
[29] Physics Department, Brookhaven National Laboratory, Upton, NY, USA
[30] Instituto de Física de Buenos Aires (IFIBA), Departamento de Física, y CONICET, Facultad de Ciencias Exactas y Naturales, Universidad de Buenos Aires, Buenos Aires, Argentina
[31] California State University, Los Angeles, CA, USA
[32] Cavendish Laboratory, University of Cambridge, Cambridge, UK
[33] [a]Department of Physics, University of Cape Town, Cape Town, South Africa; [b]iThemba Labs, Western Cape, South Africa; [c]Department of Mechanical Engineering Science, University of Johannesburg, Johannesburg, South Africa; [d]National Institute of Physics, University of the Philippines, Diliman, Philippines; [e]Department of Physics, University of South Africa, Pretoria, South Africa; [f]University of Zululand, KwaDlangezwa, South Africa; [g]School of Physics, University of the Witwatersrand, Johannesburg, South Africa
[34] Department of Physics, Carleton University, Ottawa, ON, Canada
[35] [a]Faculté des Sciences Ain Chock, Réseau Universitaire de Physique des Hautes Energies-Université Hassan II, Casablanca, Morocco; [b]Faculté des Sciences, Université Ibn-Tofail, Kénitra, Morocco; [c]Faculté des Sciences Semlalia, Université Cadi Ayyad, LPHEA-Marrakech, Morocco; [d]LPMR, Faculté des Sciences, Université Mohamed Premier, Oujda, Morocco; [e]Faculté des sciences, Université Mohammed V, Rabat, Morocco; [f]Institute of Applied Physics, Mohammed VI Polytechnic University, Ben Guerir, Morocco
[36] CERN, Geneva, Switzerland
[37] Affiliated with an Institute Covered by a Cooperation Agreement with CERN, Geneva, Switzerland
[38] Affiliated with an International Laboratory Covered by a Cooperation Agreement with CERN, Geneva, Switzerland
[39] Enrico Fermi Institute, University of Chicago, Chicago, IL, USA
[40] LPC, Université Clermont Auvergne, CNRS/IN2P3, Clermont-Ferrand, France
[41] Nevis Laboratory, Columbia University, Irvington, NY, USA
[42] Niels Bohr Institute, University of Copenhagen, Copenhagen, Denmark
[43] [a]Dipartimento di Fisica, Università della Calabria, Rende, Italy; [b]INFN Gruppo Collegato di Cosenza, Laboratori Nazionali di Frascati, Frascati, Italy
[44] Physics Department, Southern Methodist University, Dallas, TX, USA
[45] Physics Department, University of Texas at Dallas, Richardson, TX, USA

[46] National Centre for Scientific Research "Demokritos", Agia Paraskevi, Greece
[47] [(a)]Department of Physics, Stockholm University, Stockholm, Sweden; [(b)]Oskar Klein Centre, Stockholm, Sweden
[48] Deutsches Elektronen-Synchrotron DESY, Hamburg and Zeuthen, Germany
[49] Fakultät Physik , Technische Universität Dortmund, Dortmund, Germany
[50] Institut für Kern- und Teilchenphysik, Technische Universität Dresden, Dresden, Germany
[51] Department of Physics, Duke University, Durham, NC, USA
[52] SUPA-School of Physics and Astronomy, University of Edinburgh, Edinburgh, UK
[53] INFN e Laboratori Nazionali di Frascati, Frascati, Italy
[54] Physikalisches Institut, Albert-Ludwigs-Universität Freiburg, Freiburg, Germany
[55] II. Physikalisches Institut, Georg-August-Universität Göttingen, Göttingen, Germany
[56] Département de Physique Nucléaire et Corpusculaire, Université de Genève, Genève, Switzerland
[57] [(a)]Dipartimento di Fisica, Università di Genova, Genova, Italy; [(b)]INFN Sezione di Genova, Genova, Italy
[58] II. Physikalisches Institut, Justus-Liebig-Universität Giessen, Giessen, Germany
[59] SUPA-School of Physics and Astronomy, University of Glasgow, Glasgow, UK
[60] LPSC, Université Grenoble Alpes, CNRS/IN2P3, Grenoble INP, Grenoble, France
[61] Laboratory for Particle Physics and Cosmology, Harvard University, Cambridge, MA, USA
[62] [(a)]Department of Modern Physics and State Key Laboratory of Particle Detection and Electronics, University of Science and Technology of China, Hefei, China; [(b)]Institute of Frontier and Interdisciplinary Science and Key Laboratory of Particle Physics and Particle Irradiation (MOE), Shandong University, Qingdao, China; [(c)]School of Physics and Astronomy, Shanghai Jiao Tong University, Key Laboratory for Particle Astrophysics and Cosmology (MOE), SKLPPC, Shanghai, China; [(d)]Tsung-Dao Lee Institute, Shanghai, China; [(e)]School of Physics and Microelectronics, Zhengzhou University, China
[63] [(a)]Kirchhoff-Institut für Physik, Ruprecht-Karls-Universität Heidelberg, Heidelberg, Germany; [(b)]Physikalisches Institut, Ruprecht-Karls-Universität Heidelberg, Heidelberg, Germany
[64] [(a)]Department of Physics, Chinese University of Hong Kong, Shatin, N.T., Hong Kong, China; [(b)]Department of Physics, University of Hong Kong, Hong Kong, China; [(c)]Department of Physics and Institute for Advanced Study, Hong Kong University of Science and Technology, Clear Water Bay, Kowloon, Hong Kong, China
[65] Department of Physics, National Tsing Hua University, Hsinchu, Taiwan
[66] IJCLab, Université Paris-Saclay, CNRS/IN2P3, 91405 Orsay, France
[67] Centro Nacional de Microelectrónica (IMB-CNM-CSIC), Barcelona, Spain
[68] Department of Physics, Indiana University, Bloomington, IN, USA
[69] [(a)]INFN Gruppo Collegato di Udine, Sezione di Trieste, Udine, Italy; [(b)]ICTP, Trieste, Italy; [(c)]Dipartimento Politecnico di Ingegneria e Architettura, Università di Udine, Udine, Italy
[70] [(a)]INFN Sezione di Lecce, Lecce, Italy; [(b)]Dipartimento di Matematica e Fisica, Università del Salento, Lecce, Italy
[71] [(a)]INFN Sezione di Milano, Milan, Italy; [(b)]Dipartimento di Fisica, Università di Milano, Milan, Italy
[72] [(a)]INFN Sezione di Napoli, Naples, Italy; [(b)]Dipartimento di Fisica, Università di Napoli, Naples, Italy
[73] [(a)]INFN Sezione di Pavia, Pavia, Italy; [(b)]Dipartimento di Fisica, Università di Pavia, Pavia, Italy
[74] [(a)]INFN Sezione di Pisa, Pisa, Italy; [(b)]Dipartimento di Fisica E. Fermi, Università di Pisa, Pisa, Italy
[75] [(a)]INFN Sezione di Roma, Rome, Italy; [(b)]Dipartimento di Fisica, Sapienza Università di Roma, Rome, Italy
[76] [(a)]INFN Sezione di Roma Tor Vergata, Rome, Italy; [(b)]Dipartimento di Fisica, Università di Roma Tor Vergata, Rome, Italy
[77] [(a)]INFN Sezione di Roma Tre, Rome, Italy; [(b)]Dipartimento di Matematica e Fisica, Università Roma Tre, Rome, Italy
[78] [(a)]INFN-TIFPA, Povo, Italy; [(b)]Università degli Studi di Trento, Trento, Italy
[79] Department of Astro and Particle Physics, Universität Innsbruck, Innsbruck, Austria
[80] University of Iowa, Iowa City, IA, USA
[81] Department of Physics and Astronomy, Iowa State University, Ames, IA, USA
[82] Istinye University, Sariyer, Istanbul, Türkiye
[83] [(a)]Departamento de Engenharia Elétrica, Universidade Federal de Juiz de Fora (UFJF), Juiz de Fora, Brazil ; [(b)]Universidade Federal do Rio de Janeiro COPPE/EE/IF, Rio de Janeiro, Brazil; [(c)]Instituto de Física, Universidade de São Paulo, São Paulo, Brazil; [(d)]Rio de Janeiro State University, Rio de Janeiro, Brazil; [(e)]Federal University of Bahia, Bahia, Brazil
[84] KEK, High Energy Accelerator Research Organization, Tsukuba, Japan
[85] Graduate School of Science, Kobe University, Kobe, Japan

86 (a) AGH University of Krakow, Faculty of Physics and Applied Computer Science, Krakow, Poland; (b) Marian Smoluchowski Institute of Physics, Jagiellonian University, Krakow, Poland
87 Institute of Nuclear Physics Polish Academy of Sciences, Krakow, Poland
88 Faculty of Science, Kyoto University, Kyoto, Japan
89 Research Center for Advanced Particle Physics and Department of Physics, Kyushu University, Fukuoka , Japan
90 L2IT, Université de Toulouse, CNRS/IN2P3, UPS, Toulouse, France
91 Instituto de Física La Plata, Universidad Nacional de La Plata and CONICET, La Plata, Argentina
92 Physics Department, Lancaster University, Lancaster, UK
93 Oliver Lodge Laboratory, University of Liverpool, Liverpool, UK
94 Department of Experimental Particle Physics, Jožef Stefan Institute and Department of Physics, University of Ljubljana, Ljubljana, Slovenia
95 School of Physics and Astronomy, Queen Mary University of London, London, UK
96 Department of Physics, Royal Holloway University of London, Egham, UK
97 Department of Physics and Astronomy, University College London, London, UK
98 Louisiana Tech University, Ruston, LA, USA
99 Fysiska institutionen, Lunds universitet, Lund, Sweden
100 Departamento de Física Teorica C-15 and CIAFF, Universidad Autónoma de Madrid, Madrid, Spain
101 Institut für Physik, Universität Mainz, Mainz, Germany
102 School of Physics and Astronomy, University of Manchester, Manchester, UK
103 CPPM, Aix-Marseille Université, CNRS/IN2P3, Marseille, France
104 Department of Physics, University of Massachusetts, Amherst, MA, USA
105 Department of Physics, McGill University, Montreal, QC, Canada
106 School of Physics, University of Melbourne, Victoria, Australia
107 Department of Physics, University of Michigan, Ann Arbor, MI, USA
108 Department of Physics and Astronomy, Michigan State University, East Lansing, MI, USA
109 Group of Particle Physics, University of Montreal, Montreal, QC, Canada
110 Fakultät für Physik, Ludwig-Maximilians-Universität München, Munich, Germany
111 Max-Planck-Institut für Physik (Werner-Heisenberg-Institut), Munich, Germany
112 Graduate School of Science and Kobayashi-Maskawa Institute, Nagoya University, Nagoya, Japan
113 Department of Physics and Astronomy, University of New Mexico, Albuquerque, NM, USA
114 Institute for Mathematics, Astrophysics and Particle Physics, Radboud University/Nikhef, Nijmegen, The Netherlands
115 Nikhef National Institute for Subatomic Physics and University of Amsterdam, Amsterdam, The Netherlands
116 Department of Physics, Northern Illinois University, DeKalb, IL, USA
117 (a) New York University Abu Dhabi, Abu Dhabi, United Arab Emirates; (b) United Arab Emirates University, Al Ain, United Arab Emirates
118 Department of Physics, New York University, New York, NY, USA
119 Ochanomizu University, Otsuka, Bunkyo-ku, Tokyo, Japan
120 Ohio State University, Columbus, OH, USA
121 Homer L. Dodge Department of Physics and Astronomy, University of Oklahoma, Norman, OK, USA
122 Department of Physics, Oklahoma State University, Stillwater, OK, USA
123 Joint Laboratory of Optics, Palacký University, Olomouc, Czech Republic
124 Institute for Fundamental Science, University of Oregon, Eugene, OR, USA
125 Graduate School of Science, Osaka University, Osaka, Japan
126 Department of Physics, University of Oslo, Oslo, Norway
127 Department of Physics, Oxford University, Oxford, UK
128 LPNHE, Sorbonne Université, Université Paris Cité, CNRS/IN2P3, Paris, France
129 Department of Physics, University of Pennsylvania, Philadelphia, PA, USA
130 Department of Physics and Astronomy, University of Pittsburgh, Pittsburgh, PA, USA
131 (a) Laboratório de Instrumentação e Física Experimental de Partículas-LIP, Lisbon, Portugal; (b) Departamento de Física, Faculdade de Ciências, Universidade de Lisboa, Lisbon, Portugal; (c) Departamento de Física, Universidade de Coimbra, Coimbra, Portugal; (d) Centro de Física Nuclear da Universidade de Lisboa, Lisbon, Portugal; (e) Departamento de Física, Universidade do Minho, Braga, Portugal; (f) Departamento de Física Teórica y del Cosmos, Universidad de Granada, Granada, Spain; (g) Departamento de Física, Instituto Superior Técnico, Universidade de Lisboa, Lisbon, Portugal

[132] Institute of Physics of the Czech Academy of Sciences, Prague, Czech Republic
[133] Czech Technical University in Prague, Prague, Czech Republic
[134] Charles University, Faculty of Mathematics and Physics, Prague, Czech Republic
[135] Particle Physics Department, Rutherford Appleton Laboratory, Didcot, UK
[136] IRFU, CEA, Université Paris-Saclay, Gif-sur-Yvette, France
[137] Santa Cruz Institute for Particle Physics, University of California Santa Cruz, Santa Cruz, CA, USA
[138] (a)Departamento de Física, Pontificia Universidad Católica de Chile, Santiago, Chile; (b)Millennium Institute for Subatomic Physics at High Energy Frontier (SAPHIR), Santiago, Chile; (c)Instituto de Investigación Multidisciplinario en Ciencia y Tecnología y Departamento de Física, Universidad de La Serena, La Serena, Chile; (d)Department of Physics, Universidad Andres Bello, Santiago, Chile; (e)Instituto de Alta Investigación, Universidad de Tarapacá, Arica, Chile; (f)Departamento de Física, Universidad Técnica Federico Santa María, Valparaíso, Chile
[139] Department of Physics, University of Washington, Seattle, WA, USA
[140] Department of Physics and Astronomy, University of Sheffield, Sheffield, UK
[141] Department of Physics, Shinshu University, Nagano, Japan
[142] Department Physik, Universität Siegen, Siegen, Germany
[143] Department of Physics, Simon Fraser University, Burnaby, BC, Canada
[144] SLAC National Accelerator Laboratory, Stanford, CA, USA
[145] Department of Physics, Royal Institute of Technology, Stockholm, Sweden
[146] Departments of Physics and Astronomy, Stony Brook University, Stony Brook, NY, USA
[147] Department of Physics and Astronomy, University of Sussex, Brighton, UK
[148] School of Physics, University of Sydney, Sydney, Australia
[149] Institute of Physics, Academia Sinica, Taipei, Taiwan
[150] (a)E. Andronikashvili Institute of Physics, Iv. Javakhishvili Tbilisi State University, Tbilisi, Georgia; (b)High Energy Physics Institute, Tbilisi State University, Tbilisi, Georgia; (c)University of Georgia, Tbilisi, Georgia
[151] Department of Physics, Technion, Israel Institute of Technology, Haifa, Israel
[152] Raymond and Beverly Sackler School of Physics and Astronomy, Tel Aviv University, Tel Aviv, Israel
[153] Department of Physics, Aristotle University of Thessaloniki, Thessaloniki, Greece
[154] International Center for Elementary Particle Physics and Department of Physics, University of Tokyo, Tokyo, Japan
[155] Department of Physics, Tokyo Institute of Technology, Tokyo, Japan
[156] Department of Physics, University of Toronto, Toronto, ON, Canada
[157] (a)TRIUMF, Vancouver, BC, Canada; (b)Department of Physics and Astronomy, York University, Toronto, ON, Canada
[158] Division of Physics and Tomonaga Center for the History of the Universe, Faculty of Pure and Applied Sciences, University of Tsukuba, Tsukuba, Japan
[159] Department of Physics and Astronomy, Tufts University, Medford, MA, USA
[160] Department of Physics and Astronomy, University of California Irvine, Irvine, CA, USA
[161] University of Sharjah, Sharjah, United Arab Emirates
[162] Department of Physics and Astronomy, University of Uppsala, Uppsala, Sweden
[163] Department of Physics, University of Illinois, Urbana, IL, USA
[164] Instituto de Física Corpuscular (IFIC), Centro Mixto Universidad de Valencia-CSIC, Valencia, Spain
[165] Department of Physics, University of British Columbia, Vancouver, BC, Canada
[166] Department of Physics and Astronomy, University of Victoria, Victoria, BC, Canada
[167] Fakultät für Physik und Astronomie, Julius-Maximilians-Universität Würzburg, Würzburg, Germany
[168] Department of Physics, University of Warwick, Coventry, UK
[169] Waseda University, Tokyo, Japan
[170] Department of Particle Physics and Astrophysics, Weizmann Institute of Science, Rehovot, Israel
[171] Department of Physics, University of Wisconsin, Madison, WI, USA
[172] Fakultät für Mathematik und Naturwissenschaften, Fachgruppe Physik, Bergische Universität Wuppertal, Wuppertal, Germany
[173] Department of Physics, Yale University, New Haven, CT, USA

[a] Also Affiliated with an Institute Covered by a Cooperation Agreement with CERN, Geneva, Switzerland
[b] Also at An-Najah National University, Nablus, Palestine
[c] Also at Borough of Manhattan Community College, City University of New York, New York, NY, USA

[d] Also at Center for High Energy Physics, Peking University, Beijing, China
[e] Also at Center for Interdisciplinary Research and Innovation (CIRI-AUTH), Thessaloniki, Greece
[f] Also at Centro Studi e Ricerche Enrico Fermi, Rome, Italy
[g] Also at CERN, Geneva, Switzerland
[h] Also at Département de Physique Nucléaire et Corpusculaire, Université de Genève, Geneva, Switzerland
[i] Also at Departament de Fisica de la Universitat Autonoma de Barcelona, Barcelona, Spain
[j] Also at Department of Financial and Management Engineering, University of the Aegean, Chios, Greece
[k] Also at Department of Physics, California State University, Sacramento, USA
[l] Also at Department of Physics, King's College London, London, UK
[m] Also at Department of Physics, Stanford University, Stanford, CA, USA
[n] Also at Department of Physics, Stellenbosch University, Stellenbosch, South Africa
[o] Also at Department of Physics, University of Fribourg, Fribourg, Switzerland
[p] Also at Department of Physics, University of Thessaly, Thessaly, Greece
[q] Also at Department of Physics, Westmont College, Santa Barbara, USA
[r] Also at Hellenic Open University, Patras, Greece
[s] Also at Institucio Catalana de Recerca i Estudis Avancats, ICREA, Barcelona, Spain
[t] Also at Institut für Experimentalphysik, Universität Hamburg, Hamburg, Germany
[u] Also at Institute for Nuclear Research and Nuclear Energy (INRNE) of the Bulgarian Academy of Sciences, Sofia, Bulgaria
[v] Also at Institute of Applied Physics, Mohammed VI Polytechnic University, Ben Guerir, Morocco
[w] Also at Institute of Particle Physics (IPP), Toronto, Canada
[x] Also at Institute of Physics and Technology, Mongolian Academy of Sciences, Ulaanbaatar, Mongolia
[y] Also at Institute of Physics, Azerbaijan Academy of Sciences, Baku, Azerbaijan
[z] Also at Institute of Theoretical Physics, Ilia State University, Tbilisi, Georgia
[aa] Also at Lawrence Livermore National Laboratory, Livermore, USA
[ab] Also at National Institute of Physics, University of the Philippines, Diliman, Philippines
[ac] Also at Technical University of Munich, Munich, Germany
[ad] Also at The Collaborative Innovation Center of Quantum Matter (CICQM), Beijing, China
[ae] Also at TRIUMF, Vancouver, BC, Canada
[af] Also at Università di Napoli Parthenope, Naples, Italy
[ag] Also at Department of Physics, University of Colorado Boulder, Boulder, CO, USA
[ah] Also at Washington College, Chestertown, MD, USA
[ai] Also at Physics Department, Yeditepe University, Istanbul, Türkiye
* Deceased